

Compaction of DNA into an Origami-like Structure for Efficient Gene Delivery

Konstantinos Giarentis

Master's Thesis





Department of Materials and Production
Aalborg University

AALBORG UNIVERSITY

STUDENT REPORT

Title:

Compaction of DNA into an Origami-like Structure for Efficient Gene Delivery

Project:

Master's Thesis

Project Period:

September 2021 - June 2022

Participant:

Konstantinos Giarentis

Supervisors:

Leonid Gurevich
Evamaria Petersen

Total Page Number: 90

Appendix Pages: 7

Date of Completion:

June 1, 2022

Abstract:

During this Master's thesis, it was attempted to design and produce a DNA origami-like structure, able to be *in vivo* transfected into mammalian cells and express a fluorescent protein. Initially, the pHAGE-EF1 α L-eGFP-W plasmid was utilized, but its poor sequencing proved it unsuitable. Next, a DNA origami design, which had as a template the TagRFP gene of the pTagRFP-C vector, was created through the aid of caDNA2 and Maya's vHelix plugin. The structure's stability was *in silico* tested with oxDNA2. Asymmetric PCR was used to create the scaffold DNA, while an attempt to produce ten ssDNA fragments, essential for the origami structure, was performed. The annealing of the structure was evaluated through AGE and AFM imaging. Finally, different DNA origami annealing protocols were tested for their transfection efficiency on HeLa cell cultures, along with a carrier-free pTagRFP-C vector and the vector mixed with poly-L-lysine.

The content of this report is freely available, but publication (with reference) may only be pursued due to agreement with the author.

Preface

This Master's thesis was conducted throughout the 3rd and 4th semesters of the academic year 2021-2022 for the Master's programme in Nanobiotechnology at the Department of Materials and Production at Aalborg University. HeLa cell cultures and imaging of transfection were conducted at the Department of Health Science and Technology at Aalborg University.

In this report, theory regarding gene delivery, cellular uptake, and the transcription of a gene will be covered. Next, DNA origami will be described, followed by a presentation of the main plasmid which will be used in this project and a description of the general protocol of an asymmetric PCR reaction. Afterwards, the materials and methods used in this project will be described. Furthermore, the results will be demonstrated and discussed, and a conclusion will be presented. Finally, suggestions for further experimentations will be shown.

The "List of Abbreviations" presents the abbreviations used in this project. References appear on the report as numbers in brackets, which refer to the referenced source in Bibliography. References before a full stop refer to the sentence into which they are included, while references after the full stop refer to the whole subsection after the last appearing reference. Figures, equations, and tables are numbered in separate ascending order throughout the report.

I would like to thank my supervisors, Leonid Gurevich and Evamaria Petersen, for their valuable assistance during the whole project period. I would also like to thank Cristian Pablo Pennisi, associate professor of the Regenerative Medicine group, at the Department of Health Science and Technology at Aalborg University, for his contribution to the HeLa cell cultures and the imaging of transfection.

Konstantinos Giarentis

Konstantinos Giarentis

List of Abbreviations

2D	Two-Dimensional
3D	Three-Dimensional
AGE	Agarose Gel Electrophoresis
AFM	Atomic Force Microscopy
Ala (A)	Alanine
AmpR	Ampicillin Resistant
aPCR	Asymmetric Polymerase Chain Reaction
APS	Ammonium Persulfate
ATF	Activating Transcription Factor
BRE	B Recognition Element
CCV	Clathrin-Coated Vehicle
CG	Coarse-Grained
CME	Clathrin-Mediated Endocytosis
CMV_{IE}	Cytomegalovirus Immediate Early
CPP	Cell-Penetrating Peptide
CREB	cAMP Response Element-Binding Protein
CRS	Cis-Repressional Signal
CTP	Cell-Targetting Peptide
DMEM	Dulbecco's Modified Eagle's Medium
DNA	Deoxyribonucleic Acid
dNTP	Deoxyribonucleotide Triphosphate
DPE	Downstream Promoter Element
dsDNA	Double-Stranded Deoxyribonucleic Acid
DSN	Duplex-Specific Nuclease
DTS	DNA Nuclear Targetting Sequence
<i>E. coli</i>	<i>Escherichia coli</i>
ERF	Ethylene Responsive Factor
FRET	Förster (Fluorescence) Resonance Energy Transfer
GTF	General Transcription Factor

HeLa	Henrietta Lacks
Inr	Initiator
MD	Molecular Dynamics
mRNA	Messenger Ribonucleic Acid
NF-κB	Nuclear Factor Kappa-Light-Chain-Enhancer of Activated B Cells
NLS	Nuclear Localization Signal
nn	Nearest Neighbours
NPC	Nuclear Pore Complexes
PAGE	Polyacrylamide Gel Electrophoresis
PEG	Polyethylene Glycol
PCR	Polymerase Chain Reaction
PLL	Poly-L-Lysine
RFP	Red Fluorescent Protein
RNA	Ribonucleic Acid
SOC	Super Optimal broth with Catabolite Repression
SP-1	Specificity Protein 1
SRE	Serum Response Element
ssDNA	Single-Stranded Deoxyribonucleic Acid
SV40	Simian Vacuolating Virus 40
TAF	TBP-Associated Factor
TAE	Tris-Acetate-EDTA
TAT	Trans-Activator of Transcription
TB	Tris-Boric
TBE	Tris-Boric-EDTA
TBP	TATA-Binding Protein
TEM	Transmission Electron Microscopy
TEMED	Tetramethylethylenediamine
T_m	Melting Temperature
UV	Ultra Violet
YY1	Yin Yang 1

Contents

1	Introduction	1
1.1	Gene Delivery Systems	1
1.2	Uptake of Nanostructures	3
1.2.1	Clathrin-Mediated Endocytosis	4
1.2.2	Caveolin-Mediated Endocytosis	4
1.2.3	Macropinocytosis	5
1.2.4	Cell-Penetrating Peptides	5
1.2.5	Cholesterol	6
1.2.6	Endosomal Escape	6
1.2.7	Nucleus Targetting	8
1.3	Transcription	8
2	DNA Origami	10
2.1	Applications of DNA Origami	10
2.2	Limitations of DNA Origami	11
2.3	DNA Origami Delivery	12
2.4	Gene Delivery with DNA Origami	14
3	Theory	16
3.1	The pTagRFP-C Plasmid	16
3.1.1	The CMV _{IE} Enhancer-Containing Promoter	18
3.2	Polymerase Chain Reaction	19
3.2.1	Asymmetric PCR	20
4	Project Approach	21
5	Materials And Methods	22
5.1	Materials and Chemicals	22
5.2	Medium for Cell Growth and Growth Plates	24
5.3	DNA Transformation	26
5.4	DNA Isolation	26
5.5	Agarose Gel Electrophoresis	27

5.5.1	Denaturing Gels	27
5.5.2	Agarose Gel Electrophoresis for DNA Origami	27
5.6	Polyacrylamide Gel Electrophoresis	28
5.7	Plasmid Digestion With Restriction Enzymes	28
5.8	ssDNA Production	28
5.8.1	PCR Reactions	28
5.8.2	DNA Extraction from Agarose Gel	29
5.8.3	Asymmetric PCR	29
5.9	DNA Purification	30
5.9.1	dsDNA Purification	30
5.9.2	ssDNA Purification	31
5.10	DNA Origami-like Structure Formation	32
5.11	DNA Origami Dialysis	32
5.12	Atomic Force Microscopy	33
5.13	Poly-L-Lysine	33
5.14	HeLa Cell Cultures	33
5.15	Cholesterol Annealing	34
6	Simulations	35
6.1	CaDNAno2	35
6.1.1	Design of Primers and Staples	35
6.2	Maya 2019	36
6.2.1	Design of the DNA Origami-like Structure	38
6.3	oxDNA	39
7	Results	44
7.1	Testing of the pHAGE-EF1 α L-eGFP-W Plasmid	44
7.1.1	DNA Isolation and Digestion of the Plasmid	44
7.1.2	Attempt of Production of the Single-Stranded Scaffold	45
7.2	DNA Origami-like Structure with the pTagRFP-C Vector	45
7.2.1	DNA Transformation, Isolation and Digestion of the Vector	45
7.2.2	Production and Purification of ssDNA Fragments	46
7.2.3	DNA Origami-like Structure Annealing	50
7.2.4	DNA Origami-like Structure Dialysis	51
7.2.5	AFM Imaging	52
7.2.6	HeLa Cell Cultures	60
8	Discussion	64
8.1	The pHAGE-EF1 α L-eGFP-W Plasmid	64
8.2	The pTagRFP-C Vector	64
8.2.1	Design of the DNA Origami-like Structure	64
8.2.2	Molecular Dynamics Simulations	66

8.2.3	Production of ssDNA Fragments	68
8.2.4	DNA Origami-like Structure Annealing	70
8.2.5	Transfection of HeLa Cells	72
9	Conclusion	74
10	Future Considerations	75
A	Appendix	84
B	Appendix	89

1 Introduction

1.1 Gene Delivery Systems

Gene therapy is a promising strategy to treat diseases or genetic disorders by transferring therapeutic nucleic acid materials into cells, thereby regulating cellular processes and responses [1]. The main procedure of gene delivery is presented in Figure 1.1, and its steps will be analyzed afterwards. One of the main tools of gene therapy is gene delivery, a technique also used in studying gene function. The concept of gene delivery involves the transfection of genes into target cells. [2] The two general categories of gene delivery include viral and nonviral methods. There are also the physical methods, but they are mainly combined with one of the previous two to increase their efficiency. [3]

Regarding the viral vectors, the virus used must be replication-defective, or else it will be harmful to the host cell. The retrovirus is one of the most common RNA viruses, while the adenovirus is a famous DNA virus. The transfection of the cells can be performed both *in vivo* and *in vitro*. Some benefits include long-term gene expression, high efficiency, and the ability of the virus to assure transport of its genomic DNA to the nucleus of the host cell without degradation by lysosomes. On the other hand, insertional mutagenesis, poor target specificity, delayed immune responses, and the inability to transfer large-sized genes are some of the drawbacks arising. [1], [3], [4]

The nonviral gene delivery methods use synthetic or natural compounds to deliver a piece of DNA into a cell. DNA, proteins, polymers, and lipids are among the most common building blocks of nonviral vectors. [5], [6] Some of the main polymers used for *in vivo* transfection are poly-L-lysine (PLL), polyethylene glycol (PEG) and polyethylenimine, due to their positive charge which can interact with the negatively charged cell membranes [7]. Compared to viral vectors, some of their advantages include the almost unlimited production of uniform vectors, the fact that nearly none of these compounds invoke an inflammatory response, higher flexibility in gene size, and lower immunogenicity. Additionally, low toxicity and potential tissue specificity by modifying the vectors with ligands are observed. [2]–[4] Although therapeutic be-

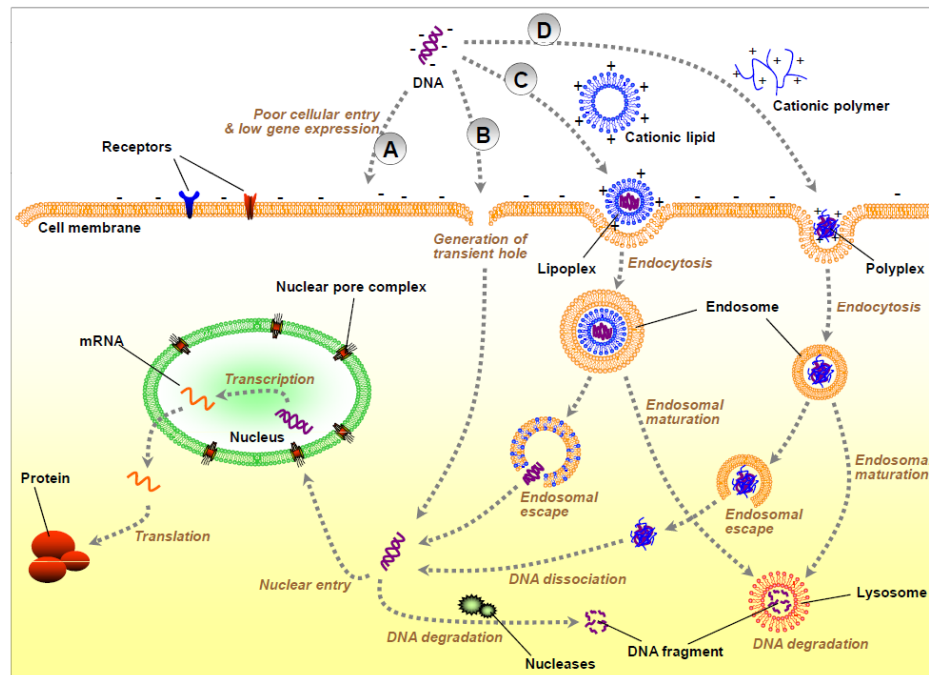


Figure 1.1: The main route of a gene delivery system: The gene is packed in a structure which will protect it until it reaches the targeted cell. Next, the complex needs to overcome the membrane barrier, escape the endosomal route and DNA degradation, and transfer the gene into the nucleus, where it will be transcribed. Obtained from [1].

enefits have been demonstrated in animal models, nonviral gene carriers are less efficacious and short-lived than viral vectors [4].

Physical methods facilitate the transfer of genes to the nucleus by creating transient membrane holes/defects using physical forces, such as local or rapid systemic injection, particle impact, electric pulse, ultrasound, or laser irradiation. Some of these techniques include needle and jet injection, hydrodynamic gene transfer, gene gun, and electroporation. [4] They are less complicated than viral and nonviral systems and highly effective for localized gene delivery. A fragment of DNA or a plasmid containing a transgene, and the regulatory elements for its expression, is directly delivered into cells without involving any substances which could be cytotoxic or immunogenic as commonly seen in viral or nonviral vectors. [3]

To reduce the risk of clinical gene therapy, minimization of the toxicity associated with viral vectors and nonviral gene carriers needs to be achieved. For that reason, a stable and reliable method for the production of a carrier-free gene delivery system would be very beneficial. [8]

1.2 Uptake of Nanostructures

The delivery of a biological therapeutic, such as a DNA molecule able to be transcribed, is crucial for biomedical research and precision cell-based therapies [9]. Different challenges arise from the delivery and endocytosis of particles, depending on their nature and the type of the cell [10]. Endocytosis is a fundamental process which is used by cells to internalise molecules [11]. For animal cells, there are several possible uptake pathways. No special targeting or penetration designs are needed for 50-200 nm molecules. This case works for cells whose *in vivo* role is the uptake of foreign particles, e.g. for macrophages, monocytes and dendritic cells. In cases where the particle is immunomodulatory, these cell types can be quite useful. Although, in most cell types, the uptake is selective and a targeting mechanism should exist on the nanoparticle to stimulate internalization. This precise targeting is very useful for therapeutic delivery. [10]

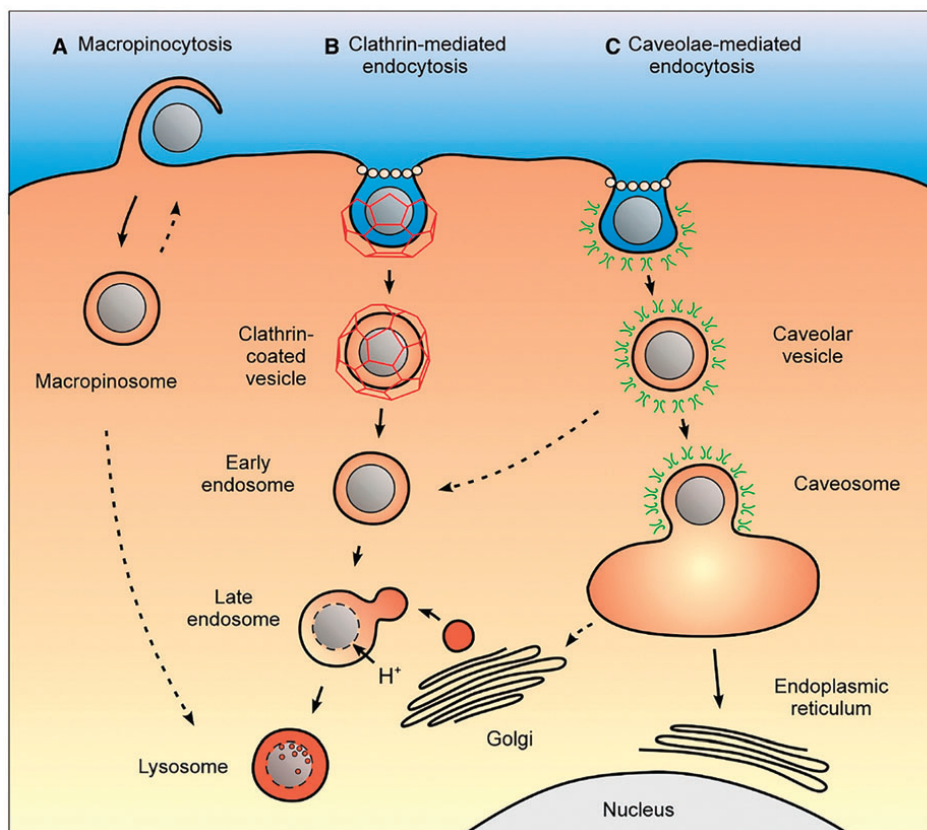


Figure 1.2: The three main sub-types of pinocytosis: Macropinocytosis, clathrin-mediated endocytosis, and caveolin-mediated endocytosis. Obtained from [12].

Passive diffusion through the cell membrane could be possible for smaller particles and molecules, such as amino acids and ions, depending on their charge. On the other hand, larger molecules are transported over the membrane in a more controlled manner. In this case, endocytosis takes place. There are two main types of endocytosis; phagocytosis and pinocytosis. [10] Phagocytosis exists only in a few specialized cells, while pinocytosis is present in almost any eukaryotic cell [11]. When molecules are bigger than 250 nm, phagocytosis occurs. It is a common case for the immune system. Pinocytosis is the pathway which is utilized for the uptake of fluids and smaller particles. It includes three sub-types: clathrin-mediated endocytosis, caveolin-mediated endocytosis, and macropinocytosis. These three sub-types are illustrated in Figure 1.2. [10]

1.2.1 Clathrin-Mediated Endocytosis

Clathrin-mediated endocytosis (CME) is the most well-studied endocytosis mechanism [11]. Its main roles involve the nutrient, antigen, pathogen, and growth factors uptake. Initially, a ligand binds strongly to a specific cell surface receptor. The resulting complex is clustered in coated pits on the plasma membranes. The main protein of the cluster is clathrin, combined with adaptor protein complexes. Next, the pits invaginate and detach from the plasma membrane, forming clathrin-coated vehicles (CCVs) in the cytosol. Afterwards, depolymerization of the clathrin coat takes place and early endosomes are created, which fuse with other early endosomes, finally forming late endosomes, and after further fusion, lysosomes are being created. [13] In this process, pH decreases from 7.4 under normal conditions, to 6.5 on early endosomes, 6 on late endosomes, and finally to 5 in lysosomes [9]. When CME is used for gene delivery, it can be targeted by ligands, such as transferrin, which are attached to the nanoparticle. The specific targeting increases the internalization rate, but for the increase of the gene expression, the endosome creation must be avoided, or endosomal escape should take place. [13]

1.2.2 Caveolin-Mediated Endocytosis

Caveolin-mediated endocytosis participates in cell signalling, lipid regulation, vesicular transport, and in a number of diseases, including diabetes and cancer. It is also a route for the insertion of various viruses and molecules, such as folic acid and the cholera toxin. Caveolae, flask-shaped invaginations on the plasma membrane, also act as membrane tension regulators and assist in transcytosis, except for their use on the specific endocytosis route. [11] The internalization process is slower than the CME, but it also is non-acidic and non-digestive. There is no drop in pH, and lysosomal degradation is avoided. Therefore, this route is advantageous for gene delivery, especially if the particle is combined with caveolae-specific receptors. [13]

1.2.3 Macropinocytosis

In macropinocytosis, a large quantity of external fluid is engulfed through the formation of waving sheet-like extensions of the plasma membrane. Macropinosomes are formed at a size of around 4.2 μm . Actin is the molecule that regulates macropinocytosis and neither the cargo nor the receptors. The cell types affect the shape of the ruffling of the plasma membrane across the cell surface. Growth factor receptors or various particles, such as apoptotic bodies, bacteria, necrotic cells, and viruses, can stimulate these membrane protrusions, but not all of these lead to the formation of macropinosomes. [11]

1.2.4 Cell-Penetrating Peptides

Before a DNA-containing particle reaches the cell, it initially has to overcome various barriers. The anatomical barriers are epithelial and endothelial cell linings, as well as the extracellular matrix surrounding the cells, leading to the prevention of the macromolecules' direct access to target the cell. [4]

The cellular barriers appearing when a particle finally reaches the cell are the most important for the efficiency of DNA transfection. The entrance of nucleic acids in the cell is possible by endocytosis, through the creation of transient holes, or by using cell-penetrating peptides (CPPs). [4]

Various proteins perform a translocation process, like the TAT protein from the HIV1 virus and the *Drosophila melanogaster* Antennapedia homeodomain. The minimum sequence needed to achieve the translocation can be used as a CPP. Although the exact entrance mechanism of CPPs is a debate, it is probably affected by the nature of the cargo, the type of CPP, the cell line, and the conditions of incubation. The formation of micromicelles at the membrane is a possibility for the insertion of CPPs in the cell. Certain proteins, when they have a small cargo attached, can perform direct translocation into the cell. Another reported way for the internalization of CPPs with high cationic residues is their adsorption at the cell surface and afterwards the insertion into an endocytosis route. [14] Unfortunately, the endosomolytic activity of CPPs is poor. Some strategies to perform the endosomal escape include the aid of multivalent CPPs, pH-dependent membrane-active peptides or photochemical internalization. [15]

CPPs are an efficient way to deliver molecules into cells, but they lack cell-type specificity, while the cell-targeting peptides (CTPs) offer specific binding activity and are being inserted into the cell through endocytosis. These peptides are 3-10 amino acids long and have high specificity and affinity with ligands which are found on specific cell types. [14]

1.2.5 Cholesterol

One of the many molecules existing in animal cell membranes is cholesterol, which modulates the fluidity of the membrane, as it regulates the lipid organisation [16], [17]. Its structure can be seen in Figure 1.3. The natural occurrence of cholesterol in the cells and its minimal toxicity makes it an efficient tool for the uptake of molecules [18]. It can be conjugated either on its own on oligonucleotides (introduction of spermine or spermidine can increase the cellular uptake even further) or be attached to cationic lipids and lipopolymers for *in vivo* or *in vitro* transfection [19], [20].

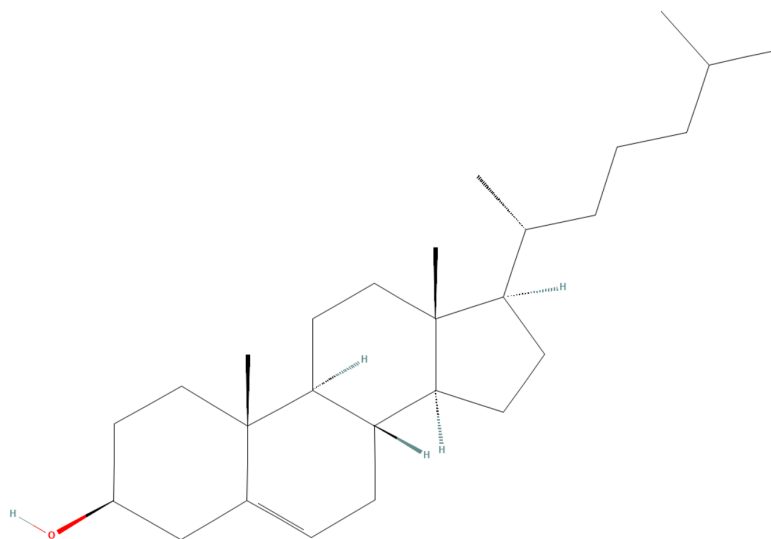


Figure 1.3: 2D structure of cholesterol. Obtained from [21].

Another advantage of cholesterol on the uptake pathway is its endosomal escape ability. It contains a tertiary amine, which has a low pK, and the acidic environment of the endosome can be buffered, leading to the protection of the transferred molecule. [16]

1.2.6 Endosomal Escape

Mostly in the case of clathrin-mediated endocytosis, an endosome is formed, leading to lysosomes which would finally destroy the nanoparticle. If the caveolin-mediated endocytosis is targeted, then no endosomes are formed. [22]. Here, different routes of endosomal escape will be exploited.

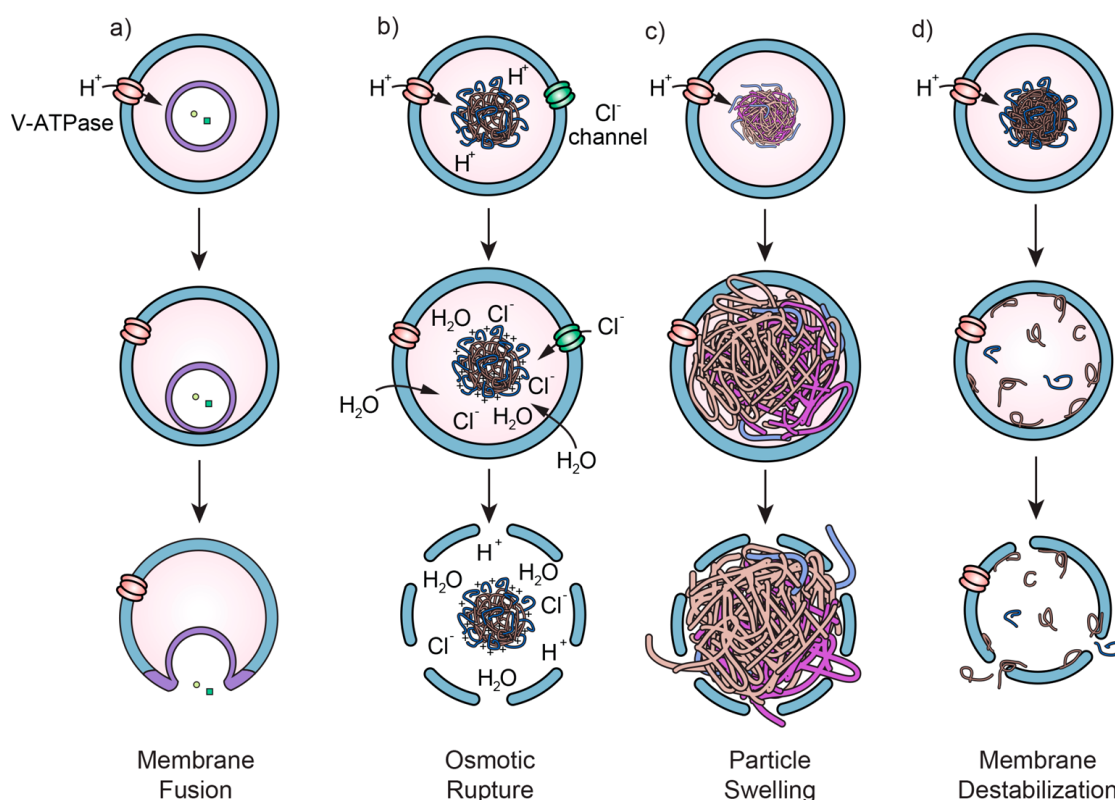


Figure 1.4: Routes of Endosomal escape: (a) Membrane fusion, (b) osmotic rupture, which is based on osmotic pressure, (c) particle swelling, which is based on mechanical strain, and (d) membrane destabilization, a pH-based route. Obtained from [9].

The first route is the endosomal escape via membrane fusion. A membrane fusion between the particle structure and the endosomal membrane is created and releases the encapsulated cargo into the cytosol. [4] Endosomal escape using osmotic pressure is another route, where the influx of chloride counterions is increased by the buffering of the acidifying endosome, due to the proton sponge mechanism. In this case, protons are absorbed by weak amine compounds and slow down the acidification process, which is crucial for the transition to the lysosome. This results in higher osmotic pressure, leading to the burst of the endosome. [4], [9] A third case is endosomal escape induced by nanoparticle swelling. Here, the increased mechanical strain, which is caused due to the swelling of a pH-responsive nanogel, ruptures the endosomal membrane, releasing its content. The last case is endosomal escape through membrane destabilization, where pH-responsive nanoparticles escape through particle disassembly and destabilization of the membrane. These routes can be seen in Figure 1.4. [23]

1.2.7 Nucleus Targetting

After the endosomal escape, or just after the insertion into the cell, in the case where no endosomes are formed, the particle must travel through the cytoplasm into the nucleus, where transcription takes place. Barriers which may appear in the cytoplasm include its viscous protein solution and the cytoskeleton matrix. The diffusion movement is insufficient and slow, resulting in weak expression levels. [4]

The final crucial barrier is the nuclear envelope for the entry of the DNA particle. It is a double-membrane envelope which has large protein structures separating the two membranes, finally forming the nuclear pore complexes (NPC). They have a diameter of around 9 nm, allowing the free diffusion of only small particles. [4] To overcome this barrier, an active transport process could take place, where the membrane's pores expand to a 30 nm diameter [13]. Here, an importin recognizes the nuclear localization signal (NLS) peptide sequence and this complex docks at the NPC. One of the main NLS is the PKKKRKV sequence of the SV40 Large T-antigen [24]. This is the case for stable cells. An easier process for nucleus targetting takes place on replicating cells, for mostly *in vitro* transfection. In this case, the majority of the DNA molecules are inserted into the nucleus during mitosis through the dissolution and reorganization of the nuclear envelope. [4], [25]

Another route to transfer a DNA molecule into the nucleus is through the binding of a specific sequence onto a transcription factor, which exists in the cytoplasm and will be translocated into the nucleus. These sequences are named DNA nuclear targetting sequences. [26] For example, The transcription factor nuclear factor κ B (NF- κ B) recognises a short 10 bp DNA sequence and binds to it. If the sequence is repeated on the DNA molecule, the nuclear transfer efficiency will be increased. Its transfer into the nucleus can be additionally stimulated by the tumour necrosis factor- α . [27]

1.3 Transcription

After the gene of interest has reached the nucleus, the transcription must be initiated, for the inserted gene to be expressed. The transcription procedure needs a series of enzymes which are combined to create an mRNA molecule complementary to the transcribing strand. The three main steps for the transcription procedure are initiation, elongation, and termination. [28]

Initially, RNA polymerase, in combination with several initiation factors, binds in a specific orientation to the promoter, a DNA sequence mainly located upstream of the transcription start point. The complex formed is called a closed complex, in which the DNA sequence is still double-stranded, and RNA polymerase is bound to one side

of the helix. This binding initiates the unwinding of DNA at the point where transcription starts. This results in a transcription bubble of single-stranded DNA (with an extension of 13 bp), which will be used as a template for this 5'-to-3' directive reaction. The complementary DNA nucleotide of the first ribonucleotide of the transcribed molecule is marked as +1. The initiation step is finished when the transcript has reached ten ribonucleotides in length. This procedure is inefficient, and ribonucleotides may be removed and replaced several times. [28]

After the transcript has reached a length of 10 bases, the elongation phase is initiated. Here, RNA polymerase performs the catalysis of the RNA synthesis, unwinds the downstream DNA and reanneals the upstream DNA. Additionally, it performs proofreading functions while dissociating the RNA transcript from the template. [28]

Finally, when the desired sequence is transcribed, termination is initiated, where transcription stops and the RNA product is released. Termination can be triggered by some well-characterized sequences in some cells, while in others, the termination procedure is unclear. [28]

In eukaryotic transcription, RNA polymerase II is the main polymerase of the transcription complex, transcribing the majority of the genes. For the initiation step, several other factors are used to aid the binding of the polymerase, as well as to escape from the promoter. These factors are called general transcription factors (GTFs), and their combination with the polymerase creates the preinitiation complex. These factors include the TFIIA, TFIIB, TFIID, TFIIIE, TFIIF, and TFIIH. [28]

The minimal set of sequence elements required for the accurate transcription initiation is called the core promoter. The length of the core promoter is typically 40 to 60 nucleotides. [28] It can be located 35 bp upstream or downstream of the transcription start site [29]. Usual elements of the core promoter include the TATA box, the TFIIB recognition element (BRE), the initiator (Inr), and the downstream promoter elements (DPE, DCE, and MTE). Only a subset of these elements is typically used for the core promoter, with Inr being the most common of these elements to be found. [30], [31]

2 DNA Origami

DNA origami is an idea which was initially demonstrated by Paul Rothemund in 2006 and refers to the construction of small, arbitrary-shaped nanoparticles by using DNA molecules [32]. It is a promising branch of structural DNA technology, which offers various utilities in the bottom-up fabrication of well-defined nanostructures [33]. The concept of DNA origami implements a long single-stranded DNA (ssDNA) used as a template (scaffold), with an approximate length of 7 kb. It folds due to smaller 20-80 bp ssDNA strands (staples) which hybridize to the scaffold via Watson-Crick base pairing. [10], [33], [34] Thanks to its high programmability, a computer-aided design makes DNA origami an easy-to-use technology, amenable to automated fabrication [33].

The general principle of DNA origami design and assembly has four steps. Initially, DNA origami structures are designed through software, such as caDNAo2. Next, staple strands, in excess, are mixed with the scaffold, and assembly takes place through thermal annealing. Afterwards, purification is usually performed by using extraction from an agarose gel. Finally, to observe the two-dimensional (2D) and single-layer origami structures and the three-dimensional (3D) origami structures, Atomic force microscopy (AFM) and Transmission electron microscopy (TEM) are utilized, respectively. [33], [35], [36]

2.1 Applications of DNA Origami

Different attributes can be added to a DNA origami structure by chemically modifying the staples. Binding sites for various biomolecules and nanoparticles can be introduced, offering the ability of cellular imaging, targeted payload delivery and controlled drug release. [37]

More specifically, DNA origami can be used as a versatile engineering platform where the manipulation of nanoscale entities in highly programmable manners is possible. Secondly, it can be used as a template or framework for the assembly or synthesis of diverse materials with nanometer precision. It has thus shown great promise in

the nanofabrication of inorganic, polymeric, and biomolecular assemblies and patterns, with enhanced structural stability and/or desired physicochemical properties. One application of this kind of assemblies is the design of masks or stamps for nanolithography. Furthermore, it can be used to offer an excellent platform for organizing enzymes spatially due to the unique addressability of DNA origami, offering an environment for the production of metabolites, biomolecules and energy conversion in living systems. [33]

DNA origami can also be created by an *in situ* synthesis approach, where precursors in solution adsorb on DNA origami templates with or without prescribed nucleation sites generating continuous architectures shaped by the morphologies of the templates or their cavities. [38]

Site-specific anchors can be included for user-defined interactions. The anchors, thanks to the high degree of thermodynamic and kinetic programmability of DNA origami, can be employed to create a substrate for *in vitro* signalling networks and molecular computation. The reversibility of the Watson-Crick pairing can be used to synthesize molecular machinery and motors. [39], [40]

2.2 Limitations of DNA Origami

Even though DNA origami has high designability and programmability, some aspects which need to be addressed include *in vivo* stability, high reproducibility, purification, storage, targetability, immune-modulation, and cost. [10]

Regarding the high reproducibility, different problems arise. In the case where the self-assembly happens in a one-pot reaction, many defects occur. Therefore, optimization of the annealing procedure by changing the annealing temperature and the cationic strength is crucial for high yield self-assembly. The most commonly used buffer, adopted in most DNA self-assembly protocols, is the Tris-acetate-EDTA (TAE) buffer with Mg^{2+} in a range of 5-20 mM. [33], [41], [42]

To purify DNA origami, different techniques are selected. This selection is based on the yield, duration, volume limitation, dilution, residuals, and damages. There are mainly five purification methods: PEG precipitation, gel purification, filter purification, ultracentrifugation, and size-exclusion chromatography. [33], [43]

Next, storage and stability are also crucial. To be thermally stable, generally, DNA origami should be at temperatures of $\sim 55^{\circ}C$ or below in solution. In cases of photocrosslinking-assisted thermal stability, temperatures above $85^{\circ}C$ can be reached. The lyophilization of DNA origami can also help its storage under freezing conditions.

Again, cationic strength serves a vital role in the stability of the structure, and the correct concentration for each mixture is crucial. [33], [44]

DNA origami also possesses intrinsic properties of DNA, such as its negative charge and susceptibility to enzyme degradation, which may lead to certain limitations. To avoid them, different methods can be applied, such as photo-crosslinking DNA nucleotides, wrapping exposed DNA surfaces with lipid bilayers, shielding DNA backbones with poly-cationic polymers, and coating DNA with silica. High-heat, low salt, and nuclease digestion resistances can be obtained by the above modifications, as well as the evasion of immune surveillance and the surface deformation. [33]

Various off-target complications occur with the insertion of DNA origami into cells. These include the activation of a potent immune response, sequence-specific interference with mRNAs or microRNAs leading to unwanted gene regulation, and long-term integration into the genome. The staple strands can be chemically modified to improve the above problems. Such modifications include post-synthetic modification to render the strands biologically or the inert introduction of modified phosphoramidites. [41]

Last but not least, the cost of DNA origami construction arises as a problem, as it is a relatively more expensive technique compared to other systems. More specifically, the production cost of 10 nmol of staples for a 7 kb structure arises at several hundreds of dollars. Additional expenses arise, such as the production of the scaffold, the purification and the actual cost for every single DNA origami design. Therefore, these costs must be reduced for DNA origami to be improved as a gene delivery system. [41] One solution to reduce the costs of the procedure would be the *in vivo* production of the DNA strands, or even the whole DNA structure [45].

2.3 DNA Origami Delivery

One significant application of DNA origami is drug and gene delivery. Different materials have been used as delivery systems, but limitations have appeared, such as limited biocompatibility and the inability to engineer spatially addressable surfaces which can be utilized for multi-functional activity. DNA origami seems like a capable delivery system candidate. Even though the phosphate groups on the backbone of the DNA make the structure negatively charged, making the passive diffusion of DNA origami through a negatively charged membrane improbable, this problem can be overcome by concealing the charges. [37]

A cell-targeted ability can be added to DNA origami by incorporating ligands on the staple strands, while in some instances this modification is not necessary for cell targeting. The uptake pathway of the DNA origami can also be observed by adding a

fluorescent tag to the structure. [37]

A DNA origami delivery system must possess the ability to reach the cell, recognize, bind, and penetrate it without being destroyed through that process. For example, in the case of intravenous administration, it means that it must survive in the blood. [12] After the insertion in the cell, it may need to target a specific organelle of the cell, or even the nucleus, as well as to avoid the endosomal pathway and DNA degradation.

Different methods have been developed for DNA origami to target cells and stimulate uptake. In one case, ligands decorating DNA origami target specific cell types, such as folate targeting the folate receptor, which is overexpressed on many cancer cells. Also, DNA aptamer 'locks' and 'keys' can be employed to control the opening/closing of DNA origami containers only in the presence of desired ligands. [12] Furthermore, in a case where no specific receptors or uptake pathways are targeted, cell-penetrating molecules may allow entry into the cells. These molecules could be CPPs, while the encapsulation into larger structures may improve cell penetration. [10], [33]

In the case where the reduction of undesirable immune stimulation is needed, immune-silent materials can be added. Enveloping the DNA origami in lipid bilayers can offer nuclease protection, significantly decreased immune activation, and increased bioavailability and half-life of the DNA origami. On the other hand, if immunostimulation is needed, decoration with CpG motifs can be an efficient addition. [10], [46]

One of the aspects which affect DNA origami's entry into cells is its size and shape, comparing them to a cell type-specific manner. Generally, large, high-compacted origamis were internalized more effectively than their elongated counterparts. Additionally, the sizes of compact DNA origami structures with low aspect-ratio range for the most effective internalization between 50 to 80 nm. [47]

When DNA origami is inserted into the cell, the endosomal uptake route must be avoided. One *in vitro* technique for that reason is the direct delivery to the cytosol through cell-squeezing. Cells undergo constriction as they are passed through a device to create holes in the membranes for small particles to pass through. This technique is one of the least disruptive to cells among other permeabilization techniques and can be combined effectively with DNA origami delivery. [48], [49]

Electrotransfection can offer direct *in vitro* and *in vivo* delivery to the cytoplasm while avoiding the endosomal uptake. In this technique, a strong electric field is employed, stripping away the Mg^{+2} counterions, which are crucial for the stability of DNA origami. To avoid the probable loss of structural integrity, the folding of 3D DNA origami structures can be performed in absence of $MgCl_2$ and the presence of sper-

midine. Spermidine is a natural DNA condensation agent and can thus mimic the properties of $MgCl_2$ in the folding buffer. [10], [50]

2.4 Gene Delivery with DNA Origami

One important application of DNA origami is gene delivery. The Watson-Crick base-pairing offers the ability to design precise shapes by using a specific sequence mixed with several staples. While DNA origami is mainly used as a nanoscale material, it also has the potential to interact with cells. [51]

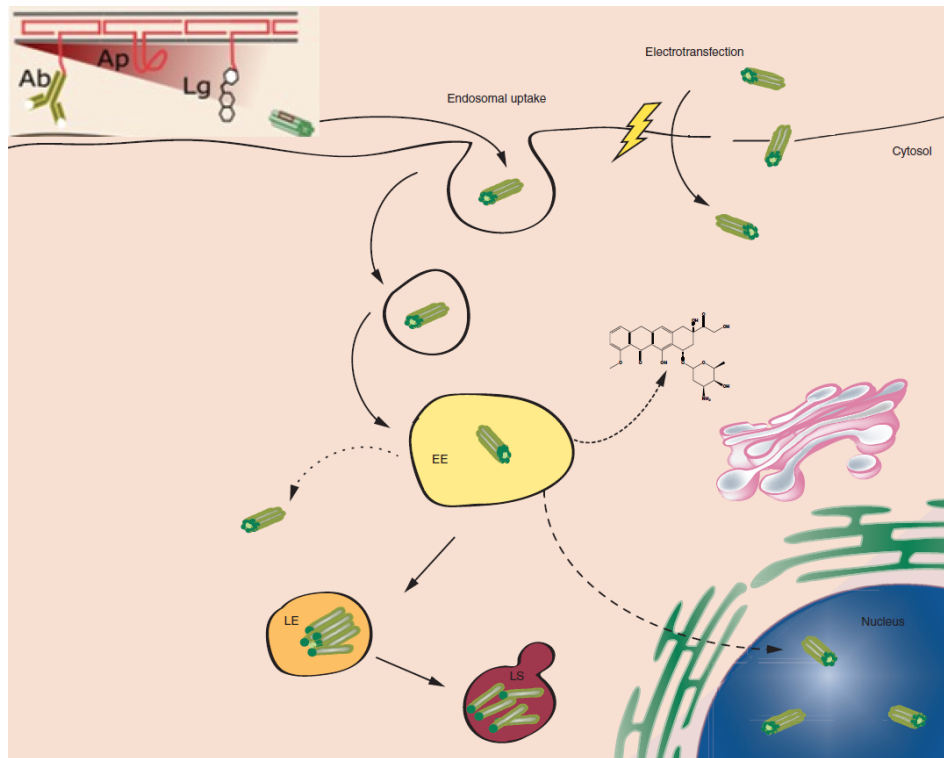


Figure 2.1: The path of a DNA origami molecule towards the nucleus of the cell: The DNA molecule needs to target the cell through a molecule attached to a staple, which will target an antibody, aptamer, or ligand of the desired cell type if it is intended to be inserted through an uptake pathway. Another route for insertion of the cell is electrotransfection. When the molecule is inserted into the cell, it must finally target the nucleus and overcome the nuclear envelope barrier. *Ab: Antibody; Ap: Aptamer; EE: Early endosome; LE: Late endosome; Lg: Ligand; LS: Lysosome.* Obtained from [10].

Since the transfer molecule which needs to be delivered is a DNA molecule, there is a potential for using this sequence as the single-stranded scaffold DNA and eliminating the need for a carrier. This process is more complicated than just using a standard scaffold for DNA origami but offers the ability to add localization signals or a fluores-

cent dye to the staples.

This carrier-free gene delivery system would eliminate the toxicity of a gene carrier, but it still needs to be stable enough, effective and reliable [8]. The packaging of the gene offers protection from nucleases, possibly increasing the efficiency of the process. Since no additional vectors are used, this leads to a reduction of immune activation. [46]

The first barrier which needs to be overcome is the initial administration of the molecule into the organism. In this process, the molecule needs to withstand different conditions until it is inserted into the cell. Additionally, to reach a specific cell type, a targeting molecule needs to be present in the DNA origami. Another barrier is the membrane of the cell. Since DNA is negatively charged, the electrostatic repulsion will not allow the passive uptake of the gene into the cell. [12] Therefore, a technique to introduce the DNA origami structure to an uptake pathway needs to be considered, or electrotransfection can be applied. Finally, the molecule must be able to be inserted into the nucleus, where it needs to be transcribed. An overview of the targeting, insertion to the cell, and finally the nucleus of a DNA origami molecule can be seen in Figure 2.1. [10]

3 Theory

3.1 The pTagRFP-C Plasmid

For this project, the pTagRFP-C vector is going to be used. Its elements can be seen in Figure 3.1. Another plasmid, the pHAGE-EF1 α L-eGFP-W, was initially chosen, but it was proven insufficient, as it will be seen in chapter 7 and chapter 8.

The pTagRFP-C vector contains a pUC origin for replication for propagation in *E. coli* and an f1 origin of replication for ssDNA production. To make the selection of transfected *E. coli* cells, a bacterial promoter (AmpR promoter) aids the expression of the kanamycin resistance gene, while for eukaryotic cells selection, an SV40 early promoter aids the expression of the neomycin resistance gene. Geneticin (G418) can be utilized to select the transfected eukaryotic cells. Suitable host strains for propagation in *E. coli* include DH5 α cells, and the vector confers resistance of 30 $\mu\text{g}/\text{mL}$ kanamycin. [52], [53]

The protein that this plasmid encodes is the red (orange) fluorescent protein pTagRFP. For a higher expression efficiency, the codon usage is optimized for expression in mammalian cells, a Kozak consensus translation initiation site is located upstream of the TagRFP coding sequence, and an SV40 polyadenylation signal exists downstream of the coding sequence, which is required for transcriptional termination [54]–[56]. Finally, the cytomegalovirus immediate early (CMV_{IE}) enhancer-containing promoter is located upstream of the coding site to increase the TagRFP expression. [52]

The red fluorescent TagRFP is a monomeric protein which is produced from the wild-type RFP from sea anemone *Entacmaea quadricolor* [57]. It has high pH-stability (with pK_a=3.8), is proven suitable to generate stably transfected mammalian cell lines, and can be used in both *in vivo* and *in vitro* FRET experiments. Its excitation and emission maxima are 555 nm and 584 nm, respectively. It additionally has high brightness, a maturation half-time of 100 min and no observable cell toxicity. Its fluorescence appears 10-12 hours after the gene's transfection in mammalian cells. The protein's crystal structure can be seen in Figure 3.2. [57]–[59]

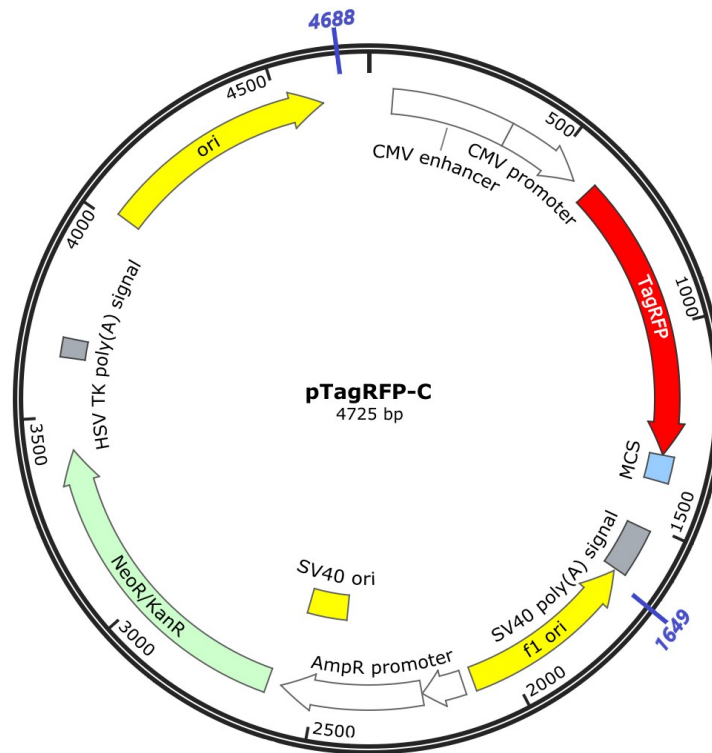


Figure 3.1: The pTagRFP-C vector. The positions 4688 and 1649, marked with blue lines, are the beginning and the end of a 1677 bp sequence which is intended to be amplified. Modified from [60].

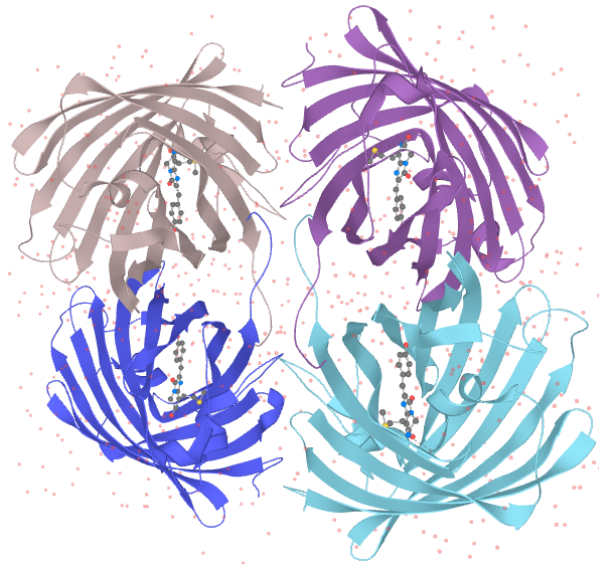


Figure 3.2: The crystal structure of the TagRFP protein. Obtained from [59].

3.1.1 The CMV_{IE} Enhancer-Containing Promoter

Upstream of the TagRFP gene, the robust and efficient CMV_{IE} promoter contains an enhancer with cis-acting binding sites for several transcription factors [61], [62]. These cis-acting elements can act independently or in conjunction to increase the transcription efficiency of RNA polymerase II. Therefore, the promoter can activate or repress TagRFP expression in response to cellular signal transduction events. [63] A map of the binding sites of the CMV_{IE} enhancer-containing promoter can be seen in Table 3.1.

Both YY1 and SP-1 bind to the 21-bp repeat, as well as the transcriptional repressor ERF. Given the frequent presence of YY1 sites adjacent to SP-1 sites, it may be possible that YY1 interacts with SP-1 to stimulate transcription. [64], [65]

The 19-bp repeat contains a CREB/ATF binding site. CREB and ATF play a role depending on the physiology of the cell. Human fibroblasts, for instance, contribute significantly to constitutive enhancing properties. Another repeat, the 18-bp repeat, contains an NF- κ B/rel binding site. All the aforementioned elements respond to chemicals, cytokines, and viral proteins, offering a rapid activation reaction. [66]

Furthermore, there is an NF-1 and an SRE site, but the former's function is unknown since it does not seem to affect transcription from transfected promoter enhancer segments. These sites, in combination with the SP-1 site, contribute collectively and individually to the transcriptional activation. Their repression would negatively affect the expression of the pTagRFP protein. [67]

The TATA box is also located in the CMV promoter. It is where the pre-initiation complex formation starts. TFIID is the GTF that recognizes and binds to the TATA box and specifically its TBP (TATA-binding protein) component. TFIID also has other subunits, the TBP-associated factors (TAFs). Some of these subunits can recognize other core promoter elements. [30]

Finally, at the downstream end of the promoter exists the initiator-like sequence and the cis-repression signal (CRS). A 150 kDa cellular protein binds to the initiator-like sequence and the binding site of the cellular sequence overlaps the CRS. Therefore, the repression of the CRS binding site is silenced, and the expression efficiency is increased. When the initiator-like sequence is mutated, the cellular protein is no longer bound to the enhancer and transcription from the enhancer is reduced significantly. [66]

Table 3.1: Sequence of the CMV_{IE} enhancer-containing promoter. Enhancer Sequence: 1-465. Promoter sequence: 466-589. **Orange Sequence:** Nf1-t binding site. **Light Blue Sequence:** SRE binding site. **Grey Sequence:** 21-nt binding site (the grey highlighted text refers to the SP-1 binding site only). **Green Sequence:** 19-nt binding site. **Blue Sequence:** 18-nt binding site. **Brown Sequence:** AP-1 binding site. **Red Sequence:** TATA box. **Purple Sequence:** CRS/Inr binding site.

1	TAG TTA TTA ATA GTA ATC AAT TAC GGG GTC	30
31	ATT AGT TCA TAG CCC ATA TAT GGA GTT CCG	60
61	CGT TAC ATA ACT TAC GGT AAA TGG CCC GCC	90
91	TGG CTG ACC GCC CAA CGA CCC CCG CCC ATT	120
121	GAC GTC AAT AAT GAC GTA TGT TCC CAT AGT	150
151	AAC GCC AAT AGG GAC TTT CCA TTG ACG TCA	180
181	ATG GGT GGA GTA TTT ACG GTA AAC TGC CCA	210
211	CTT GGC AGT ACA TCA AGT GTA TCA TAT GCC	240
241	AAG TAC GCC CCC TAT TGA CGT CAA TGA CGG	270
271	TAA ATG GCC CGC CTG GCA TTA TGC CCA GTA	300
301	CAT GAC CTT ATG GGA CTT TCC TAC TTG GCA	330
331	GTA CAT CTA CGT ATT AGT CAT CGC TAT TAC	360
361	CAT GGT GAT GCG GTT TTG GCA GTA CAT CAA	390
391	TGG GCG TGG ATA GCG GTT TGA CTC ACG GGG	420
421	ATT TCC AAG TCT CCA CCC CAT TGA CGT CAA	450
451	TGG GAG TTT GTT TTG GCA CCA AAA TCA ACG	480
481	GGA CTT TCC AAA ATG TCG TAA CAA CTC CGC	510
511	CCC ATT GAC GCA AAT GGGCGG TAG GCG TGT	540
541	ACG GTG GGA GGT CTA TAT AAG CAG AGC TGG	570
571	TTT AGT GAA CCG TCA GAT CCG	591

3.2 Polymerase Chain Reaction

One of the main techniques for the amplification of a specific site of a nucleotide chain is the polymerase chain reaction (PCR). It was first introduced by Kary Mullis in 1983 and was utilized for various purposes since. The elements of the PCR include: [68]

- The template DNA, which contains the sequence of interest.
- Two different primers, which bind on the 3' and 5' ends of the sequence of interest. The 3' ends of the two primers are oriented towards each other.
- A polymerase, which will perform the replication on the amplification of the sequence.
- Nucleotides, MgCl₂, and PCR buffer, which are crucial for the correct amplification of the target sequence.

The three main steps of PCR are the annealing, the denaturation, and the extension. In denaturation, the temperature rises to 94-98°C and the two strands of the template

DNA are separated and are accessible for the primers to bind on the annealing step. In annealing, the temperature is usually reduced by 3–5°C below the melting temperature (T_m) of the primers, making their binding to the template possible. Finally, in extension, the temperature is risen until the optimum temperature of the polymerase, resulting in the extension of the primers. These steps are repeated, and after the final cycle, the PCR is terminated, and the temperature is lowered to 4°C. [68], [69]

Before the first cycle starts, the denaturation step lasts a little longer than the following ones to activate the polymerase. From the second annealing step and afterwards, the primers can bind to the newly created DNA strands, finally producing a fragment with the desired sequence. The number of cycles following, which usually varies between 25-35, depends on the amount of the template DNA and the desired product yield. If the number of cycles is very high, this may create nonspecific bands. The final extension step lasts 5-15 minutes to provide a full-length polymerization and a good yield of the target DNA. [69]

3.2.1 Asymmetric PCR

While PCR produces double-stranded DNA (dsDNA) fragments, asymmetric PCR (aPCR) is applied whenever a ssDNA molecule is needed. As a first step of the aPCR protocol, a typical PCR reaction is performed. In this reaction, the primer which is used for the replication of the antisense strand binds a little further than the desired sequence's ending nucleotide. The second primer binds at the position where the final product needs to stop extending. The product of this reaction is used as a template for a second PCR reaction, where only one primer is added, which binds to the product of the initial PCR reaction. For a better yield of the aPCR reaction, the primers of the first amplification need to be discarded throughout purification. Since the products of the aPCR can't be used as a template for further steps, the product is linearly increased and not geometrically. Therefore, a greater number of cycles, compared to a typical PCR reaction, needs to be performed to have sufficient yield. [70]

4 Project Approach

This Master's thesis aims to design and produce a DNA origami-like structure. This structure is intended to offer efficient gene delivery of a gene which transcribes a fluorescent protein. Rather than serving as an encapsulation system, the origami structure is designed to be transcribed. Hence, the scaffold sequence will include the promoter and the gene region of the desired protein.

Initially, a region containing the eGFP gene from the pHAGE-EF1 α L-eGFP-W plasmid was utilized [71]. However, it was deemed insufficient for reasons further explained in the thesis. The plasmid which was eventually used is the pTagRFP-C plasmid, and more specifically, its region containing the TagRFP gene and its promoter.

In the origami-like structure, only its ends will contain staples. The remainder scaffold will be double-stranded due to the binding of ssDNA fragments produced through aPCR. Therefore, the first step of the procedure is the design of the primers which will yield these fragments. Afterwards, the staples for the structure will be designed. After designing the structure through the assistance of caDNAno and Maya's vHelix plugin, a simulation will be performed in oxDNA2 to test its stability.

When the staples, the scaffold, and the ssDNA sequences are mixed, a honeycomb cylinder with ten long strands is expected to be assembled. Compared to a typical DNA origami design, this design will have lower production costs, sufficient stability, and better accessibility of the promoter for the initiation of transcription. For an efficient uptake of the structure into the cell, the tails of the staples are designed to have a specific sequence, where a cholesterol molecule conjugated with an oligomer can bind. The correct folding of the structure will be evaluated through AFM imaging.

Finally, for efficiency testing, the DNA origami-like structure will be transfected into mammalian cells by three different transfection complexes: carrier-free, encapsulated into PLL, and annealed with cholesterol. The controls which will be used will be the carrier-free plasmid and the plasmid mixed with PLL. The fluorescent nature of the protein can be used as a marker for the evaluation of transfection efficiency.

5 Materials And Methods

5.1 Materials and Chemicals

Table 5.1: Materials and equipment utilised throughout the project period.

Device	Description	Supplier	Use
Mini-Sub Cell GT	N/A	BioRad	AGE
Turbo Cyclor	112649	Blue-Ray Biotech	PCR
GeneAmp PCR System 9700	Part No. N8050200	Applied Biosystems	PCR
GenElute TM PCR Clean-Up Kit	SLCL6932	Sigma-Aldrich	PCR Product Purification
ChargeSwitch [®] Pro: PCR Cleanup Kit	Lot 1968672	Thermo Fischer Scientific TM	PCR Product Purification
GeneJet Plasmid Miniprep Kit	Cat. No: K0502	Thermo Fischer Scientific TM	DNA Plasmid Isolation
MiniSpin Plus	112620	Eppendorf	Centrifugion
Centrifuge 5804R	12813	Eppendorf	Centrifugion
Centrifuge 5424R	123812	Eppendorf	Centrifugion
Pico200 Picodrop Microliter Spectrophotometer	SKU: P200P	Souther Labware	DNA Concentration Evaluation
Ultrafree [®] -DA DNA Extraction kit	Lot: R8NA39074	Merck Millipore	DNA Extraction
Monarch [®] PCR & DNA Cleanup Kit	Lot: 10113874	Thermo Fisher	ssDNA Purification
QIAEX II Gel Extraction Kit	Lot: 11547755	QIAGEN	ssDNA Gel Extraction
Biotech CE Tubing MWCO:100 kD	Lot: 3312526	Spectrum	DNA Origami Dialysis
Thermomixer Comfort	N/A	Eppendorf	PAGE/ ssDNA Gel Extraction
Power PAC	N/A	BioRad	PAGE
Enduro TM GDS Touch II	133503	Labnet International	PAGE/AGE
Nanoscope IIIA	68706	Bruker Inc	AFM
EnSpire [®] Plate Reader	N/A	Perkin Elmer	Transfection
AxioObserver Z1	N/A	Carl Zeiss	Transfection

Table 5.2: Overview of the chemicals utilised throughout the project period.

Chemical	Cas/Cat No.	Lot No.	Supplier	Use
Tryptone Plus	91079-40-2	BCCCC2953	Sigma-Aldrich	LB Medium
Sodium Chloride	7647-14-5	17L184138	VWR Chemicals	LB Medium
Yeast Extract	8013-01-2	VM619326 346	EMD Millipore	LB Medium
Agar	9002-18-0	BCBP0217V	Sigma-Aldrich	LB-Agar Plates
Ampicillin	69-53-4	N/A	N/A	LB-Agar Plates
Kanamycin Monosulfate	25389-94-0	104K01645	Sigma-Aldrich	LB-agar Plates
10x CutSmart® Buffer	B7204S	0051404	NEB	DNA Digestion
SOC Medium	15544-034	N/A	Thermo Scientific	DNA Digestion
1x TAE Buffer	N/A	N/A	In-House	AGE
Agarose I TM	9012-36-6	19G0256361	Biotechnology Grade	AGE
Ethidium Bromide	1239-45-8	SLBF7132V	Sigma-Aldrich	AGE
10,000x PAGE GelRed®	41003	19G0819	Biotium	AGE
Gel loading Dye	B7025S	10055732	NEB	AGE
1 kbp DNA Ladder	B7025S	N/A	NEB	AGE
GeneRuler® 1kbp DNA Ladder	SM0311	N/A	Fermentas	AGE
100 bp DNA Ladder	N3231L	10025275	NEB	AGE
Trizma Base	77-86-1	SLCH2550	Sigma-Aldrich	AGE
Urea	57-13-6	BCBN1959V	Sigma Life Science	AGE
Bromophenol Blue	115-39-9	N/A	Sigma-Aldrich	AGE
Triton X-100	9002-93-1	023K0005	Sigma-Aldrich	AGE
TB-Buffer	N/A	N/A	In-House	AGE
MgCl ₂ ·6H ₂ O	7791-18-6	N/A	Sigma-Aldrich	AGE
Molecular Biology Water	BE51200	8MB248	Lonza AccuGene	PCR
50 mM MgCl ₂	N/A	N/A	PCR Bio	PCR
5 nmol/μL dNTP mix	N/A	N/A	In-house	PCR
10x Taq Buffer w. (NH ₄) ₂ SO ₄	N/A	00933106	Thermo Scientific	PCR
10X Taq Buffer w. KCl & 15 mM MgCl ₂	N/A	00933107	Thermo Scientific	PCR
30 % Acrylamide/Bis	79-06-1	N/A	BioRad	PAGE
30 % Ammonium Persulfate	7727-54-0	N/A	N/A	PAGE
TEMED	110-18-9	036K0694	Sigma-Aldrich	PAGE
5x TBE Buffer	N/A	N/A	In-house	PAGE
NuSieve® GTG® Agarose	50080	0000306214	Lonza	ssDNA Gel Extraction
Tilibit 10x Folding Buffer	N/A	M2-1-2	Tilibit	Annealing
Mica	N/A	N/A	EMS	AFM
0.01% Poly-L-Lysine	75K2381	N/A	Sigma-Aldrich	Transfection
DMEM medium	7N/A	N/A	Thermo-Fisher	Transfection
10% Fetal Calf Serum	N/A	N/A	N/A	Transfection
Penicillin	N/A	N/A	N/A	Transfection
Streptomycin	N/A	N/A	N/A	Transfection

Table 5.3: Overview of the biological components used throughout the project period.

Cells/Vectors/Enzymes/DNA	Description	Supplier	Use
<i>Escherichia coli</i>	DH5 α	N/A	Cloning
pHAGE-EF1aL-eGFP-W	CAT: 126686	Addgene	Cloning
pTagRFP-C Plasmid	CAT: FP141	Evrogen	Cloning
Taq DNA Polymerase	Lot 00815450	Thermo Scientific	Cloning
EcoRI-HF	Product No. R3101	NEB	DNA Digestion
SmaI	Product No. R0141	NEB	DNA Digestion
NdeI	Product No. R0111	NEB	DNA Digestion
Duplex-Specific Nuclease	CAT: EA001	Evrogen	dsDNA Digestion
HeLa Cells	CCL-2 TM	ATCC	Transcription

Table 5.4: Staples designed for the DNA origami-like structure of the pTagRFP-C vector's TagRFP gene. Obtained from TAG Copenhagen.

Sequence from 5' to 3'	Bases
GGAGAACATGGTGTCTTATG	21
AAAACCTTCAAGACTGGGCGG	21
GTGTTGTGATGGCCCTGAGAACCTT	25
GTGTTGTGCGGCCCTTCCAAAATCCACCC	29
TGGCATTACATGACTAAGGGCGTGTGTG	30
GTGTTGTGACTGGGGCAACCTCCCTCTACAA	31
CGACATCGCACCAAGGAGTTTGTGTGTTGTG	31
TATCTTACCCCTGAAGGACGGTGATTAAGTGTGTG	36
GTGTTGTGGGGCCACACCAGCTCATTGACAATGACG	36
CTCCCCCTCGGCAGCAAGCTCGCACATACAGATCCATTTACTT	42
GGACTTTGTAAATGGATAACCCAAACTCAATTCCGGTGTGTG	43
CTACCGGTCGCCACCATGCACAGGACACCATCAGAGGGCCAGA	43
GTGTTGTGCGTCAAGAGCCTCCTTCTGTGGCCCCGCCGTGTGTG	44
AATGAGGAAAGTCCCACGAGGAAAGTCCCCAGCGAGGAAAGTCCCCTA	48
GTGTTGTGCATTGACCCATAGTCAACGACTAAAATGGCTTTAAGTGTGTG	51
GTGTTGTGCTGCAACTCCACACCTGAACCTGAAACACCCCGCCTCATGTA TCGCCTT	58
GTGTTGTTTACTGCGCAAACCTTATCAATGTTTTAGGGGACTTTCCTCGCTGGG GACTTTCCTCGTGGGACTTTCCTCATT	80
TAGGGGACTTTCCTCGCTGGGGACTTTCCTCGTGGGACTTTCCTCATTTTTTT ATGTTTCGTCATGAATCAACGGGACTT	80

5.2 Medium for Cell Growth and Growth Plates

The LB medium, which was prepared for the bacterial growth of *Escherichia coli* cells, contained: 10 g/L tryptone, 5 g/L yeast extract, and 5 g/L NaCl. For the LB agar plates, 15 g/L agar were added and mixed with the liquid growth medium before autoclaving. The mixture was dialysed in Mili-Q water in a BlueCap bottle and auto-

claved at 121°C for 30 min.

After the autoclave, the liquid growth medium was stored at 4°C. For the agar plates, when the medium cooled down to approximately 55°C, the desired antibiotic was added, 100 mg/L ampicillin for the pHAGE-EF1 α L-eGFP-W plasmid or 30 mg/L kanamycin for the pTAGRFP-C vector. The mixture was finally poured into Petri dishes and stored at 4°C.

Table 5.5: Primers designed for PCR and asymmetric PCR. Obtained from TAG Copenhagen.

Name	Sequence	T _m	Pos. in Table B.1
EF-1alpha forward	5'-GGACAGCAGAGATCCAG-3'	59.0°C	N/A
EF-1alpha reverse	5'-AGCACTCAAGGCAAGC-3'	60.0°C	N/A
EF-1alpha asym rev	5'-CTTAAAGGATCTCAGGCGG-3'	60.0°C	N/A
CMV-TagRFP-forw	5'-CCCCTGATTCTGTGG-3'	58.1°C	1-15
CMV-TagRFP-rev	5'-GATGGTTACAGTAGTGG-3'	59.4°C	N/A
CMV-TagRFP-rev as	5'-CGCGTTAAGATACATTGATG-3'	59.5°C	1677-1658
pRFP-C-for_as1	5'-CCGCCATGCATTAG-3'	56.6°C	28-41
pRFP-C-rev1	5'-CGGTCAGCCAGG-3'	57°C	138-127
pRFP-C-for1	5'-CGGAACAGGAGAGC-3'	57.9°C	N/A
pRFP-C-for_as2	5'-GGGACTTTCCATTGACGTC-3'	62.8°C	199-217
pRFP-C-rev2	5'-GTCATTGACGTCAATAGGGG-3'	62.6°C	306-287
pRFP-C-for2	5'-GGTCGGAACAGGAGAGC-3'	63.9°C	N/A
pRFP-C-for_as3	5'-CCTACTTGGCAGTACATCTACG-3'	63.9°C	358-379
pRFP-C-rev3	5'-GACTTGGAATCCCCGTGAG-3'	64.7°C	469-450
pRFP-C-for3	5'-GTTCCGCGTTACATAACTTACGG-3'	65.3°C	93-115
pRFP-C-for_as4	5'-GTCGTAACAACCTCCGC-3'	59.9°C	533-548
pRFP-C-rev4	5'-CGCTAGCGGATCTGAC-3'	61.4°C	635-620
pRFP-C-for4	5'-GGGACTTTCCATTGACG-3'	60.1°C	199-215
pRFP-C-for_as5	5'-GAAGCTGTACATGGAGGGC-3'	64.7°C	695-713
pRFP-C-rev5	5'-CCCTCGACCACCTTGATTC-3'	64.3°C	805-787
pRFP-C-for_as6	5'-CATCAACCACACCCAGGG-3'	64.8°C	869-886
pRFP-C-rev6	5'-GGGTAGCGGTCAGCAC-3'	64.4°C	978-963
pRFP-C-for_as7	5'-GGGTGAACTTCCATCCAAC-3'	65.1°C	1030-1049
pRFP-C-rev7	5'-GTCGCTTCTGCCTTCCAG-3'	64.9°C	1139-1122
pRFP-C-for_as8	5'-GAAACCCGCTAAGAACCCTC-3'	62.5°C	1205-1223
pRFP-C-rev8	5'-CAGCCACCTCGTGC-3'	62.2°C	1314-1301
pRFP-C-for8	5'-CATCAACCACACCCAGG-3'	62.4°C	869-885
pRFP-C-for_as9	5'-GACTCAGATCTCGAGCTCAAG-3'	63.6°C	1366-1386
pRFP-C-rev9	5'-CCTCTACAAATGTGGTATGGC-3'	62.9°C	1476-1456
pRFP-C-for_as10	5'-GCAATTGTTGTTGTTAACTTG-3'	59.9°C	1536-1556
pRFP-C-rev10	5'-CCACAACCTAGAATGCAGTG-3'	60.9°C	1645-1627

Table 5.6: Single-stranded DNA fragments replacing the products of the aPCR reactions 2-11 of Table 5.9. Obtained from IDT.

Sequence from 5' to 3'	Bases
GTATTACCGCCATGCATTAGTTATTAATAGTAATCAATTACGGGGTCATTAGTTCATAG	59
CCCATATATGGAGTTCGCGTTACATAACTTACGGTAAATGGCCCCGCTGGCTGACCG	58
AACGCCAATAGGGACTTTCCATTGACGTCAATGGGTGGAGTATTACGGTAAACTGCC	59
ACTTGGCAGTACATCAAGTGTATCATATGCCAAGTACGCCCCCTATTGACGTCAATGAC	59
CCTACTTGGCAGTACATCTACGTATTAGTCATCGCTATTACCATGGTGTATGCGGTTTTG	59
GCAGTACATCAATGGGCGTGGATAGCGGTTTACTCACGGGGATTTCCAAGTC	53
GTCGTAACAACCTCCGCCCCATTGACGCAAATGGGCGGTAGGCGTGTACGGTGG	53
GAGGTCTATATAAGCAGAGCTGGTTTAGTGAACCGTCAGATCCGCTAGCG	50
GAAGCTGTACATGGAGGGCACCGTGAACAACCACCTTCAAGTGCACATCCGAGGG	57
CGAAGGCAAGCCCTACGAGGGCACCCAGACCATGAGAATCAAGGTGGTTCGAGGG	54
CATCAACCACACCCAGGGCATCCCCGACTTCTTTAAGCAGTCCTTCCCTGAGGGCTT	57
CACATGGGAGAGAGTACCACATACGAAGACGGGGGCGTGTGACCGCTACCC	53
GGGTGAACTTCCCATCCAACGGCCCTGTGATGCAGAAGAAAACACTCGGCTGGGAG	56
GCCAACACCGAGATGCTGTACCCCGCTGACGGCGGCCTGGAAGGCAGAAGCGAC	54
GAAACCCGCTAAGAACCTCAAGATGCCCGCGTCTACTATGTGGACCACAGACTG	55
GAAAGAATCAAGGAGGCCGACAAAGAGACCTACGTCGAGCAGCAGGAGGTGGCTG	55
GACTCAGATCTCGAGCTCAAGCTTCGAATTCTGCAGTCGACGGTACCGCGGGCCC	55
GGGATCCACCGGATCTAGATAACTGATCATAATCAGCCATAACCATTTGTAGAGG	56
GCAATTGTTGTTGTTAACTTGTATTGTCAGCTTATAATGGTTACAAATAAAGCAATA	58
GCATCACAATTTTCAAAATAAAGCATTTTTTTCCTGCACTTCTAGTTGTGGTTTGTG	58

5.3 DNA Transformation

Competent DH5 α *E. coli* cells, stored at -80°C, were briefly centrifuged and thawed on ice. For the procedure, two Eppendorf tubes were prepared. The first contained 10 μ L of DH5 α *E. coli* cells (control), while the second contained 5 μ L of the pTagRFP-C plasmid, mixed with 40 μ L of DH5 α *E. coli* cells. The Eppendorf tubes were mixed by patting gently and put on ice for 30 min. The samples were then exposed to heat shock for 45 seconds at 42°C in a water bath and put back on the ice for 2 min. 0.5 mL SOC-medium preheated to 37°C was then added to the samples and put on the shaker for 1 hour at 37°C and 400 rpm. Next, the plasmid-containing mixture was inoculated onto preheated LB-agar-kanamycin plates (30 mg/L kanamycin). Finally, the plates were incubated overnight at 37°C.

5.4 DNA Isolation

For the plasmid isolation, a quantity of transformed *E. coli* cells containing the desired plasmid were spread on a petri dish and left to grow overnight at 37°C. The next day, a single colony was added to a 5 mL LB-medium containing 100 mg/L ampicillin for the

pHAGE-EF1 α L-eGFP-W plasmid or 30 mg/L kanamycin for the pTagRFP-C plasmid and left to grow overnight at 37°C and 300 rpm.

The culture was afterwards centrifuged at 8000 rpm for 8 min, and the supernatant was discarded. The extraction of the DNA was performed by using the GeneJET Plasmid Miniprep Kit (Thermo Scientific) and following the instructions contained in the kit. Finally, the presence of the desired plasmid was confirmed through agarose gel electrophoresis (AGE).

5.5 Agarose Gel Electrophoresis

For the agarose gel, agarose (1g/100mL for 1% agarose gels) was dissolved in a 1xTAE buffer. Next, 30 mL of the mixture, in which 0.5 μ L Ethidium Bromide (EtBr) was added, were poured into a casting tray with the required comb. When stabilized, the gel was set in an electrophoresis tray and covered with 1xTAE buffer. 1 μ L of gel loading dye was mixed in 5 μ L of each sample. 5 μ L of a DNA ladder were added to estimate the DNA size. The gel was afterwards run at a Mini-Sub Cell GT from BioRad, at 90 V, until the samples moved to the desired distance. Finally, the samples were imaged under UV light.

5.5.1 Denaturing Gels

Regarding the AGE for the aPCR reactions, a different protocol should be followed due to the single-stranded nature of the products. A 2% agarose gel was prepared, additionally containing 1 M of urea. Instead of EtBr, 10 μ L of 10,000x PAGE GelRed® from Biotium were utilized. After stabilized, the gel was set in an electrophoresis tray and covered with 1xTAE buffer containing 1 M of urea. 5 μ L of each sample were mixed with 20 μ L of a loading dye. The loading dye was composed of: 0.5 mg/mL bromophenol blue, 8M urea, 1% (v/v) triton, and 1 mM Tris pH 8. The samples were heated for 5 min at 80°C to denature and left on ice for 1 min before loading on the gel. The gel was afterwards run at 70 V for 130 min in the cold room. Finally, the samples were imaged under UV light.

5.5.2 Agarose Gel Electrophoresis for DNA Origami

The last protocol for an agarose gel was made to observe the origami-like structure. The gel contained 2% agarose into a 0.5x TB-buffer (the 1x TB contains 45 mM Boric acid and 45 mM Trizma base). A 50 mL mixture was briefly microwaved and left to cool down. Next, 550 μ L of a 1 M MgCl₂ solution was added, followed by 8 μ L of EtBr. Afterwards, the gel was placed on a 0.5x TB buffer containing 11 mM MgCl₂ and run at 60 V for 4 hours. The buffer was changed after 2 hours to avoid MgCl₂ depletion.

5.6 Polyacrylamide Gel Electrophoresis

Polyacrylamide gel electrophoresis (PAGE) was performed for the observation of the aPCR products. The 10% PAGE gel (12 mL) contained 4 mL 30% acrylamide (29:1), 2.4 mL 5x TBE Buffer, 200 μ L 10% Ammonium Persulfate (APS), 24 μ L TEMED, 10 μ L of 7 M urea, and Mili-Q water. The gel was run in the cold room in a 1xTBE buffer containing 1 M of urea for 90 min at 90V. [72] The samples were denatured either at 80°C for 5 min or at 95°C for 2 min and put immediately on ice for 1 min before loading on the gel. Afterwards, the gel was stained in a 50 μ L staining solution, which contained Mili-Q water and 5 μ L of 10,000x PAGE GelRed®, while being agitated, for 30 min. The gel was visualized under UV light.

5.7 Plasmid Digestion With Restriction Enzymes

The vectors were cut with two restriction enzymes, EcoRI-HF and SmaI for the pHAGE-EF1 α L-eGFP-W plasmid or EcoRI-HF and NdeI for the pTagRFP-C plasmid, to confirm their presence. For this procedure, a 50 μ L mix was created. Each restriction enzyme had an initial concentration of 20,000 units/mL and was supplied from NEB.

The pHAGE-EF1 α L-eGFP-W mix contained 12 μ L of the DNA template (which concentration was 158 μ g/mL, as it was calculated on the Pico200 Picodrop), 2 μ L of each restriction enzyme needed, and 5 μ L of the 10x SmartCut Buffer. The mix was incubated for 1 h at 37°C.

The pTagRFP-C mix contained 4 μ L of the DNA template (which concentration was 445 μ g/mL), 2 μ L of each restriction enzyme needed, and 5 μ L of the 10x SmartCut Buffer. The mix was incubated for 1 h at 37°C. The results were observed through AGE.

5.8 ssDNA Production

For the production of the ssDNA scaffold, as well as the 10 ssDNA fragments, an aPCR protocol was followed.

5.8.1 PCR Reactions

Initially, the templates for the aPCR reactions were produced throughout the PCR reactions seen in Table 5.8. For a better yield of the products, different conditions were tested and the conditions stated in the table are indicative of the most efficient ones. The PCR products needed to be purified in order to remove the primers, the initial template, and the salts from the mixture.

5.8.2 DNA Extraction from Agarose Gel

To obtain the desired DNA fragments, a preparative agarose gel was run, with a 5 μL DNA ladder and a well containing the DNA mixture mixed with 1:6 DNA loading dye, at 90 V for 1 hour. The desired fragment was extracted from the gel with a scalpel, cut into small pieces and left at -20°C for 1 h.

For the extraction of the DNA from the gel, the Ultrafree[®]-DA DNA extraction kit, from Merck Millipore, was used. A small piece of the frozen gel was added to the tube and centrifuged at 5.000 g for 2 min. When the last piece was centrifuged, a final 15 min centrifugation at 5.000 g was performed, and the flow-through was kept.

The TAE buffer of the extracted DNA solution needed to be removed. For that reason, NaAc at a volume of 1/10 of the DNA solution's volume was added, as well as 96% ethanol at 2x the volume of the DNA solution. The mix was centrifuged for 30 min at 4°C and 15000 g. The liquid was discarded quickly, 400 μL of 70% ethanol were added, and the mix was centrifuged for 15 min at 4°C and 15000 g. Ethanol was quickly discarded and left to evaporate. Finally, 30 μL of DNA water were added.

5.8.3 Asymmetric PCR

After the purified templates were obtained, the aPCR reactions were ready to be performed. The primer sequences, ingredients, and protocols of the various aPCR reactions can be seen in Table 5.5, Table 5.7, and Table 5.9. Similar to Table 5.8, the conditions stated for each reaction are indicative of the most efficient ones, and different temperatures and reaction times for each step were tested.

Table 5.7: Mixtures for the PCR and aPCR reactions.

Components of PCR Mix	100 μL PCR Mix	50 μL Asymmetric PCR Mix
dNTPs (20 nmol/ μL)	4x1 μL	2x1 μL
MgCl ₂ (50 mM)	6 μL	3 μL
10x PCR Buffer	10 μL	5 μL
Template DNA	1 μL	3 μL
Primer 1 (100 μM)	1 μL	2 μL
Primer 2 (100 μM)	1 μL	-
Taq Polymerase	0.5 μL	0.5 μL
Molecular Biology Water	76.5 μL	34.5 μL

Table 5.8: PCR reactions. Steps 2-4 are repeated 35 times. When finished, the products remain at 4°C. The temperatures of step 3 and the reaction times of step 4 are indicative of the reaction which performed better. Different temperatures and reaction times were also tested.

No	Primer 1	Primer 2	Step 1	Step 2	Step 3	Step 4	Step 5
1	EF-1alpha forward	EF-1alpha reverse	3 min 94°C	0.5 min 94°C	0.5 min 53/55/57°C	1 min 72°C	7 min 72°C
2	EF-1alpha forward	EF-1alpha assym rev	3 min 94°C	0.5 min 94°C	0.5 min 53/55/57°C	1 min 72°C	7 min 72°C
3	CMV-TagRFP forward	CMV-TagRFP reverse	5 min 94°C	0.5 min 94°C	0.5 min 53°C	2 min 72°C	10 min 72°C
4	pRFP-C-for1	pRFP-C-rev1	5 min 94°C	0.5 min 94°C	0.5 min 52°C	1 min 72°C	7 min 72°C
5	pRFP-C-for2	pRFP-C-rev2	5 min 94°C	0.5 min 94°C	0.5 min 58.2°C	1 min 72°C	7 min 72°C
6	pRFP-C-for3	pRFP-C-rev3	5 min 94°C	0.5 min 94°C	0.5 min 59°C	1 min 72°C	7 min 72°C
7	pRFP-C-for4	pRFP-C-rev4	5 min 94°C	0.5 min 94°C	0.5 min 56.3°C	1 min 72°C	7 min 72°C
8	pRFP-C-for5	pRFP-C-rev5	5 min 94°C	0.5 min 94°C	0.5 min 59.6°C	1 min 72°C	7 min 72°C
9	pRFP-C-for6	pRFP-C-rev6	5 min 94°C	0.5 min 94°C	0.5 min 59.6°C	1 min 72°C	7 min 72°C
10	pRFP-C-for7	pRFP-C-rev7	5 min 94°C	0.5 min 94°C	0.5 min 60°C	1 min 72°C	7 min 72°C
11	pRFP-C-for8	pRFP-C-rev8	5 min 94°C	0.5 min 94°C	0.5 min 57.4°C	1 min 72°C	7 min 72°C
12	pRFP-C-for9	pRFP-C-rev9	5 min 94°C	0.5 min 94°C	0.5 min 60°C	1 min 72°C	7 min 72°C
13	pRFP-C-for10	pRFP-C-rev10	5 min 94°C	0.5 min 94°C	0.5 min 57.9°C	1 min 72°C	7 min 72°C

5.9 DNA Purification

5.9.1 dsDNA Purification

For the purification of the double-stranded DNA (dsDNA) products of the PCR reactions 3-13 of Table 5.8, the ChargeSwitch[®] Pro PCR Cleanup Kit from Thermo Fisher Scientific, or the GenElute[™] PCR Clean-Up Kit from Sigma-Aldrich, was used. For the procedure, 200 µL (or 100 µL for the GenElute[™] PCR Clean-Up Kit) of the PCR products were used, and the instructions of the kit were followed. The final product had a volume of 50 µL.

Table 5.9: Asymmetric PCR reactions. Steps 2-4 are repeated 75 times. When finished, the products remain at 4°C. The temperatures of step 3 and reaction times of step 4 are indicative of the reaction which performed better. Different temperatures, numbers of cycles and reaction times were also tested.

No	Primer 1	Step 1	Step 2	Step 3	Step 4	Step 5
1	CMV-TagRFP rev asym	5 min 94°C	0.5 min 94°C	0.5 min 54°C	2 min 72°C	10 min 72°C
2	pRFP-C-for_as1	5 min 94°C	0.5 min 94°C	0.5 min 51°C	2 min 72°C	10 min 72°C
3	pRFP-C-for_as2	5 min 94°C	0.5 min 94°C	0.5 min 57.7°C	2 min 72°C	10 min 72°C
4	pRFP-C-for_as3	5 min 94°C	0.5 min 94°C	0.5 min 52°C	2 min 72°C	10 min 72°C
5	pRFP-C-for_as4	5 min 94°C	0.5 min 94°C	0.5 min 54.5°C	2 min 72°C	10 min 72°C
6	pRFP-C-for_as5	5 min 94°C	0.5 min 94°C	0.5 min 59.4°C	2 min 72°C	10 min 72°C
7	pRFP-C-for_as6	5 min 94°C	0.5 min 94°C	0.5 min 59.8°C	2 min 72°C	10 min 72°C
8	pRFP-C-for_as7	5 min 94°C	0.5 min 94°C	0.5 min 59.1°C	2 min 72°C	10 min 72°C
9	pRFP-C-for_as8	5 min 94°C	0.5 min 94°C	0.5 min 56.8°C	2 min 72°C	10 min 72°C
10	pRFP-C-for_as9	5 min 94°C	0.5 min 94°C	0.5 min 60°C	2 min 72°C	10 min 72°C
11	pRFP-C-for_as10	5 min 94°C	0.5 min 94°C	0.5 min 57.9°C	2 min 72°C	10 min 72°C

5.9.2 ssDNA Purification

For the purification of the ssDNA products of the aPCR reactions in Table 5.9, the Monarch® PCR & DNA Cleanup Kit, the QIAEX II Gel extraction kit, and the Duplex-specific nuclease (DSN), from Evrogen, were utilized in three different procedures.

In the first procedure, which was performed for the product of aPCR reaction 1, which contained the scaffold ssDNA for the origami-like structure, the product was first purified through the DNA Cleanup and Concentration protocol. A 100 μ L sample was added initially, and the purified product had a volume of 12 μ L. This resulted in a mixture only containing the dsDNA scaffold of the reaction and the ssDNA product. In order to remove the dsDNA, the mixture was digested with DSN, which only digests dsDNA, and finally, the product was re-purified with the DNA Cleanup and Concentration protocol.

A second protocol for the scaffold ssDNA was performed. The ssDNA was extracted

from a low-melting agarose gel through the QIAEX II gel extraction kit. The product of the extraction was afterwards purified through the DNA Cleanup and Concentration protocol to up-concentrate the ssDNA and remove any remaining agarose.

Finally, for aPCR reactions 2-11, the Oligonucleotide Cleanup Protocol was followed. A 50 μL sample was added initially, and the purified product had a volume of 12 μL . The product was afterwards either stored or digested with the DSN and re-purified to remove the scaffold of the aPCR reaction.

5.10 DNA Origami-like Structure Formation

Two different protocols were used for the synthesis of the desired origami-like structure. The reaction steps for the two protocols used can be seen in table Table 5.10. The scaffold used was either the purified product of the aPCR reaction 1 of Table 5.9, which concentration was calculated through the Picodrop Pico 200 or the unpurified aPCR product.

Table 5.10: Conditions of the annealing protocols utilized for the synthesis of the origami structure.

Protocol 1			Protocol 2		
Cycles Number	Temperature	Time	Cycles Number	Temperature	Time
1	65°C	10 min	1	80°C	5 min
21	60-40°C	1 h	14	79-66°C	1 min
1	4°C	-	36	65-30°C	10 min
			1	4°C	-

The mixture had a final volume of 40 μL , and its components varied depending on the different experiments. The Tilbit folding buffer used was kept at 1x. The staples of Table 5.4 had a final concentration of 200 nM each. The ssDNA fragments of Table 5.6 had a final concentration of 200 nM each. The scaffold varied from 5 μL to 15 μL for the unpurified aPCR product, while the purified product had a final concentration of 20 nM. The MgCl_2 concentration varied from 5 mM to 20 mM, while in some experiments it was replaced with spermine, which concentration was either 100 μM , 200 μM or 500 μM .

5.11 DNA Origami Dialysis

After the annealing procedure of the DNA origami-like structure, the excess staples and ssDNA fragments needed to be discarded. For that purpose, a Biotech CE 100 kD dialysis tubing was filled with 40 μL of the origami mixture, combined with 80 μL of 0.5x TB buffer, which contained the same concentration of MgCl_2 or spermine

as the origami mixture. The tubing was sealed and put perpendicularly to the flow of electricity into a Mini-Sub Cell GT from BioRad, which contained the same buffer added to the tubing. Next, it was run in the cold room at 65 V for 10 min, reversed and ran for 2 more minutes. Finally, the solution was stored at 4°C.

5.12 Atomic Force Microscopy

For the confirmation of the presence of the intended DNA origami-like structure, Nanoscope IIIA (Bruker Inc) was used, with the assistance of the SPMLab Phoenix controller and software (SPM Labs LLC) and Gwyddion [73]. AFM, a scanning probe microscopy technique, offers the topography of a sample at the nanoscale level [74]. Since the desired structure has dimensions of approximately 50 nm x 20 nm x 15 nm, it can be observed through AFM.

To observe the samples, 10 µL were pipetted on a mica substrate, incubated for 10 min, rinsed with water, and finally blow-dried with N₂. In the case where the samples were highly concentrated, they needed to be diluted in their running buffer.

5.13 Poly-L-Lysine

To increase the transfection efficiency of the plasmid and the DNA origami-like structure, the molecules were mixed with positively charged PLL. In a protocol performed by Daniel Joubert et al. [75], PLL molecules, which molecular weight varied from 9-40 kD, were used. A mixture contained DNA and PLL at 2x the mass of DNA, was left for 30 min at room temperature, and was afterwards implemented in HeLa cell cultures. Additionally, for further transcription efficiency, 10⁻⁴ M of chloroquine were added to the mixture. In the experiments which followed in this thesis, PLL of molecular weight between 75-150 kD was used, while no chloroquine was added.

5.14 HeLa Cell Cultures

For the transfection testing of the DNA origami-like structure, a culture containing HeLa cells was utilized. The cells were cultured in DMEM medium supplemented with 10% fetal calf serum and 1% penicillin/streptomycin. After trypsinization, the cells were cultured in 96-well plates (Corning Costar) at a density of 6000 cells/cm² and left to grow for 1-2 days. Next, the medium was replaced, and the new medium was mixed with the transfecting molecules at a final volume of 200 µL and was incubated in a 5% CO₂ incubator at 37°C.

After 24 h or 48 h incubation, the transfection efficiency was tested on Perkin Elmer's Enspire Microplate Reader and an AxioObserver Z1 microscope from Carl Zeiss through the assistance of the ZEN blue software. The excitation and emission used were 555 nm and 584 nm, respectively.

5.15 Cholesterol Annealing

A cholesterol annealing procedure was followed, and its results were tested on AFM. A cholesterol molecule conjugated on the 3' end of an oligomer, received from IDT, was used. Its final structure was: 5'-CACAAACACAAAAA-3'CholTEG-3'. DNA origami mixtures, obtained from different protocols were mixed with cholesterol, which had a final concentration of 1 μ M, at a final volume of 20 μ L. The mixtures were heated at 95°C and cooled down to 10°C, with -1°C/min steps. Finally, the mixtures were stored at 4°C.

6 Simulations

During the DNA origami-like structure's simulations, different programs were used to assist in the design of the staples and check the molecule's stability. Initially, the staples were designed through the assistance of caDNAno2, the desired structure was formed in Maya 2019, which contained the vHelix plugin, and finally, the simulation code of oxDNA was applied to review the molecule's stability. The results were observed through oxView, an online site which can project topology and configuration files containing DNA structures. The simulations following include only the pTagRFP-C vector as a template since the pHAGE-EF1 α L-eGFP-W plasmid was not correctly sequenced, as will be later discussed.

6.1 CaDNAno2

caDNAno2 is a free and open-source program which simplifies the design of the staples for a DNA origami structure [76]. In this project, a honeycomb structure was formed by ten long parts. The number of staples was reduced compared to common origami structures. Therefore, only the ends of the structure were introduced in caDNAno2. The AutoStaple plugin offered probable staples, and manual changes were introduced.

6.1.1 Design of Primers and Staples

As a first step for the simulation, the design of the primers which were going to be used needed to take place. These primers are essential for the production of the DNA origami-like structure's scaffold, as well as the ten double-stranded parts that need to be present in the molecule. For that reason, the primers seen in Table 5.5 were designed. The first three primers were used to produce the single-stranded, 1677 nucleotide-long scaffold of the structure. The rest of the primers were utilized for the production of single-stranded sequences which would bind to the scaffold, in a way that will be further analyzed. In Table 6.1, the regions of the promoter where the staples are bound, if the aforementioned single-stranded sequences are used, are underlined.

Table 6.1: Sequence of the CMV_{IE} enhancer-containing promoter. Enhancer sequence: 1-465. Promoter sequence: 466-589. **Orange sequence:** Nf1-t binding site. **Light blue sequence:** SRE binding site. **Grey sequence:** 21-nt binding site (the grey highlighted text refers to the SP-1 binding site only). **Green sequence:** 19-nt binding site. **Blue sequence:** 18-nt binding site. **Brown sequence:** AP-1 binding site. **Red sequence:** TATA box. **Purple sequence:** CRS/Inr binding site. Underlined sequence: The part of the sequence where the staples are bound.

1	TAG TTA TTA ATA GTA ATC AAT TAC GGG GTC	30
31	ATT AGT TCA TAG CCC ATA TAT GGA GTT CCG	60
61	CGT TAC ATA ACT TAC GGT AAA TGG CCC GCC	90
91	TGG CTG ACC GCC CAA CGA CCC CCG CCC ATT	120
121	GAC GTC AAT AAT GAC GTA TGT TCC CAT AGT	150
151	AAC GCC AAT AGG GAC TTT CCA TTG ACG TCA	180
181	ATG GGT GGA GTA TTT ACG GTA AAC TGC CCA	210
211	CTT GGC AGT ACA TCA AGT GTA TCA TAT GCC	240
241	AAG TAC GCC CCC TAT TGA CGT CAA TGA CCG	270
271	TAA ATG GCC CGC CTG GCA TTA TGC CCA GTA	300
301	CAT GAC CTT ATG GGA CTT TCC TAC TTG GCA	330
331	GTA CAT CTA CGT ATT AGT CAT CGC TAT TAC	360
361	CAT GGT GAT GCG GTT TTG GCA GTA CAT CAA	390
391	TGG GCG TGG ATA GCG GTT TGA CTC ACG GGG	420
421	ATT TCC AAG TCT CCA CCC CAT TGA CGT CAA	450
451	TGG GAG TTT GTT TTG GCA CCA AAA TCA ACG	480
481	GGA CTT TCC AAA ATG TCG TAA CAA CTC CGC	510
511	CCC ATT GAC GCA AAT GGG CGG TAG GCG TGT	540
541	ACG GTG GGA GGT CTA TAT AAG CAG AGC TGG	570
571	TTT AGT GAA CCG TCA GAT CCG	591

In caDNA_{no2}, a honeycomb structure with ten straight strands was used as a template, in a form which can be observed in Figure 6.1. The staples, after a manual cutting and several modifications, for them to have the desired length, and eliminate the dimer and loop formations, can be seen in Figure 6.2. The bottom line refers to the number zero of Figure 6.1, the line above to number one, etc. Additionally, to further avoid dimer formations between the staples and make the introduction of a cholesterol-modified oligonucleotide possible, 5'-GTGTTGTG-3' sequences and a 5'-GTGTTGTT-3' were introduced either on the 3' or the 5' ends of the staples. Finally, in two of the staples, a sequence which contained three binding sites for the transcription factor Nf- κ B was added, and a complementary staple would make this sequence double-stranded. The sequences of the staples can be seen in Table 5.4.

6.2 Maya 2019

Maya 2019 is a 3D visual effects software to which the vHelix plugin can be added. vHelix was developed by the Högberg Research Group at Karolinska Institutet and offers various tools for the design of a DNA origami structure. [77]

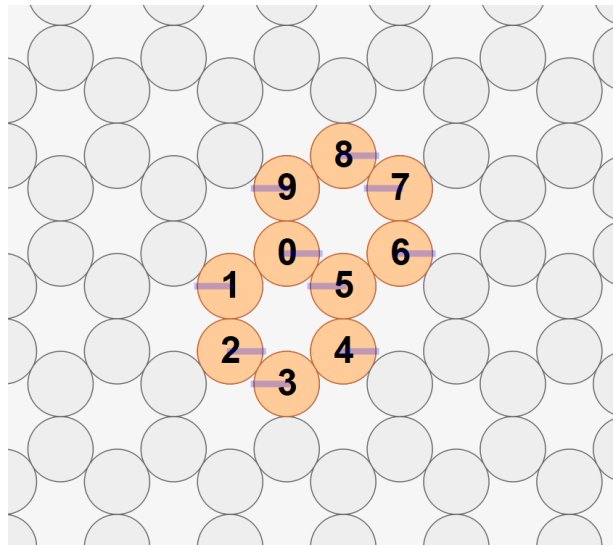


Figure 6.1: Initial design of the honeycomb structure for the origami-like molecule in caDNA2.

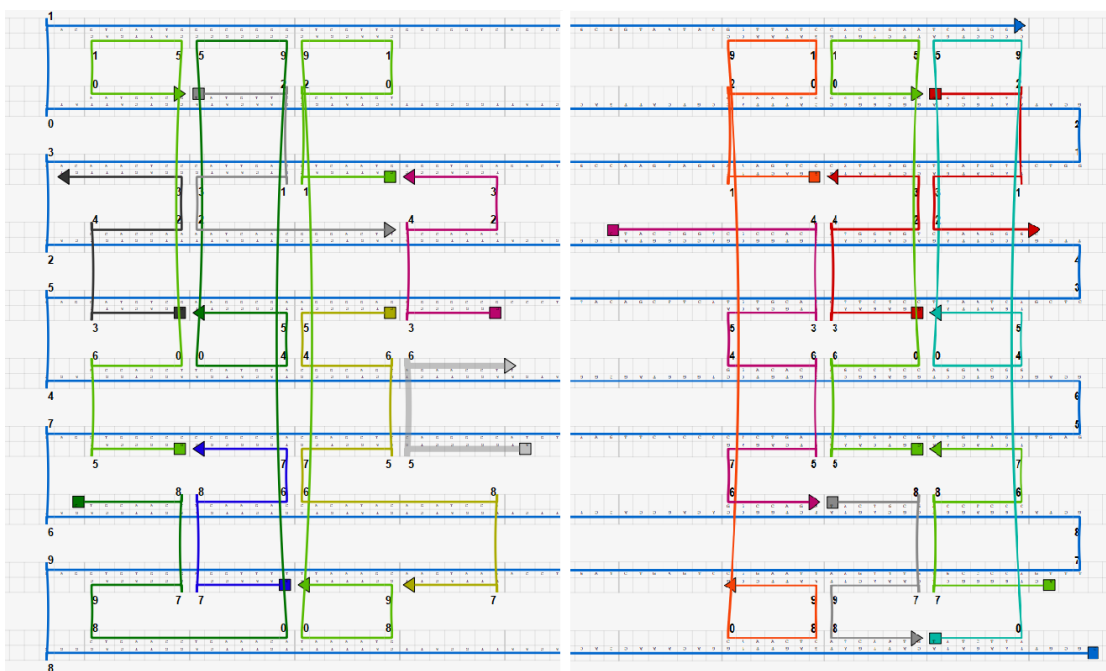
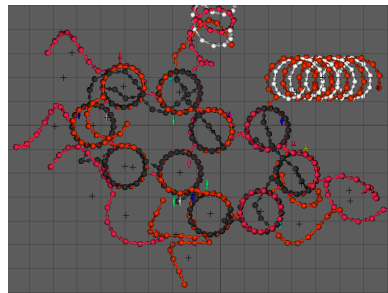


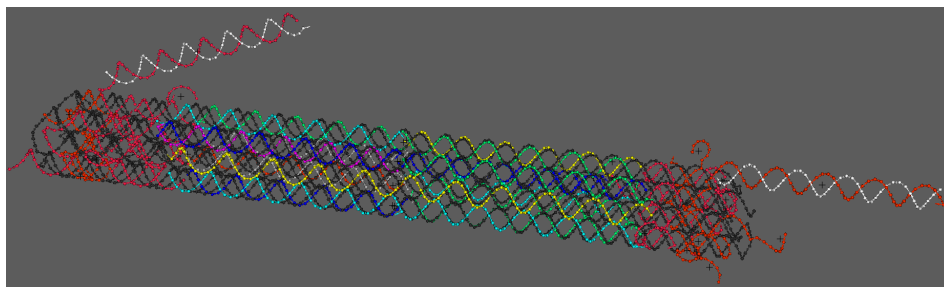
Figure 6.2: Staples designed on caDNA2 with a 1677 nt part of the pTagRFP-C vector as a template. The direction of the arrows is 5' to 3'. In the figure, only the ends of the origami structure are present, since the middle part will contain complementary single-stranded sequences, and no staples were designed for that part.

6.2.1 Design of the DNA Origami-like Structure

Using the caDNAno2 design as a map, a honeycomb cylinder was manually structured, as can be seen in Figure 6.3, where each strand had 168 nt length, except the first (164 nt) and the last strand (169 nt). Every strand was connected to the other, finally forming a long strand, where the sequence of the pTagRFP-C vector's part that was intended to be amplified was introduced. Next, the staples, which were designed previously, were manually introduced into the structure, finally providing the desired structure, as can be seen in Figure 6.3b. In this figure, the black strand is the 1677 bp DNA sequence which will be obtained through aPCR with the pTagRFP-C vector as the initial template. The multi-coloured strands are the sequences which were intended to be obtained through aPCR to reduce the number of staples needed for this structure. As will be seen later, the aPCR for these fragments was not efficient, and therefore the fragments were ordered. The red strands at the ends of the structure are the staples, and the two extended sequences containing a white strand are binding sites for the transcription factor Nf- κ B. Afterwards, the structure was saved as a topology and a configuration file. These files were used for a molecular dynamics simulation through oxDNA.



(a)



(b)

Figure 6.3: Design of the DNA origami-like structure by using a part of the pTagRFP-C vector as a scaffold, designed in Maya 2019. The black strand is the 1677 nt sequence. The multi-coloured strands, located in the middle of the structure, are the sequences which were intended to be obtained through asymmetric PCR. The red strands at the ends of the structure are the staples. The white strands are used to make the two extended staples double-stranded, for the transcription factor Nf- κ B to bind.

6.3 oxDNA

oxDNA was introduced by T. E. Ouldridge, J. P. K. Doye, and A. A. Louis and has been developed by researchers in the groups of Doye and Louis at the University of Oxford. It is a coarse-grained (CG) model which is used to implement the DNA model, where interactions are parametrized to be similar to real-life conditions. [78], [79]. The idea of this model is to treat DNA as a string of rigid nucleotides, which position and orientation affect the way they interact with one another [80].

Some simplifications have been made in the original model. First, the complementary base pairs and stacking partners interact with the same strength, while there is no attractive interaction between non-complementary bases. Also, the electrostatic interactions take place only in the short-ranged excluded volume. There is no differentiation between the major and the minor grooves, and the salt concentration cannot be modified. [80]

In this project, a newer version of oxDNA, oxDNA2, was used. In oxDNA2, different widths of the major and minor grooves are introduced, making the simulation more precise, while there is also a differentiation between AA and TT stacking strengths. Additionally, the Debye-Hückel model is included, making possible the modification of the salt concentration and offering the ability to simulate the structure in physiological conditions. Unfortunately, $MgCl_2$ cannot be used, which is usually the ion for DNA origami structures, but only NaCl. [81] The total potential energy of the oxDNA model is the sum of the potential energies occurring between the nearest neighbours (nn) and between other pairs:

$$V = \sum_{nn} (V_{backbone} + V_{stack} + V'_{exc}) + \sum_{otherpairs} (V_{HB} + V_{cross-stacking} + V_{exc} + V_{c-stack}) \quad (6.1)$$

$V_{backbone}$ refers to the covalent bond between each nucleotide of the backbone and has the form of a finitely extensive nonlinear elastic spring, which equilibrium distance equals 6.4 Å. (V_{stack}) represents the nn stacking and uses a smoothly cut-off Morse potential with a minimum at 3.4 Å. (V'_{exc} and V_{exc} are the excluded volumes for nn and next-nearest neighbours, respectively. The hydrogen bonding potential (V_{HB}) also uses a smoothly cut-off Morse potential for hydrogen bond interactions between base pairs. $V_{cross-stacking}$ and $V_{c-stack}$ correspond to cross-stacking between base-pair steps in a duplex and coaxial stacking, respectively. They provide stabilization for the duplex. These interactions can also be seen in Figure 6.4. [79], [82], [83]

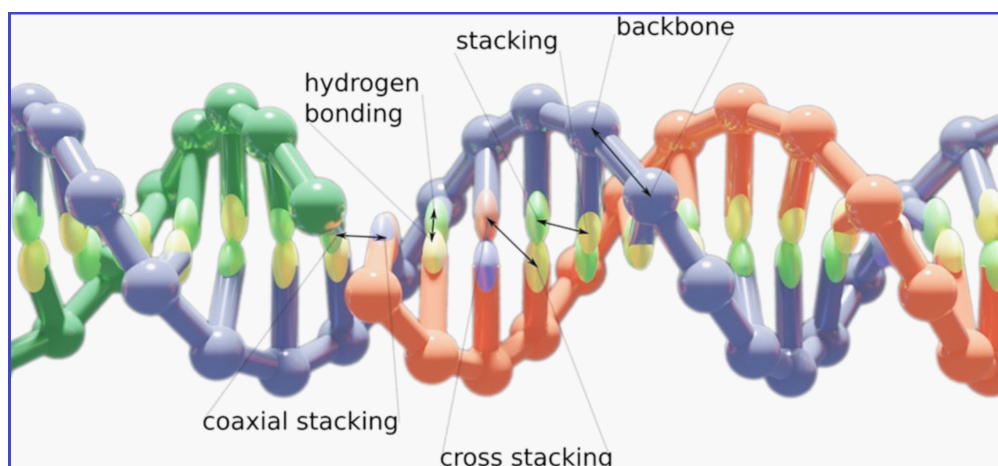


Figure 6.4: Interactions taken into consideration from the oxDNA2 CG model. Obtained from [79].

Three steps were performed for the simulation of the DNA origami-like structure: a minimization step, a relaxation step, and a final molecular dynamics simulation. The first two steps were performed to eliminate nucleotides whose excluded volumes overlap one another, or to avoid too long backbone bonds, while the final simulation was run for 500 ns to evaluate the stability of the structure over time. If the first two simulations were excluded, there was a big chance for the molecular dynamics simulation to fail. [81] The codes used for each step can be seen in Appendix A, while the shape of the final structure after the MD simulation, obtained from oxView, can be seen in Figure 6.5.

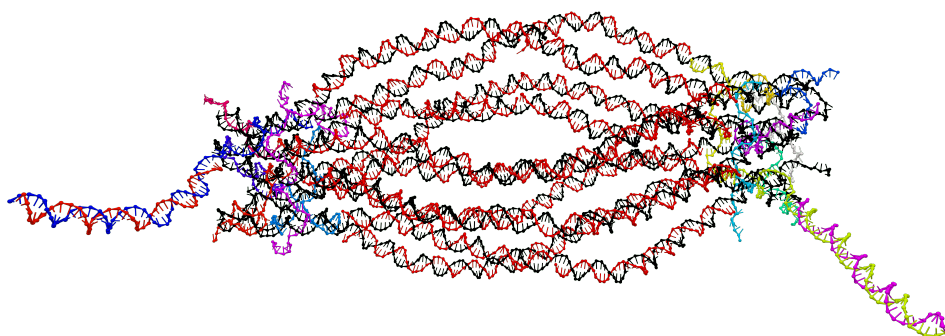


Figure 6.5: The DNA origami-like structure obtained after an MD simulation. The figure is a snapshot from the online program oxView, taken at the end of the oxDNA simulation.

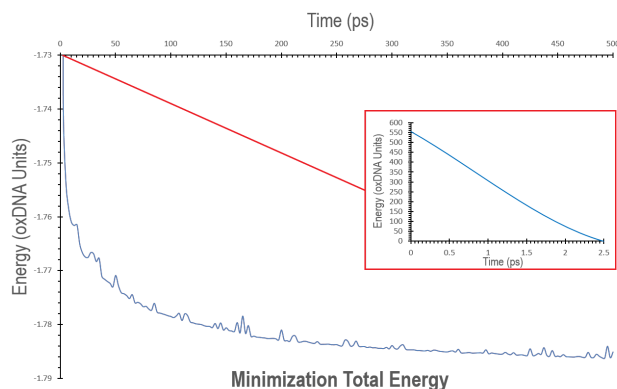


Figure 6.6: Total energy over the simulation time during the minimization step of the DNA origami-like structure.

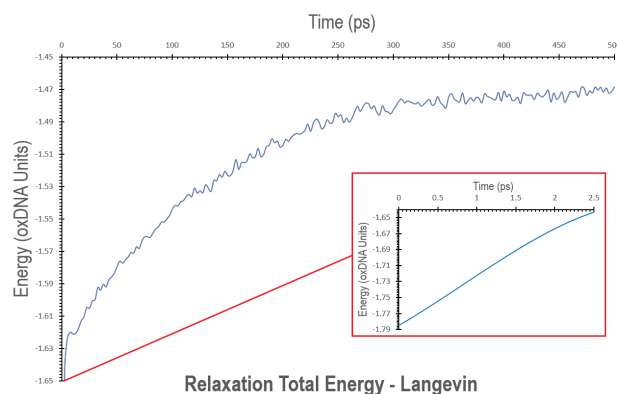


Figure 6.7: Total energy over the simulation time occurred on a relaxation simulation for the DNA origami-like structure, by using the Langevin thermostat.

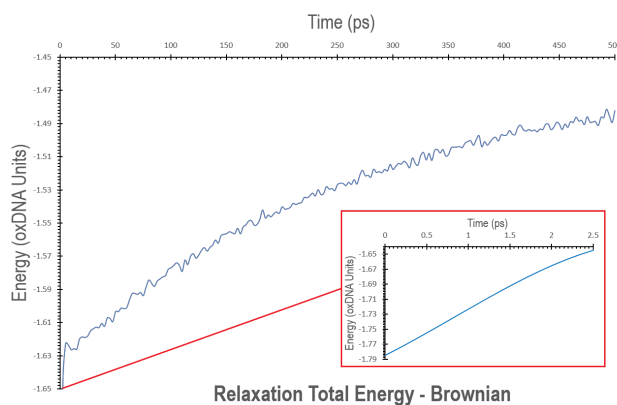


Figure 6.8: Total energy over the simulation time occurred on a relaxation simulation for the DNA origami-like structure, by using the Brownian thermostat.

From the aforementioned simulations, different data were obtained. The total energy change over time for the minimization can be seen in Figure 6.6. Figure 6.7 and Figure 6.8 show the total energy change over time for the relaxation step while using a Langevin or a Brownian thermostat, respectively.

Regarding the final simulation, two different types of graphs were obtained. The total energy variation over a simulation time of 500 ns, while using a Langevin or a Brownian thermostat, respectively, can be observed in Figure 6.9 and Figure 6.10, respectively. The dimensions' variations over a simulation time of 500 ns, while using a Langevin or a Brownian thermostat, can be observed in Figure 6.11 and Figure 6.12 respectively.

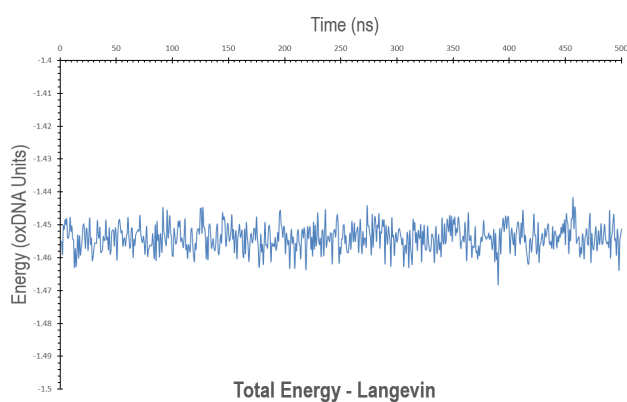


Figure 6.9: Total energy over 500 ns simulation time for the DNA origami-like structure, by using a Langevin thermostat.

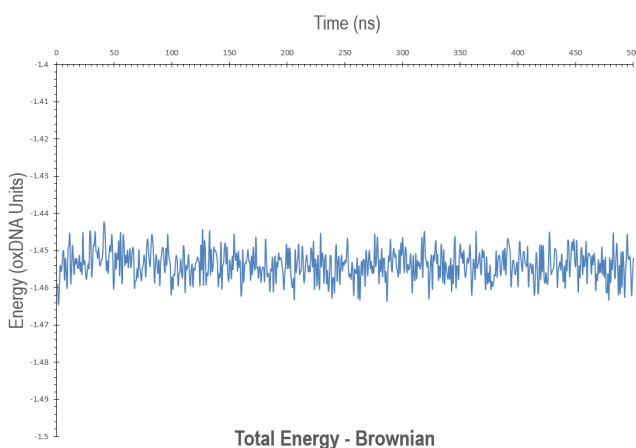


Figure 6.10: Total energy over 500 ns simulation time for the DNA origami-like structure, by using a Brownian thermostat.

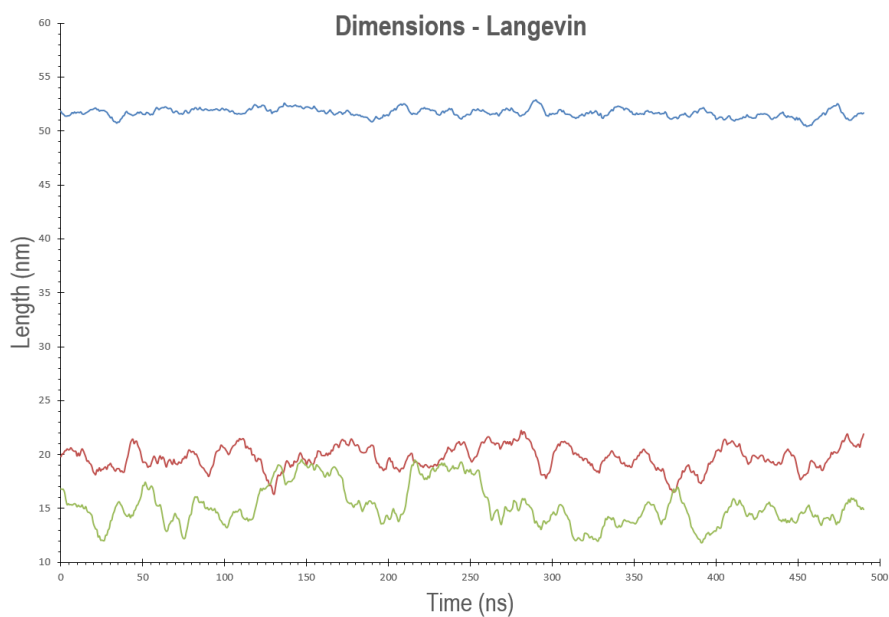


Figure 6.11: Dimensions' variations over 500 ns simulation time occurred for the DNA origami-like structure, by using a Langevin thermostat. The blue line refers to the length of the molecule, the orange line to its height, and the green line to its width.

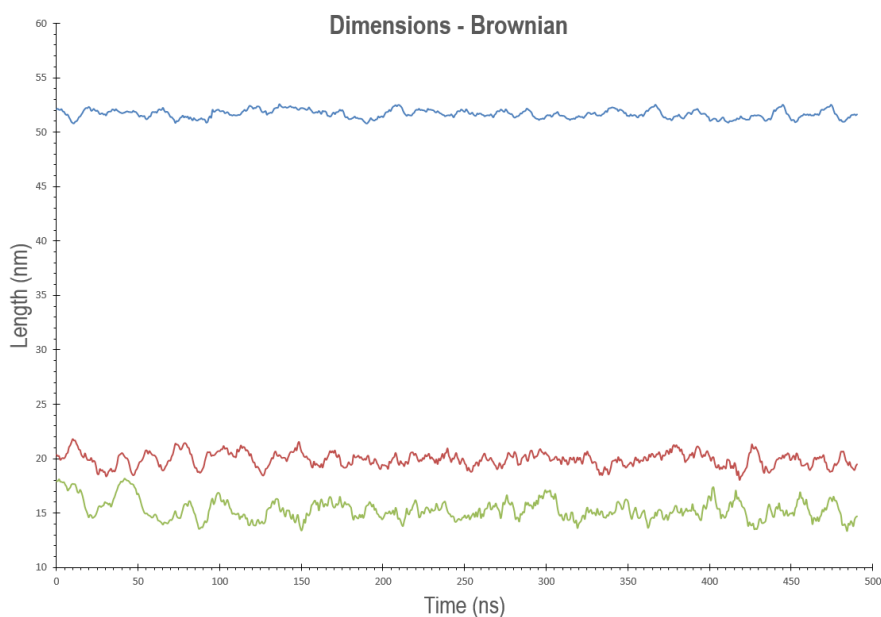


Figure 6.12: Dimensions' variations over 500 ns simulation time occurred for the DNA origami-like structure, by using a Brownian thermostat, The blue line refers to the length of the molecule, the orange line to its height, and the green line to its width.

7 Results

7.1 Testing of the pHAGE-EF1 α L-eGFP-W Plasmid

At a first attempt, the pHAGE-EF1 α L-eGFP-W plasmid was chosen as a basis for the design of a DNA origami-like structure, which was going to be inserted in mammalian cells' nuclei and express the green fluorescent protein eGFP. For that purpose, the plasmid needed to be isolated for further PCR reactions that would produce the scaffold of the DNA origami and the single-stranded sequences.

7.1.1 DNA Isolation and Digestion of the Plasmid

After overnight growth of transformed *E. coli* cells, the pHAGE-EF1 α L-eGFP-W plasmid was isolated as described in section 5.4. To verify the presence of the desired plasmid, agarose gel electrophoresis was performed, and the results can be seen in Figure 7.1.

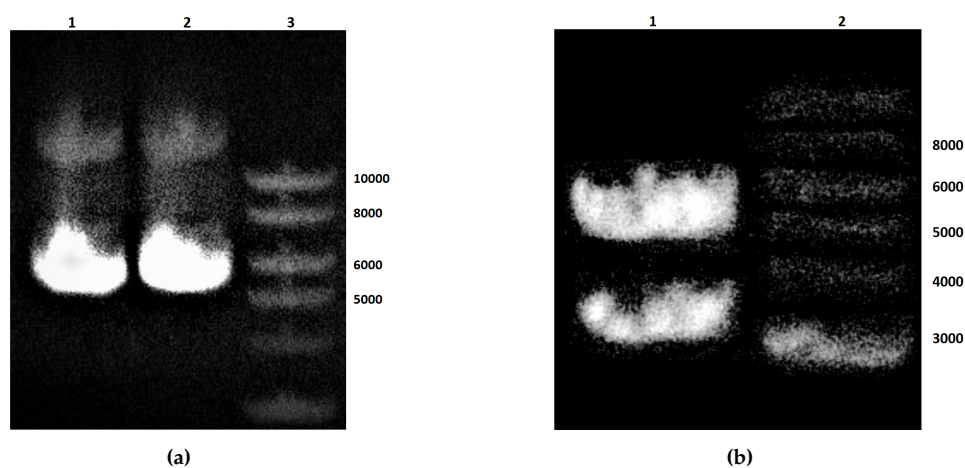


Figure 7.1: AGE of the pHAGE-EF1 α L-eGFP-W plasmid. (a) AGE after DNA isolation. Lanes 1 and 2 contain the DNA isolated from *E. coli* cells which were transformed with the pHAGE-EF1 α L-eGFP-W plasmid. Lane 3 contains the 1 kb DNA ladder. (b) AGE of the isolated plasmid, after it was digested with the EcoRI and SmaI restriction enzymes. The right band contains the 1 kb DNA ladder, while the left band contains the digested plasmid.

Three different columns can be observed. The first two columns contain the isolated plasmid, which originated from two overnight cultures. In the two cultures, the same transformed *E. coli* cells were added, and, therefore, the columns look identical, as expected. Two bands are visible, a pale band at 10 kb and a very intense band at 6 kb.

The comparison of the plasmid with the DNA ladder is not precise because the two bands contain nicked DNA and supercoiled plasmid DNA, and further verification needed to be conducted. For that reason, digestion of the plasmid with two restriction enzymes, EcoRI and SmaI, to produce linear fragments was performed. As can be seen in Figure 7.1b, two bands appeared after the digestion, a 3.1 kb band and a 4.7 kb band. Finally, the 3.1 kb band was extracted from a preparative gel to be further used as a template for PCR reactions.

7.1.2 Attempt of Production of the Single-Stranded Scaffold

Since the presence of the plasmid was confirmed, DNA could be used as a template for the production of the desired sequences. For this reason, the PCR reactions 1 and 2 in Table 5.8 took place with two different templates, either the whole pHAGE-EF1 α L-eGFP-W plasmid or the 3.1 kb sequence. Unfortunately, after various attempts in different annealing temperatures and different volumes (50 μ L or 100 μ L total volume), no results appeared on the agarose gel after electrophoresis.

The plasmid was sent for sequencing to identify the positions at which the initial sequencing suggested on the Addgene site was wrong [71]. Specific primer sequences were suggested and sent along with the plasmid at Eurofins Scientific. Unfortunately, no sequencing results were received.

7.2 DNA Origami-like Structure with the pTagRFP-C Vector

Since the pHAGE-EF1 α L-eGFP-W plasmid was not capable to be used as a template for the desired DNA origami-like structure, a different vector needed to be found. For the experiments followed, the pTagRFP-C vector was used as a template.

7.2.1 DNA Transformation, Isolation and Digestion of the Vector

As a first step of the lab procedure for the production of the DNA origami-like structure, competent DH5 α *E. coli* cells were transformed with the pTagRFP-C vectors. To check the efficiency of the transformation, non-transformed and transformed DH5 α *E. coli* cells were spread on LB-agar-kanamycin plates.

For further identification of the vector, single colonies were grown in an LB-kanamycin medium overnight, and their DNA was isolated. The product was initially run in AGE, as can be seen in Figure 7.2a. For verification of the vector's presence, the plasmid was digested with two restriction enzymes, EcoRI-HF and NdeI. The expected fragment sizes, 1.1 kb and 3.6 kb, can be seen in Figure 7.2b.

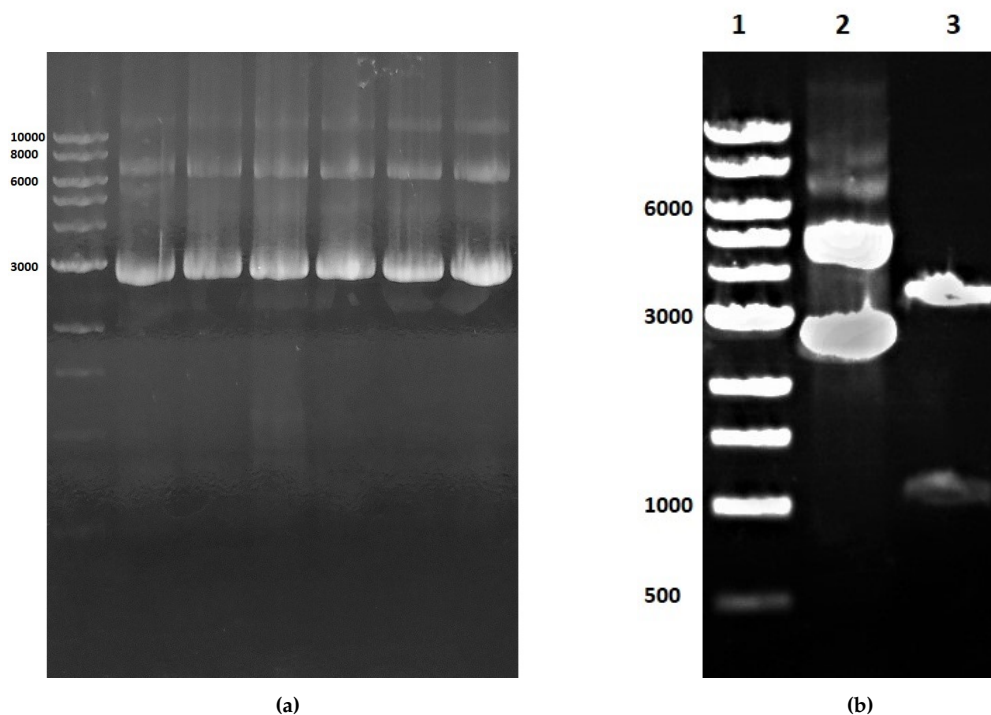


Figure 7.2: Agarose gel electrophoresis of the pTagRFP-C vector. (a) AGE after DNA isolation. The first lane contains the 1 kb DNA ladder. The rest of the lanes contain the DNA isolated from *E. coli* cells which were transformed with the pTagRFP-C plasmid. (b) AGE of the isolated plasmid, after it was digested with the EcoRI-HF and NdeI restriction enzymes. Lane 1 contains the 1 kb DNA ladder. Lane 2 contains the uncut plasmid. Lane 3 contains the digested plasmid.

7.2.2 Production and Purification of ssDNA Fragments

For the production of the DNA origami structure's single-stranded scaffold and the 10 single-stranded fragments, 11 PCR reactions were performed, which can be seen in Table 5.8, numbers 3-13. After purification with the ChargeSwitch®Pro PCR Cleanup Kit, the samples were run in AGE with the 1kb DNA ladder, as can be seen in Figure 7.3. The expected sizes of the fragments, from reaction 3 to 13, are 1915 bp, 347 bp, 518 bp, 377 bp, 437 bp, 448 bp, 621 bp, 782 bp, 446 bp, 608 bp, and 441 bp, respectively. As can be seen, the bands match the expected sizes.

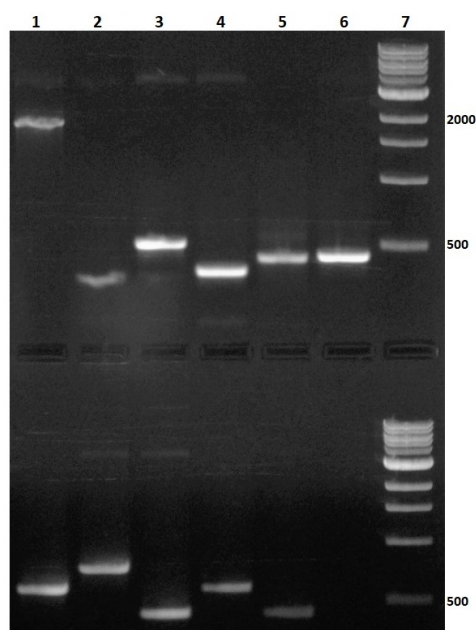


Figure 7.3: AGE for the products of the PCR reactions 3-13 of Table 5.8, after purification. The upper part of the gel contains the PCR reactions 3-8 (lanes 1-6) and the lower part the PCR reactions 9-13 (lanes 1-5). Lane 7 contains 1 kb DNA ladders.

Next, the aforementioned products were used as a template for aPCR reactions. Various aPCR reactions were performed, in different annealing temperatures, reaction times of the extension step, numbers of cycles, and amounts of template and primers. The conditions that appear to have the best product can be seen in Table 5.9.

To observe the ssDNA products and avoid loop formations and different conformations which could occur, the samples were run in a 2% agarose gel containing 1 M of urea, submerged in 1xTAE buffer also containing 1 M urea. In Figure 7.4 the results can be observed. In Figure 7.4a, Lanes 2 and 3 contained the asymmetric PCR products from reactions 3 and 8, respectively, after they were purified with the Monarch® PCR & DNA Cleanup Kit, reacted with the Duplex-specific nuclease (DSN) and re-purified with the Monarch® PCR & DNA Cleanup Kit. Lanes 4 and 5 contained asymmetric PCR reaction 1. Lanes 6 and 7 contained the aPCR reaction 4 at annealing temperatures of 57.5°C and 58.4°C, respectively. Lane 8 contained the asymmetric PCR product of reaction 7 at an annealing temperature of 59.1°C. A band at a size smaller than 100 bp appeared in each one of the lanes, but it could not be distinguished if these are the primers of each reaction or the desired product. Therefore, a second agarose gel, seen in Figure 7.4b, contained in lane 8 the pRFP-C-for_as10 primer. Additionally, lanes 2-7 were heated up at different temperatures and heating times to further avoid different conformations that would occur.

Even though the bands which appeared on each lane seemed to fit the primer's size, the size sensitivity of the agarose gel was not enough to make a distinction. Therefore, a 10% PAGE, containing 7 M of urea was run in a 1xTBE buffer at 90V for 90 min in the cold room. It was confirmed that these bands were indeed in the size of the primer, but the quality of the gel was not sufficient to be added to the results.

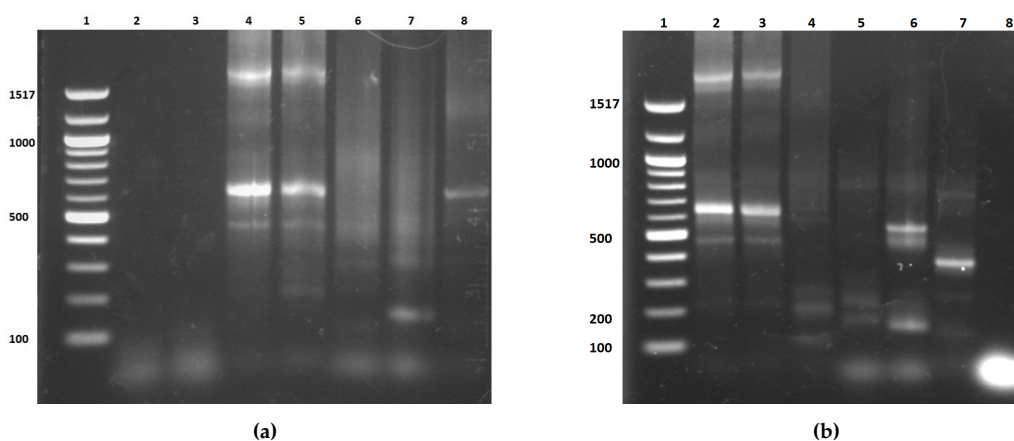


Figure 7.4: 2% AGE containing 1 M urea, run in 1xTAE buffer containing 1 M urea. (a): Lane 1: 100 bp DNA ladder. Lane 2: purified aPCR reaction 3. Lane 3: purified aPCR reaction 8. Lanes 4, 5: aPCR reaction 1, Lanes 6, 7: aPCR reaction 4. Lane 8: aPCR reaction 7. **(b):** Lane 1: 100 bp DNA ladder. Lane 2: aPCR reaction 1, after 5 min denaturation at 80°C. Lane 3: aPCR reaction 1. Lane 4: aPCR reaction 7 with annealing temperatures of 59.9°C. Lanes 5, 6: aPCR reaction 10 with annealing temperatures of 57.5°C and 59.1°C, respectively. Lane 7: aPCR reaction 11. Lane 8: pRFP-C-for_as10 primer. The samples on lanes 3-8 of **(b)** were denatured at 70°C for 10 min. All the reactions refer to Table 5.9.

Since the presence of the correct ssDNA fragments could not be confirmed, it was decided for these fragments to be purchased from IDT. Each fragment was purchased in two parts of 55 bases. Consequently, only the scaffold of the DNA origami-like structure was produced through aPCR.

To further purify the final ssDNA product, several steps were performed. First, the dsDNA product of reaction 3 of Table 5.8 was extracted from a 1% agarose gel through the Ultrafree®-DA DNA Extraction Kit to remove primers, salts, and the initial template. Next, the aPCR reaction took place, and its product was extracted from a 1% low-melting agarose gel with the QIAEX II Gel Extraction Kit. In Figure 7.5, the initial plasmid and the products of the aforementioned reactions can be observed. In lanes 4 and 6, the smear existing in lanes 3 and 5, respectively, disappears, while in lane 6, only the band extracted from the asymmetric PCR product seen in lane 5 can be observed. The size of this band appears at a 500 bp size, but this does not correspond to its actual size, due to the single-stranded nature of the molecule.

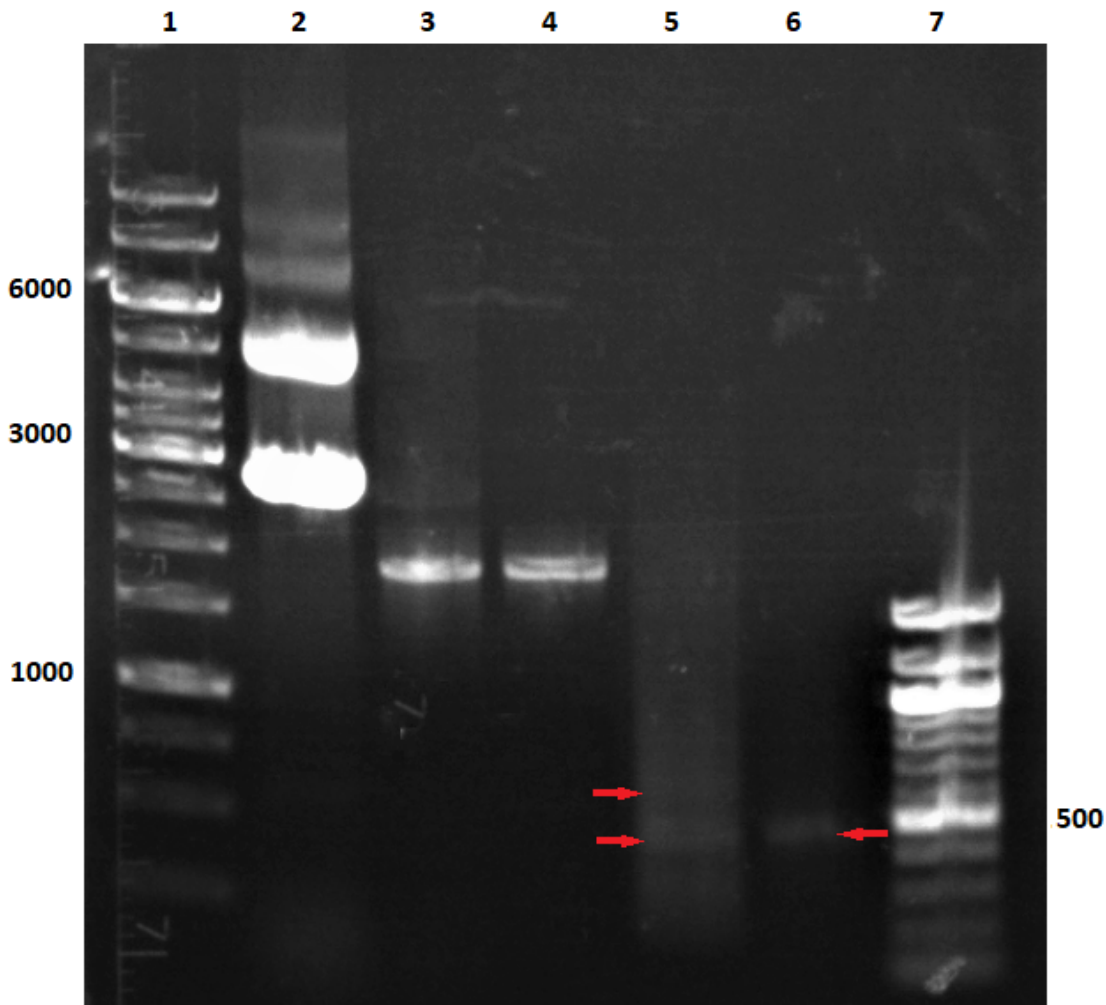


Figure 7.5: AGE of the steps for the production of the ssDNA scaffold of the DNA origami-like structure. The first lane contains a GeneRuler® 1 kb DNA ladder, while the last lane is a 100 bp DNA ladder. Lane 2: pTagRFP-C plasmid. Lane 3: PCR product of reaction 3 of Table 5.8. Lane 4: PCR product of lane 2 after it was extracted from a 1% agarose gel with the Ultrafree®-DA DNA Extraction Kit. Lane 5: asymmetric PCR product of reaction 1 of Table 5.9. Lane 6: asymmetric PCR product of lane 4 after it was extracted from a 1% Low-melting agarose gel with the QIAEX II Gel Extraction Kit.

In further asymmetric PCR experiments where the ssDNA scaffold needed to be produced, the Taq buffer was altered from KCl & 15 mM MgCl₂ to (NH₄)₂SO₄. The change in the products can be seen in Figure 7.6. Lanes 3-5 contain the product where the KCl & 15 mM MgCl₂ 10x Taq buffer was used, whereas lanes 6 and 7 contain the product where the (NH₄)₂SO₄ 10x Taq buffer was utilized.

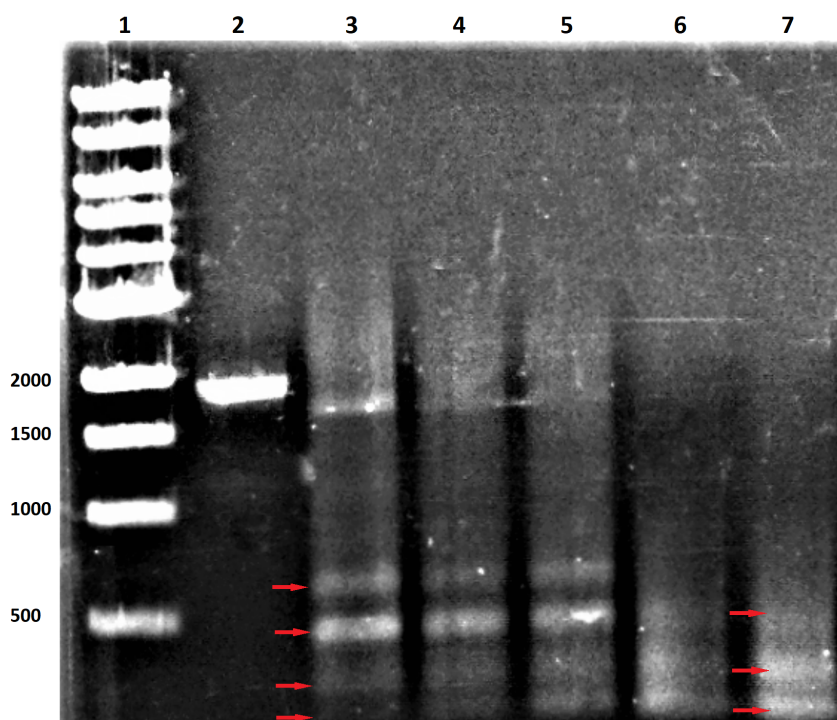


Figure 7.6: 1% AGE for the different PCR buffers used in asymmetric PCR reaction 1, of Table 5.9. Lane 1: 1 kb DNA ladder. Lane 2: template of the asymmetric PCR reaction 1 of Table 5.9. Lanes 3-5: asymmetric PCR product which contained the KCl & 15 mM MgCl₂ 10x Taq buffer. Lanes 6, 7: asymmetric PCR product which contained the (NH₄)₂SO₄ 10x Taq buffer.

7.2.3 DNA Origami-like Structure Annealing

For the annealing of the origami-like structure, two different main protocols were used, seen in Table 5.10. An attempt of their formation to be visualized in a 2% agarose gel, containing 1 M of MgCl₂, can be seen in Figure 7.7. Lanes 2 and 3 contained the templates used, unpurified and purified, respectively. The lanes which contained the purified aPCR template seem that they didn't contain anything except the staples, possibly because of the low concentration which occurred after the purification (approximately 40 ng/μL as it was measured with the PicoDrop). For the following experiments, the purified aPCR product was not used.

Further experiments were performed, where different concentrations or ingredients of the annealing mixture were tested. Different concentrations of MgCl₂, different volumes of the scaffold, and replacement of the MgCl₂ with spermine were tested. However, since the scaffold has a small size, it would not be possible to observe with certainty any difference in size throughout AGE, and therefore AFM imaging was utilized instead for the structure's observation.

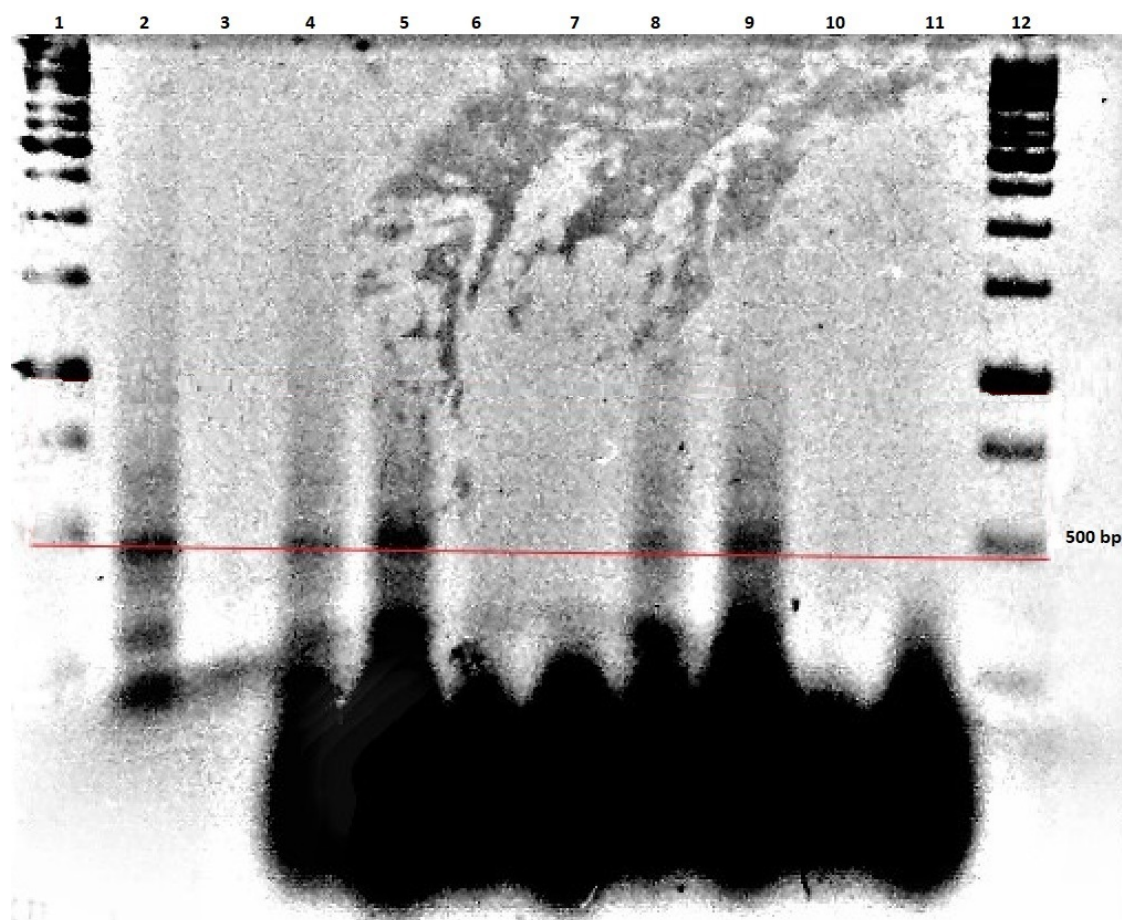


Figure 7.7: AGE, in a 2% agarose gel containing 1 M of $MgCl_2$, for the origami annealing reaction, applying the protocols 1 and 2 of Table 5.10. Lanes 1, 12: 1 kb GeneRuler[®] DNA Ladder. Lanes 2, 3: unpurified and purified scaffold at the same amount as in the origami annealing reaction, respectively. Lane 4: mixture of the DNA origami reaction 1, containing the unpurified scaffold, before the reaction. Lane 5: mixture of the DNA origami reaction 1, containing the unpurified scaffold, after the reaction. Lane 6: mixture of the DNA origami reaction 1, containing the purified scaffold, before the reaction. Lane 7: mixture of the DNA origami reaction 1, containing the purified scaffold, after the reaction. Lane 8: mixture of the DNA origami reaction 2, containing the unpurified scaffold, before the reaction. Lane 9: mixture of the DNA origami reaction 2, containing the unpurified scaffold, after the reaction. Lane 10: mixture of the DNA origami reaction 2, containing the purified scaffold, before the reaction. Lane 11: mixture of the DNA origami reaction 2, containing the purified scaffold, after the reaction.

7.2.4 DNA Origami-like Structure Dialysis

After the annealing of the structure from the different protocols, removal of the unbound staples and fragments was performed through dialysis, as it is described in section 5.11. The final products were tested for their concentration with the PicoDrop, which varied from 40-100 $\mu g/mL$ for the mixtures containing $MgCl_2$ and 30 $\mu g/mL$ for the mixtures containing spermine.

7.2.5 AFM Imaging

In order to check the formation of the desired structure, AFM imaging was implemented on the annealing mixtures. All mixtures were diluted 20 times since all the non-diluted samples appeared over-concentrated, as can be seen in Figure 7.8.

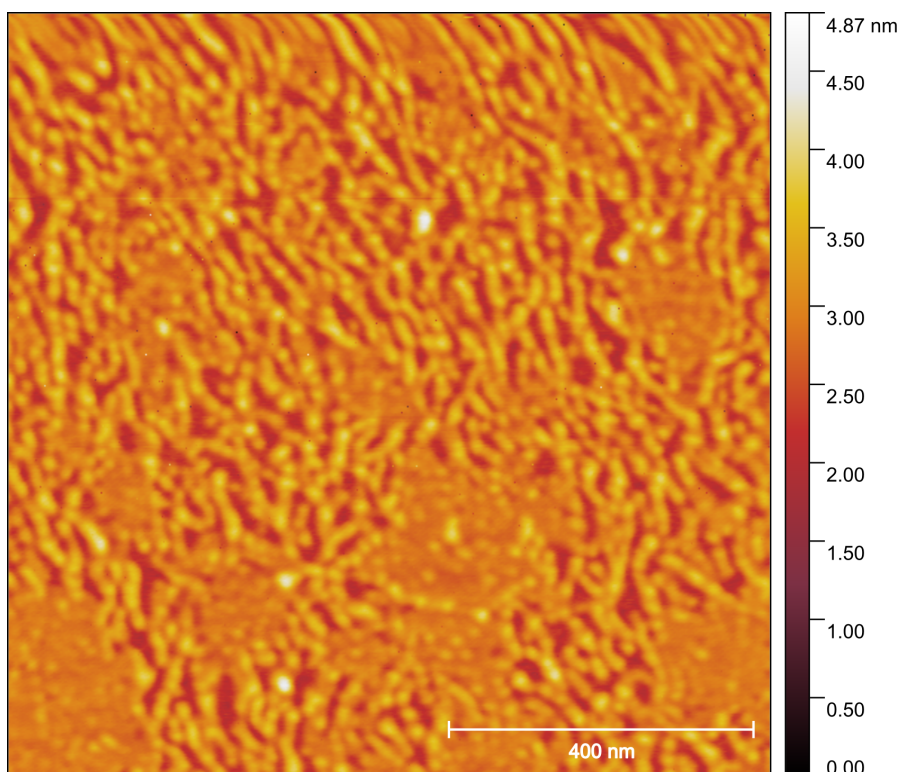


Figure 7.8: AFM of the dialysed DNA origami annealing mixture of protocol 2, Table 5.10.

First, AFM imaging for the unpurified aPCR mixture was performed, as can be seen in Figure 7.9. The biggest percentage of the surface was covered with small dots, with a diameter and height of 20 nm and 0.1 nm, respectively, which probably appear to be the aPCR products. Another structure found was the big molecule seen in the figure, which is the template DNA of the PCR reaction. This structure has a diameter and height of 350 nm and 0.7 nm, respectively.

Next, a DNA origami annealing mixture containing only the staples, without the scaffold sequence, can be seen in Figure 7.10. The structures appearing have an average diameter of 20 nm and an average height of 0.15 nm.

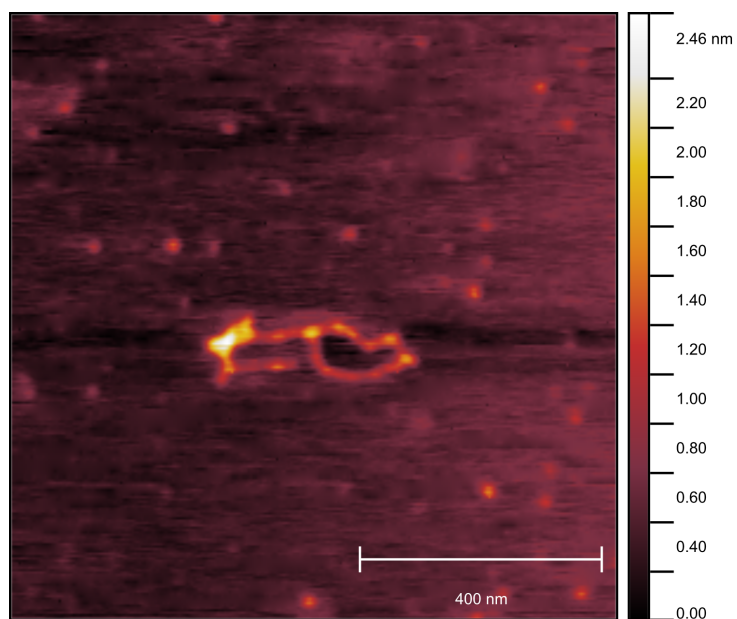


Figure 7.9: AFM imaging of the aPCR reaction 1 of Table 5.9. The mixture was not purified and was diluted 20 times.

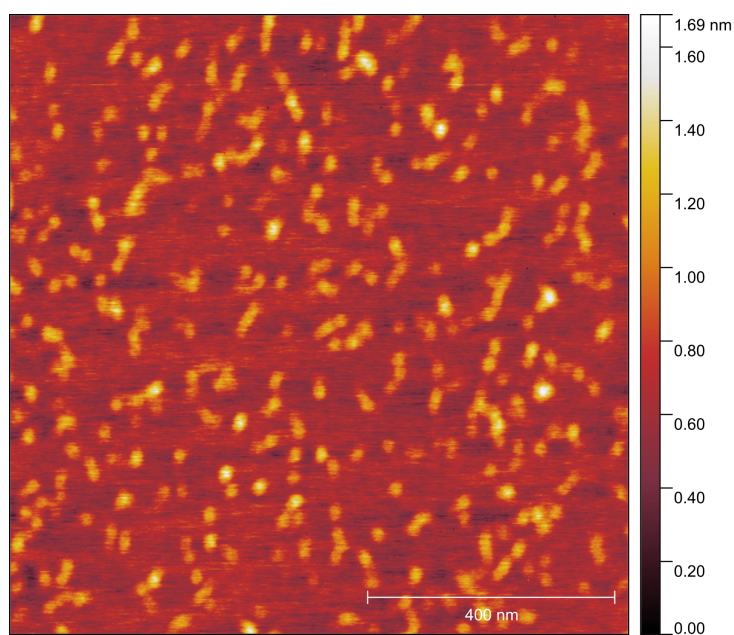


Figure 7.10: AFM imaging of the annealing protocol 2 of Table 5.10, containing 20 mM of MgCl_2 and without containing the scaffold of the reaction. The sample was diluted 20 times.

In further experiments, a comparison between the two different annealing protocols can be seen in Figure 7.11. Two reactions were performed for each protocol, which varied on the Taq buffer used for the production of the scaffold DNA. Figure 7.11a and Figure 7.11b show the products of annealing protocol 1 of Table 5.10, with 20 mM MgCl₂ and 5 μL of scaffold containing either Taq buffer with KCl and MgCl₂ or (NH₄)₂SO₄, respectively. Figure 7.11c and Figure 7.11d show the products of annealing protocol 2 of Table 5.10, with 20 mM MgCl₂ and 5 μL of scaffold containing either Taq buffer with KCl and MgCl₂ or (NH₄)₂SO₄, respectively.

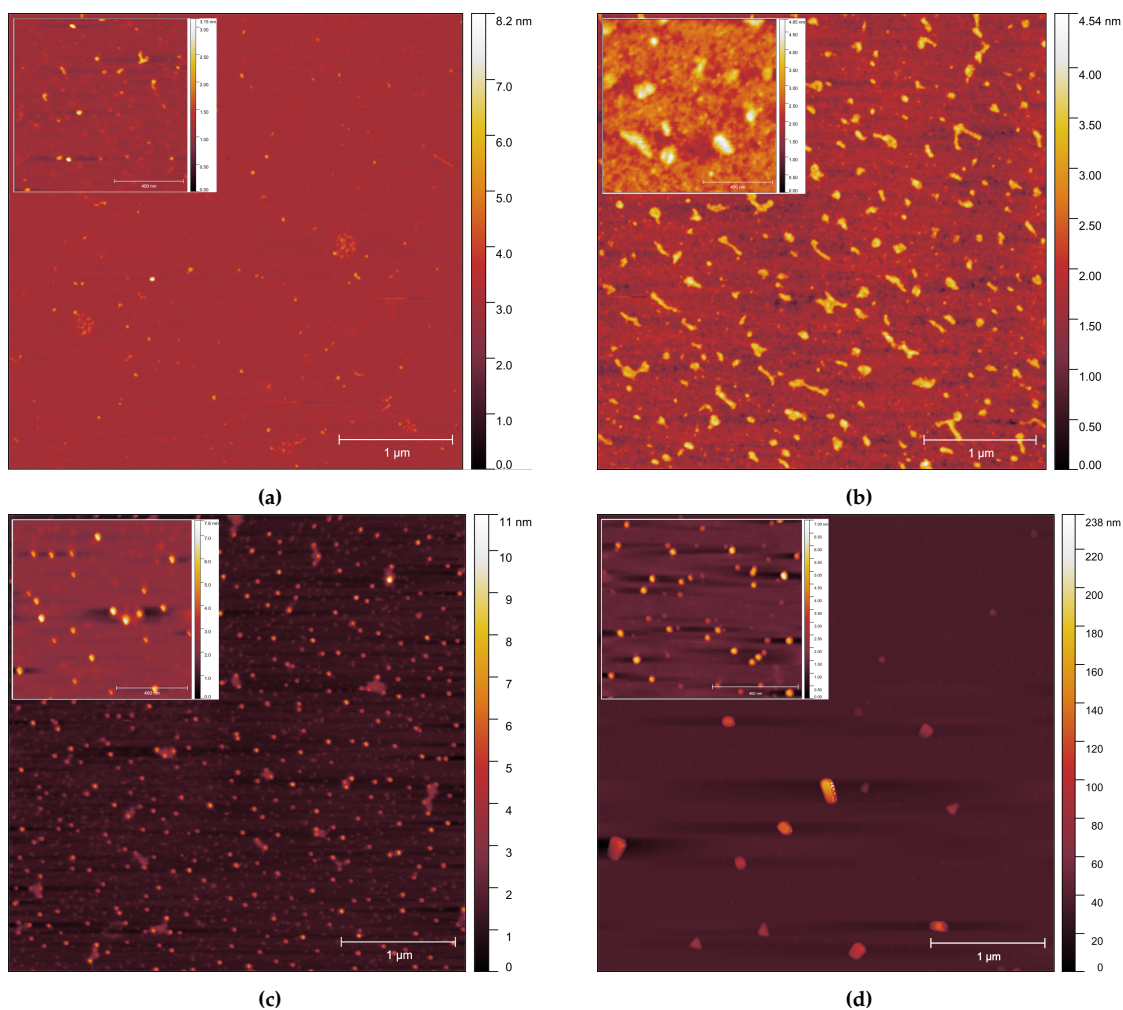


Figure 7.11: AFM imaging of the 2 different annealing protocols of Table 5.10, containing a scaffold obtained with different Taq buffers. (a) and (b) are produced by the annealing protocol 1 and their scaffold contained Taq buffer with KCl and MgCl₂ or (NH₄)₂SO₄, respectively. (c) and (d) are produced by the annealing protocol 2 and their scaffold contained Taq buffer with KCl and MgCl₂ or (NH₄)₂SO₄, respectively. The samples were diluted 20 times.

The average diameter and height of the molecules seen in Figure 7.11a is 25 nm and 0.4 nm, respectively. For Figure 7.11b, the sizes are 60 nm and 0.9 nm. For Figure 7.11c they are 45 nm and 1.6 nm, while for Figure 7.11d they are 25 nm and 1.1 nm.

In another attempt to form the desired structure, MgCl_2 was replaced with spermine, as can be seen in Figure 7.12. Three different concentrations of spermine were tested, 100 μL (Figure 7.12a), 200 μL (Figure 7.12b), and 500 μL (Figure 7.12c). The average diameter and height for the molecules seen in Figure 7.12a-Figure 7.12c was 20 nm and 0.6 nm, 20 nm and 0.2 nm, and 20 nm and 0.5 nm, respectively.

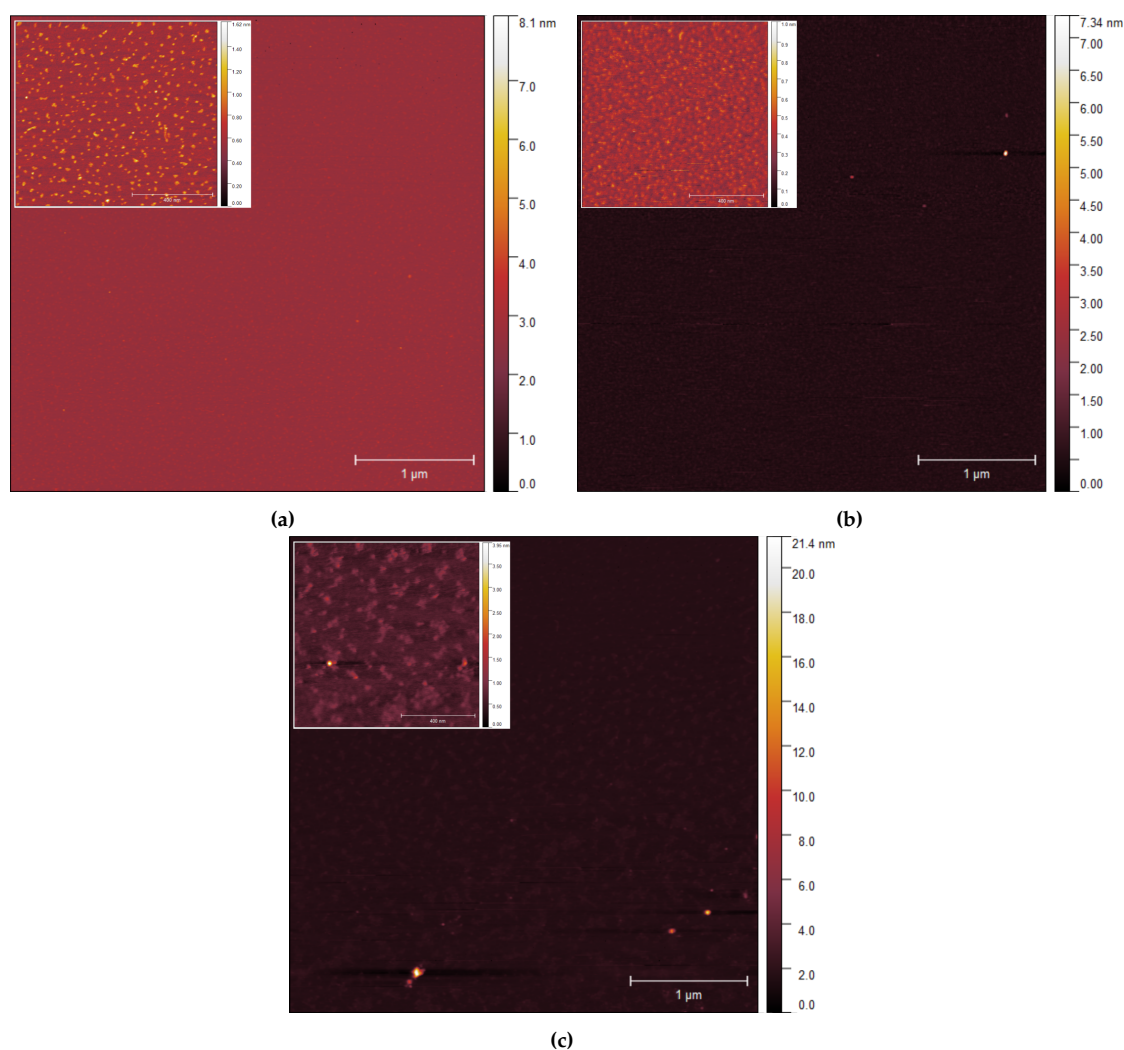


Figure 7.12: AFM imaging of annealing protocol 2, Table 5.10, without MgCl_2 and different concentrations of spermine. (a): 100 μM of spermine. (b): 200 μM of spermine. (c): 500 μM of spermine. The samples were diluted 20 times.

To increase the transfection efficiency, PLL was added to different mixtures, and its AFM imaging can be seen in Figure 7.13. Figure 7.13a contains an annealing mixture with 10 mM of MgCl_2 , Figure 7.13b contains an annealing mixture with 20 mM of MgCl_2 , and Figure 7.13c contains an annealing mixture with 200 μM of spermine. The average diameters and heights of the structures seen in Figure 7.13a-Figure 7.13c are 50 nm and 3 nm, 45 nm and 2.5 nm, and 25 nm and 0.5 nm, respectively.

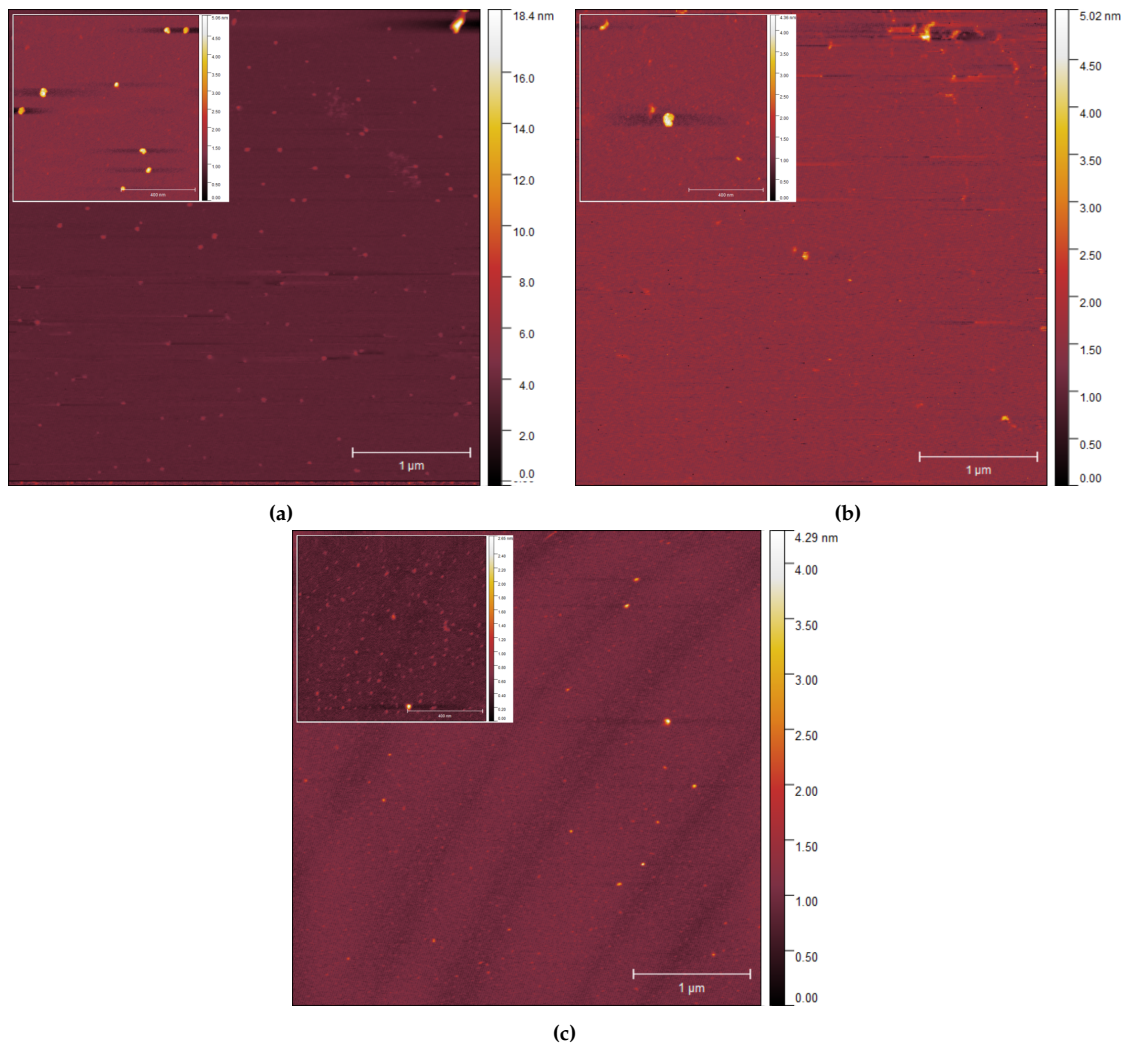


Figure 7.13: AFM imaging of DNA mixed with PLL, two times the mass of the DNA. (a): annealing mixture with 10 mM of MgCl_2 . **(b):** annealing mixture with 20 mM of MgCl_2 . **(c):** annealing mixture with 200 μM of spermine. The samples were diluted 20 times, while the annealing protocol used was protocol 2, Table 5.10.

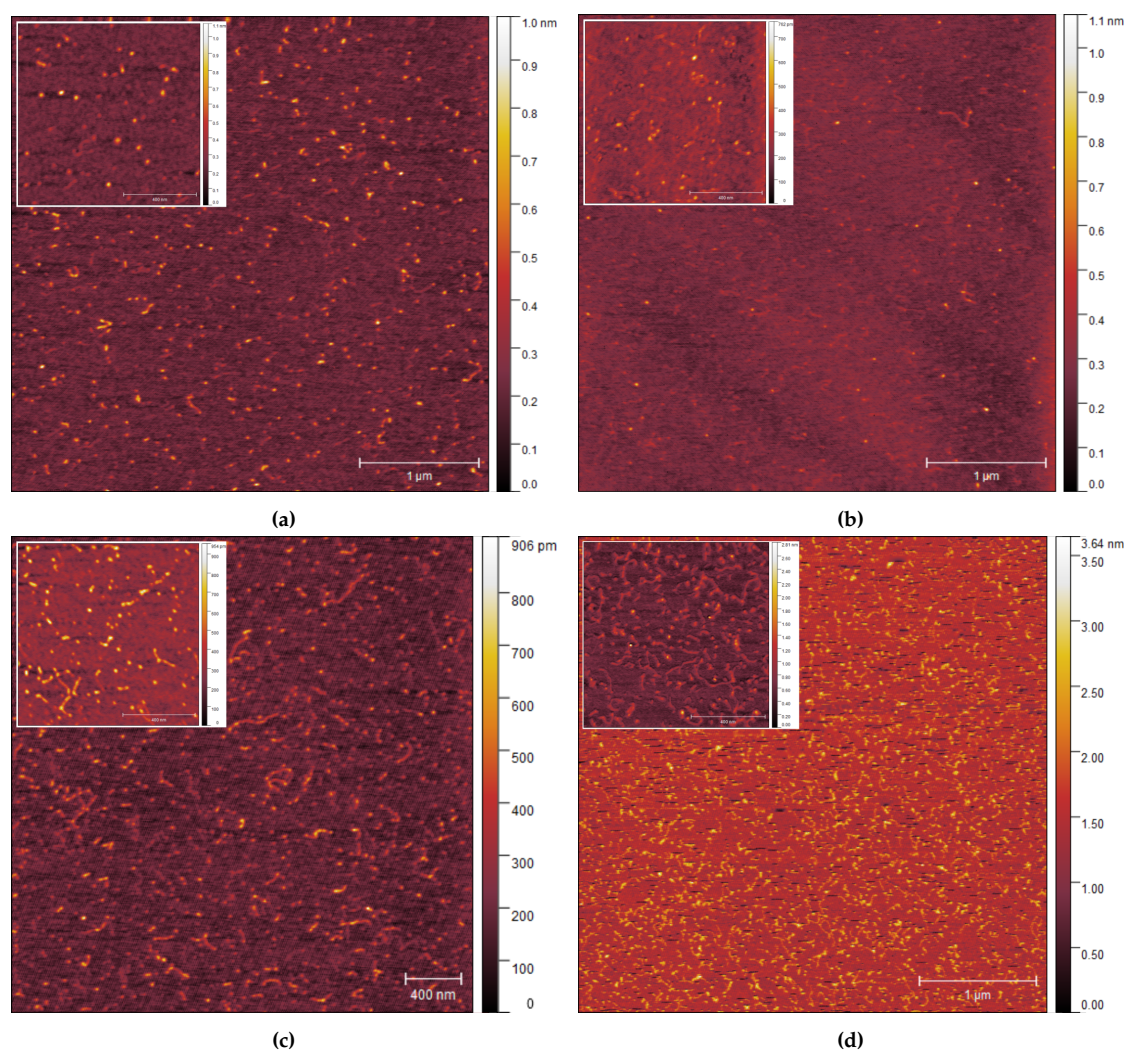


Figure 7.14: AFM imaging of annealing protocol 2, Table 5.10, containing different concentrations of MgCl₂. (a): 5 mM of MgCl₂. (b): 10 mM of MgCl₂. (c): 15 mM of MgCl₂. (d): 20 mM of MgCl₂. The samples were diluted 20 times.

In Figure 7.14, different concentrations of MgCl₂ were tested. Figure 7.14a - Figure 7.14d contained 5 mM, 10 mM, 15 mM, and 20 mM MgCl₂, respectively. For Figure 7.14a-Figure 7.14d, the average height and diameter of the structures appearing is 0.5 nm and 45 nm, 0.6 nm and 45, 0.7 nm and 45 nm, and 1.3 nm and 45 nm, respectively. The measurements were performed two weeks after the annealing, and most of the structures have been unfolded.

Since the actual concentration of the unpurified scaffold could not be estimated because the purification step was discarded due to the low final product concentration, different volumes of the scaffold were tested. This was not an accurate measurement but a rough estimate of the product which would end up if the aforementioned steps for the production of the aPCR product were followed. In Figure 7.15, three different volumes of scaffold were added: 5 μL (Figure 7.15a), 10 μL (Figure 7.15b), or 15 μL (Figure 7.15c). Similar to Figure 7.14, the measurements were performed two weeks after the annealing of the structures and most of them have been unfolded.

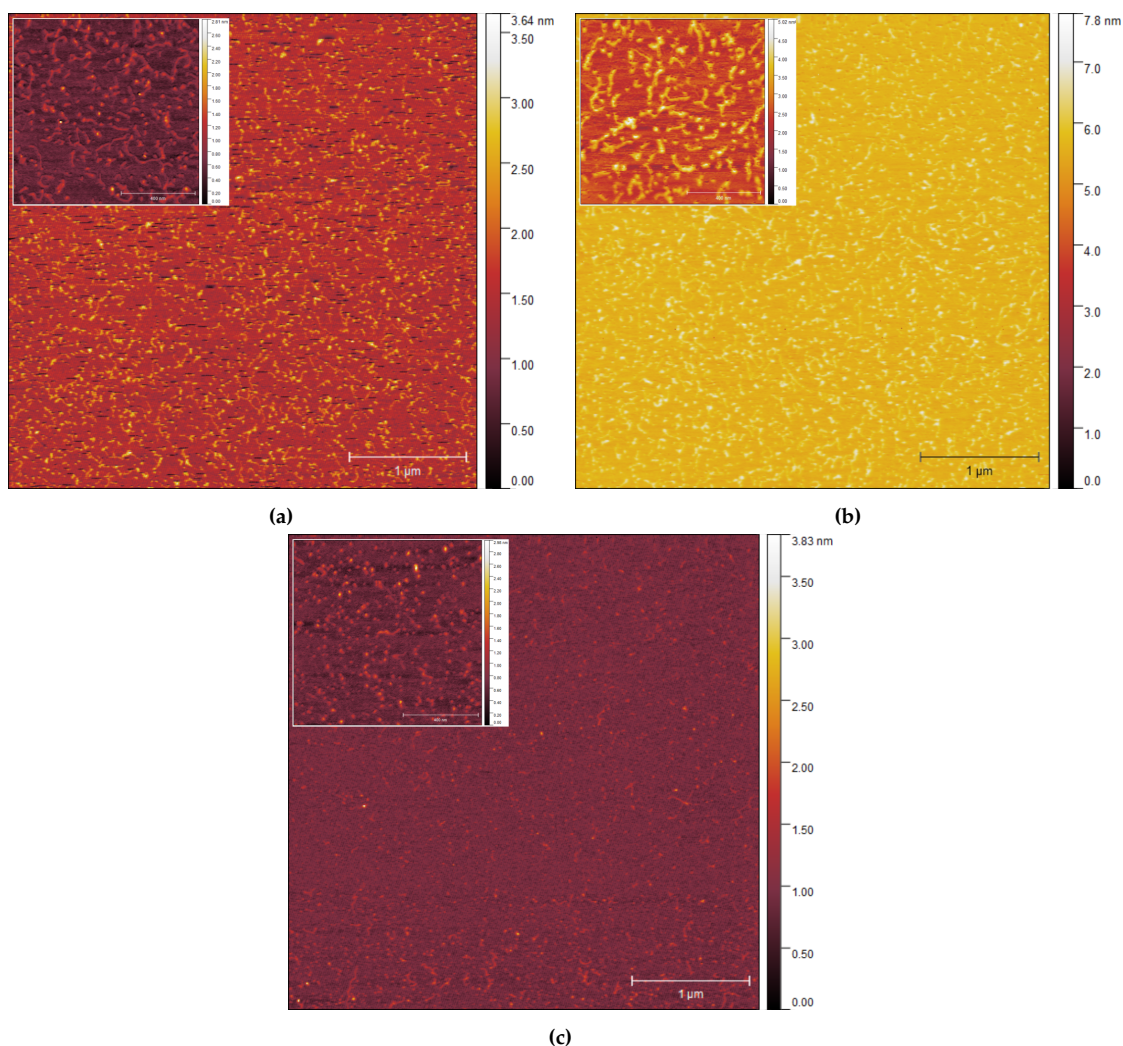
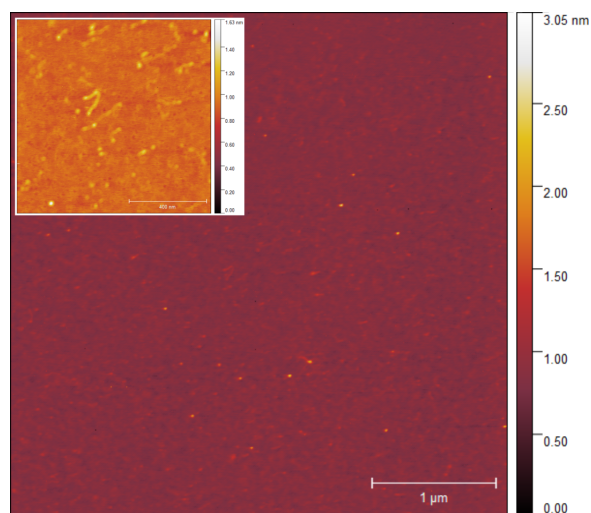
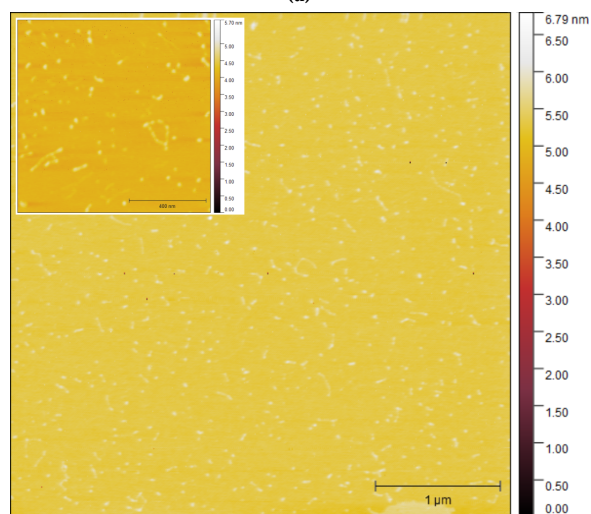


Figure 7.15: AFM imaging of annealing protocol 2, Table 5.10, containing 20 mM of MgCl_2 and different volumes of scaffold. (a): 5 μL of scaffold. (b): 10 μL of scaffold. (c): 15 μL of scaffold. The samples were diluted 20 times.

Finally, annealing mixtures were incubated with oligomer-conjugated cholesterol, in order to increase the origami's transfection efficiency, and the AFM results can be seen in Figure 7.16. For Figure 7.16a and Figure 7.16b, the average height and diameter of the structures appearing is for both cases 0.8 nm and 40 nm.



(a)



(b)

Figure 7.16: AFM imaging of annealing protocol 2, Table 5.10, incubated with oligomer-conjugated cholesterol at a final concentration of 1 μM. (a): 10 mM of MgCl₂ and 5 μL of scaffold. (b): 20 mM of MgCl₂ and 5 μL of scaffold. The samples were diluted 20 times.

7.2.6 HeLa Cell Cultures

In order to test the transfection efficiency of the DNA origami-like structure, a culture of HeLa cells was used. Different annealing protocols were tested, as well as transfection of the pTagRFP-C plasmid, either carrier-free or mixed with PLL. All the protocols which were imaged in AFM were also tested for their transfection efficiency. Unfortunately, none of the DNA origami-like structure protocols appeared to have an efficient transfection. Only the pTagRFP-C plasmid mixed with PLL was observed to be transfected to the HeLa cells.

The fluorescence of the cultures was initially measured with Perkin Elmer's Enspire microplate reader, with excitation and emission of 555 nm and 584 nm, respectively, but no observable difference was seen between the different samples. Therefore, the AxioObserver Z1 microscope from Carl Zeiss, through the assistance of the ZEN blue software, was used, and its results can be seen in the figures that follow. The yellow indications in the images were produced through a filter with excitation and emission of 555 nm and 584 nm, respectively. All samples were imaged after 24 h and after 48 h of culturing.

As a negative control, a culture containing HeLa cells and a fresh DMEM medium was used, which can be seen in Figure 7.17. The yellow dots seen occur due to the reflection of dead HeLa cells or due to buddings. Next, in Figure 7.18, the carrier-free pTagRFP-C plasmid was tested, and again no transfection efficiency was observable. Same with the negative control, the yellow dots are either buddings or dead HeLa cells.

The only efficient transfection occurred from pTagRFP-C plasmid mixed with PLL. The mixture contained 100 ng/ μ L plasmid DNA and 200 ng/ μ L PLL. In Figure 7.19, two different volumes of the mixture were tested: 3 μ L for Figure 7.19a and Figure 7.19b, and 5 μ L for Figure 7.19c and Figure 7.19d. In the first 24 h, only one cell in the whole culture was transfected, while after 48 h, Figure 7.19d was slightly more transfected.

Since no DNA origami structures were transfected, only two indicative samples are presented, DNA origami containing 200 μ M of spermine (Figure 7.20) and DNA origami with 20 mM of MgCl₂, mixed with PLL (Figure 7.21). For the different origami transfections tested, three different amounts of DNA origami were introduced each time: 100 ng, 200 ng, and 300 ng. Regarding the PLL mixtures, the samples tested contained 30 ng/ μ L DNA and 60 ng/ μ L PLL, and the volumes added in the cultures were either 3 μ L or 9 μ L. Again, the yellow dots appearing are either buddings or dead HeLa cells.

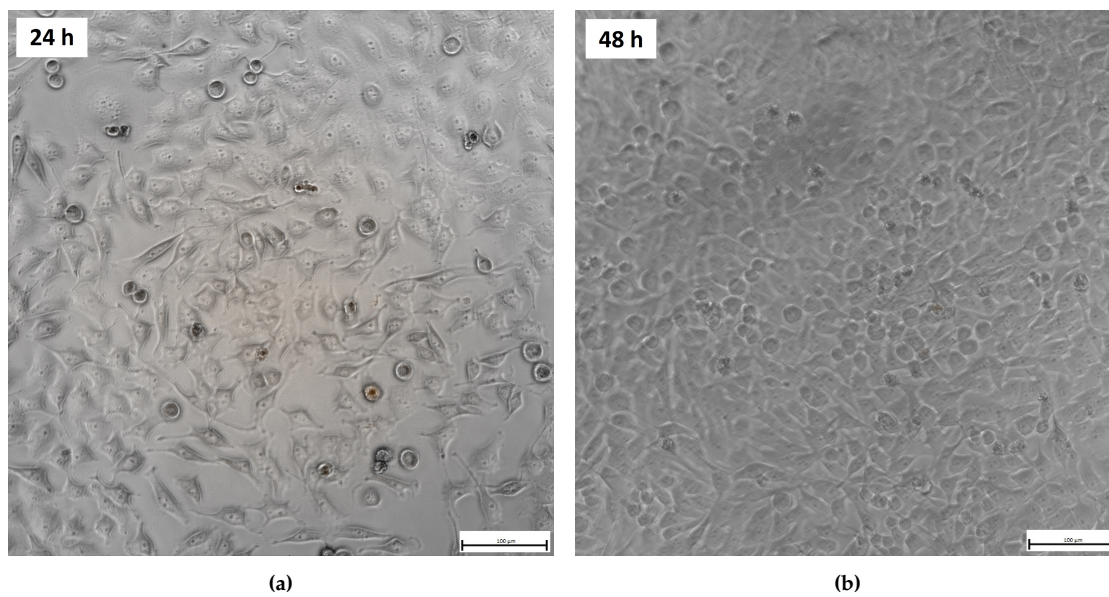


Figure 7.17: Negative control for the transfection efficiency of the TagRFP gene. HeLa cells were left for 24h (a) and 48 h (b) with 200 µL of DMEM buffer.

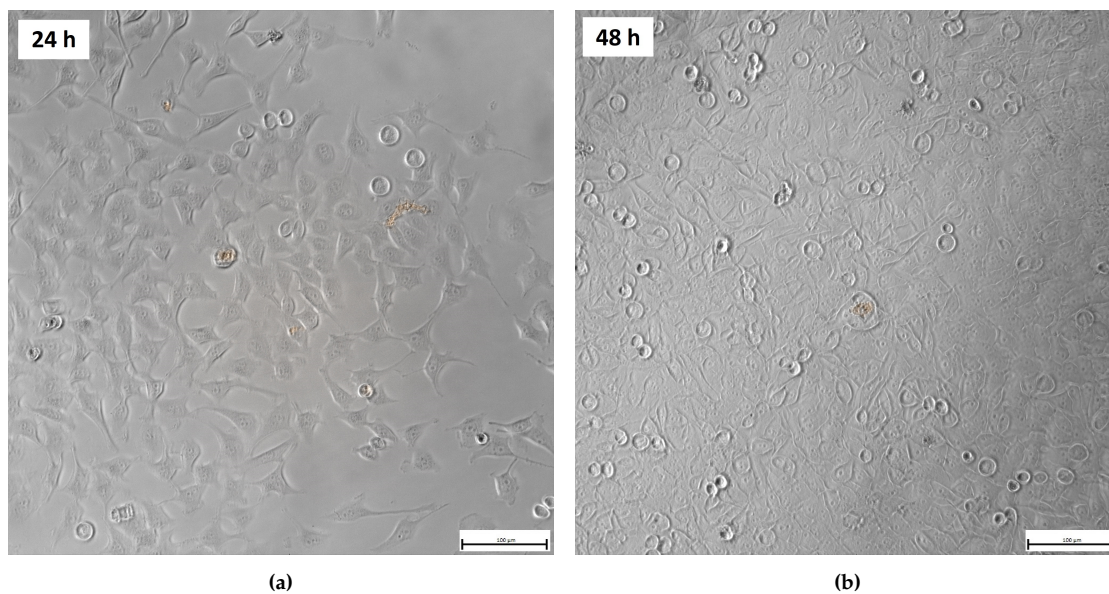


Figure 7.18: Transfection efficiency of the carrier-free pTagRFP-C plasmid. HeLa cells were left with DMEM, mixed with 2 µL of free pTagRFP-C plasmid, in a final volume of 200 µL, for 24h (a) and 48 h (b).

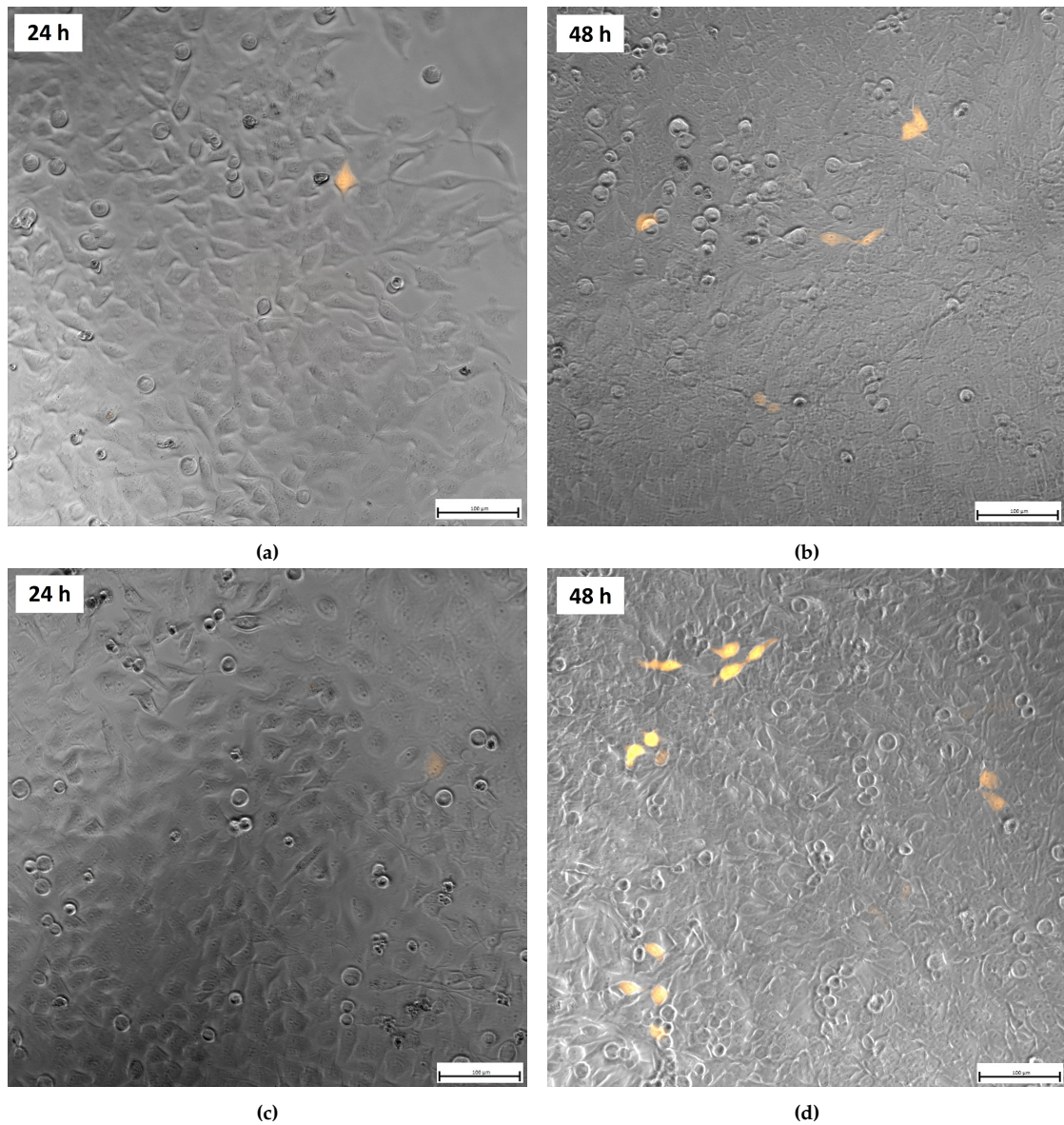


Figure 7.19: Transfection efficiency of the pTagRFP-C plasmid mixed with PLL. HeLa cells were left with DMEM, mixed with 3 μL [(a) and (b)] or 5 μL [(c) and (d)] of pTagRFP-C plasmid mixed with PLL, in a final volume of 200 μL , for 24h [(a) and (c)] and 48 h [(b) and (d)].

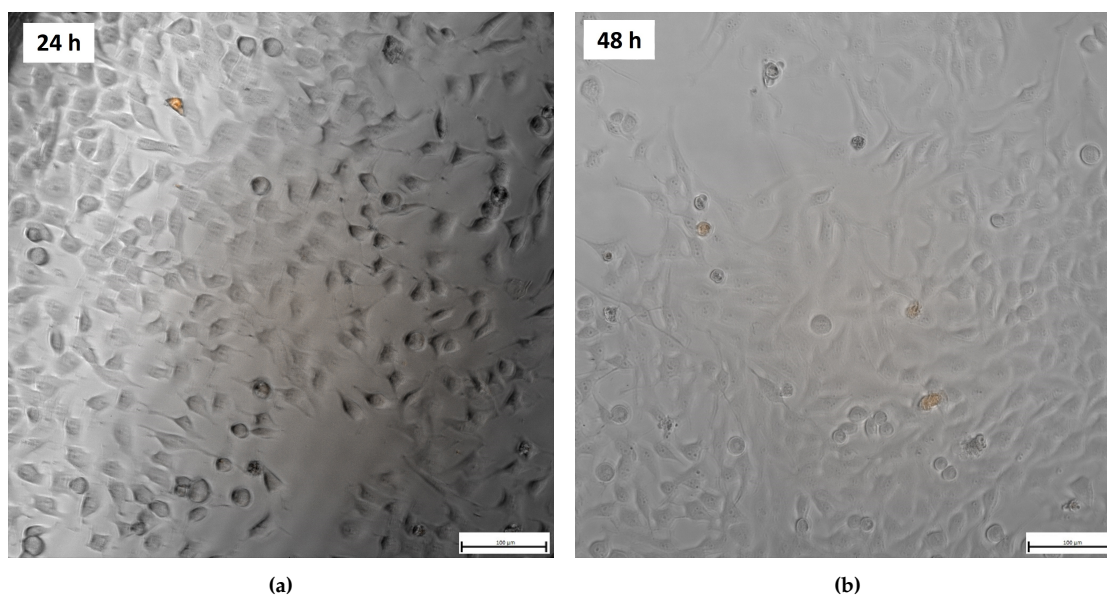


Figure 7.20: Transfection efficiency of DNA origami mixed with spermine. HeLa cells were left with DMEM, mixed with 9 μL of DNA origami, in a final volume of 200 μL , for 24h (a) and 48 h (b).

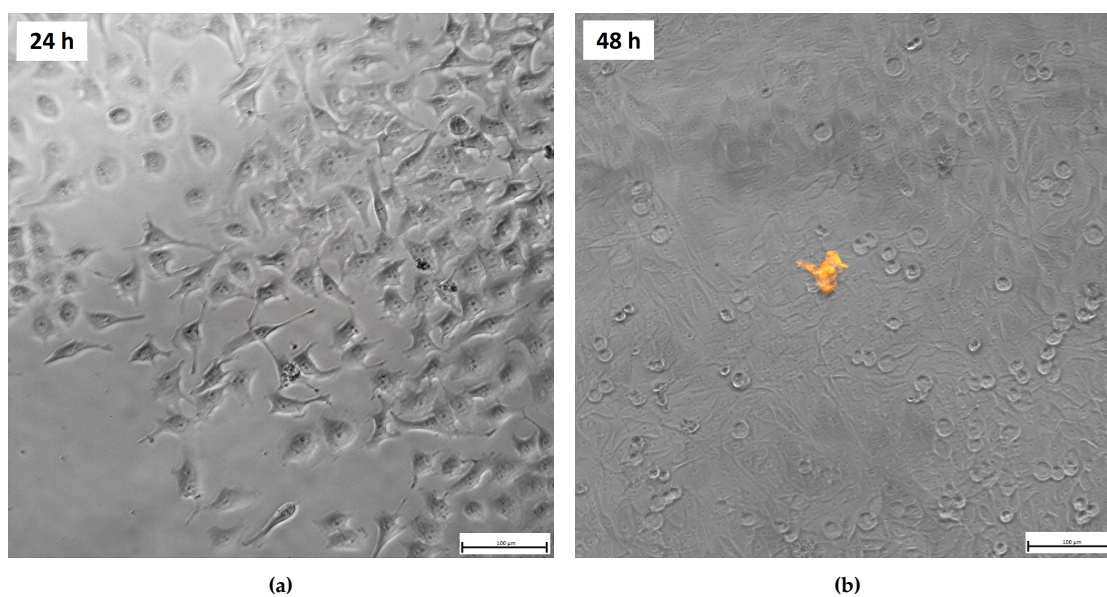


Figure 7.21: Transfection efficiency of DNA origami mixed poly-L-lysine. HeLa cells were left with DMEM, mixed with 9 μL of DNA origami/PLL, in a final volume of 200 μL , for 24h (a) and 48 h (b).

8 Discussion

8.1 The pHAGE-EF1 α L-eGFP-W Plasmid

In a first attempt to create the desired DNA origami-like structure, the pHAGE-EF1 α L-eGFP-W plasmid was used as a template [71]. Initially, primers were designed for the plasmid to create a long single-stranded sequence for the structure intended to be made. It was created in a position where the staples were offering the expected molecule enough stability. The stability was also tested in a molecular dynamics simulation, and the experimental part started to get set.

Since the plasmid was obtained, the designed primers were used for aPCR. Unfortunately, no results were obtained after various PCRs. The annealing temperature was lowered, and the volume of the PCR reaction was changed, but still, no results appeared on AGE. Since all the other ingredients were tested and worked fine in PCRs with different templates and primers, the problem in the reaction should be either the primers or the plasmid itself.

The plasmid used was not commercial, and therefore, its sequencing may not be precise. This was also observed through an attempt to be sequenced, where the plasmid and a suggestion of primers were sent at Eurofins Scientific [84], but no results were received. This was probably caused by the very poor sequencing of the Addgene site [71], since not even the suggested primers were not able to bind in order to give a sufficient sequencing result.

8.2 The pTagRFP-C Vector

8.2.1 Design of the DNA Origami-like Structure

The new template that was used eventually was the pTagRFP-C vector [60]. It contained a gene that expressed a red fluorescent protein, pTagRFP, with a potent promoter for expression in mammalian cells. The first step of the procedure was the design of the structure and an MD simulation to check its stability.

Design of Primers

A 1667 nt part of the vector was selected to be the scaffold for the DNA origami-like structure. Therefore, three primers, found in Table 5.5, were designed, which had as a final product a single-stranded DNA sequence through aPCR. The final sequence contained the antisense strand of the CMV_{IE} promoter and the TagRFP gene. The complementary DNA sequence of this product can be seen in Table B.1. The antisense strand was chosen to be produced because it needs to be continuous during the transcription procedure for the gene to be successfully transcribed.

To reduce the number of staples needed for the structure, a part of the structure was intended to be double-stranded. Therefore, the production of strands complementary to specific parts of the scaffold was necessary. For the honeycomb cylinder design, ten parts were intended to be double-stranded, and their complementary single-stranded parts were attempted to be produced through aPCR. The primers designed for the PCR reactions can be seen in Table 5.5. The stability of the molecule would be lower compared to a regular DNA origami structure, but its production costs would also be significantly reduced. Comparably, if the structure had no single-stranded parts, at least sixty staples would be needed to be ordered, while for this design only seventeen were used.

Another advantage of this kind of design appears to be the more accessible promoter. In nature, proteins that take part in transcription are binding in a double-stranded promoter, which afterwards opens into two single strands for the transcription to be initiated [28]. If the promoter contained staples everywhere, this "transcription bubble" would be harder to be created, and maybe the binding sites of these proteins would not even be accessible.

More specifically, the promoter sequence and its double-stranded parts can be seen in Table 6.1. Among the major binding sites of the promoter, the ones existing in the staples' binding territory are one out of the two 21-bp binding sites, two out of the four 19-nt binding sites, two out of the three 18-nt binding sites, and one out of the two Nf1-t binding sites [66]. Consequently, even if the proteins can't bind at these sites, there are other binding sites where they can bind, and the transcription efficiency will probably only be slightly affected.

Design of Staples

In the remaining single-stranded parts of the molecule, staples were designed to give the desired shape. They were designed to bind on the ends of the honeycomb cylinder structure. These staples should be at an adequate length to be stable, and they should form neither loops nor dimers. Additionally, every neighbouring strand of the desired

honeycomb structure should be connected with at least one staple.

The main way to avoid the loop formations is the addition of a tail in each staple that was necessary, while for the dimer formation, some extra adjustments needed to be done. The tails used, 5'-GTGTTGTG-3' and 5'-GTGTTGTT-3', also offered a binding site for any modified peptide that could be useful for the protection or the transfer of the structure into the cell [85]. Even though these sequences were not long enough for very stable annealing, in attempts to increase their length and annealing stability, the loop and dimer formations were also increased.

The caDNAno2 tool has only the ability to design the staples to create the desired 3D shape of the structure but does not take into consideration the sequence of the scaffold. Consequently, some staples needed to be cut into smaller parts or even mix two or three of the suggested staples manually. These adjustments were crucial to reduce the possibility of dimer formation as much as possible without affecting the structure of the molecule.

Two more tails were added on two different staples, which contained three binding sites for the transcription factor NF- κ B. The tails had a sequence of: 5'-TAGGGGACTT TCCTCGCTGGGGACTTTCCTCGTGGGACTTTCCTCATT-3'. The sequences which are underlined are the binding sites of the transcription factor NF- κ B. [26] These tails were also made double-stranded by a complementary DNA fragment. They were positioned on specific staples so that one of them was located inside the CMV promoter, while the second one was located at the end of the RFP gene. The binding site of the transcription factor NF- κ B, which is translated into the cytoplasm and is afterwards transferred into the nucleus, on the structure would offer a route of insertion into the nucleus for the DNA origami structure, increasing its transfection efficiency [26], [86].

8.2.2 Molecular Dynamics Simulations

After the design of the molecule with the desired staples and double-stranded sequences on Maya 2019, the structure could be extracted as a topology and a configuration file. These two files were used for three simulations on oxDNA2.

The first two simulations, which are the first three scripts in Appendix A, were a minimization and two relaxation simulations, respectively. They were both run in an oxDNA2 simulation, which offers higher precision compared to the older oxDNA. They included 100000 steps each, where each step lasted approximately 5 fs. They ran at a temperature of 300K and a salt concentration of 0.2 M NaCl to simulate the conditions of a mammalian cell. For the relaxation simulations, a Langevin or a Brownian thermostat was added.

The `diff_coeff` was set on 2.50, making the procedure slow, allowing for larger time steps and therefore longer simulation time. The `verlet_skin` was set at 0.15. This is the width of the skin that controls the maximum displacement, after which the Verlet lists need to be updated [87]. MD simulations make use of Verlet lists to maintain a list of all particles within designated proximity of one another [88]. Finally, the `max_backbone_force` was set at 50 (or 2.43 nN) for the minimization and 20 (or 0.97 nN) for the relaxation. At the end of relaxation, most of the overlapped excluded volumes, as well as any long backbone bonds, were fixed.

The third type of simulations, which are the fourth and fifth script in Appendix A, was a molecular dynamics simulation. In this case, the steps were 2500000, where each step lasted 15 fs. A repetition of this simulation was done where the input files of the simulation were the output files of the previous simulation to achieve a final time of 500 ns. It was run at a temperature of 300K in a Langevin or a Brownian thermostat and a salt concentration of 0.2 M NaCl. The `diff_coeff` was set at 2.50, whereas the `verlet_skin` was set at 0.05. Finally, a new parameter was inserted, the `newtonian_steps`, at 103. This parameter specifies the number of steps after which a procedure of thermalization will be performed.

Regarding the minimization, in Figure 6.6, a steep drop in the total energy is observed. Thanks to minimization, the nucleotides, whose excluded volumes overlapped one another, were eliminated, and the too-long backbone bonds were avoided, leading to this total energy drop. It was expected for these problems to appear on the original design, as it was manually designed. After a very short period, the total energy reached levels below zero, indicating a stable structure and only a slow decrease was observed for the rest of the minimization, reaching almost a flattened curve.

In Figure 6.7 and Figure 6.8, representing the energy variation for the relaxation simulations, a sharp increase was observed in the first 10 ps, and then the structure only slowly increased its energy. This indicated that the molecule reached the desired structure fast, foreshadowing a stable structure. Maybe the relaxation could be run for a little longer for a more flattened curve, but as it is seen in the MD simulation's results, no problem eventually occurred. The results for the Brownian and the Langevin thermostat had a slight difference, wherein in the Langevin case, the total energy was increased slightly faster and reached total energy of -1.468668 oxDNA Energy Units, while in the Brownian case reached -1.482143 oxDNA Energy Units.

From the final MD simulations, various results were obtained. As expected, the structure initially designed started to extend in the middle, while its ends remained compact, as they were the only parts which contained staples. Its final shape can be seen in

Figure 6.5. Figure 6.10 shows a steep increase in total energy in the beginning and then stabilizes for the Brownian case, while for the Langevin case, in Figure 6.9, remains stable for the whole simulation, indicating a stable structure from both cases. This increase in total energy for the Brownian case was probably caused due to the slower increase in the relaxation simulation compared to the Langevin case. Eventually, both cases ended up on the same energy level.

The same assumption can be made from Figure 6.11 and Figure 6.12, where the structure's dimensions' stability was already achieved from the end of the relaxation since no observable change was obvious for the whole MD simulation. For both the Brownian and the Langevin cases, the results were very similar, with the Brownian simulation seeming a little more stable. Consequently, the designed structure is stable, and the next step of the process, the experimental part, can be initiated.

8.2.3 Production of ssDNA Fragments

Having available the desired design of the structure, the scaffold and the ssDNA fragments binding in the middle of the DNA origami were intended to be produced throughout aPCR. A first step was the production, throughout PCR, of the templates which would be further used in aPCR. These templates had one end finishing in the base where their complementary strand was intended to stop, and the second end was around 100 bases upstream of the place where the primer of the aPCR was binding. As can be seen in Figure 7.3, all the 11 products were efficiently produced and purified. The two first bands appear a little fainter, but this occurred due to a loading issue on this specific gel. The first two samples were afterwards run in a second agarose gel, and their quality was similar to the rest of the bands in Figure 7.3.

The next step of the procedure was the production of the single-stranded fragments. For the scaffold, the desired product was the non-coding strand of the RFP gene, while the DNA fragments were on the coding strand. This choice was made for the RNA polymerase to have a consecutive strand to bind and finally produce the desired mRNA.

To visualize the aPCR products, 1 M of urea was added into the agarose gel and the 1xTAE buffer, and a loading dye containing 7 M of urea was prepared. Urea would interact with the Hydrogen bonds of the nucleotides, blocking the formation of loops and different conformations of the ssDNA fragments [89]. Since urea is not efficient enough to remove pre-existing conformations, the samples were denatured through heating and immediately put on ice before loading.

Regarding the scaffold of the DNA origami-like structure, as can be seen in Figure 7.4,

the aPCR reaction seemed to be more efficient compared to the ssDNA fragments. One band appears at a size of 1900 bp, being the template of the reaction. A considerable amount of template was used on the aPCR reaction due to its linear nature of increased product yield, and this is the reason why the template is so observable. Next, four bands appear at 600 bp, 550 bp, 450 bp, and 200 bp. The product is single-stranded, and therefore these comparisons to the DNA ladder don't correspond to the actual length of the product, but they are probably different conformations of it. As it can also be observed, the denaturation of the samples made no difference in the bands. The denaturing temperature was attempted to be increased to 95°C for a more efficient denaturation, but this made the loading of the samples to the gel impossible.

The aPCR products of the ssDNA fragments were more unclear. The bands of the scaffold appeared in each case, but depending on the different annealing temperatures, different bands occurred. Due to the folding nature of the ssDNA, it was unclear if these were just different conformations or completely different products. One band which appeared in all samples was at a size below 100 bp, but as it can be seen in Figure 7.4b, this band contained the primers of each reaction, which was further verified through urea-PAGE, where the size separation is more sensitive than AGE [72].

Another barrier to the procedure appeared to be the purification of the single-stranded fragments. The Oligonucleotide Purification protocol, which was available for the Monarch® PCR & DNA Cleanup Kit, could not remove the primers, and no gel extraction kit was able to isolate ssDNA of 100 bp size. Additionally, both the single-stranded fragments and the scaffold were incubated with DSN, which digests dsDNA, but as can be seen in Figure 7.4a, in lanes 2 and 3, the products of the asymmetric PCR reactions also disappeared, and only the primers remained. An explanation for this result is the loop formations of ssDNA sequences. If they were long and stable enough, DSN could recognise and digest them. Therefore, the single-stranded fragments needed to be ordered. Each intended fragment was ordered in two pieces of approximately 55 bases since the cost for sequences above 100 bases is significantly higher.

The focus of purification fell on the scaffold DNA, and the steps of the procedure are summarized in Figure 7.5. In Lane 2, the plasmid can be seen. The two intense bands make the other bands of the gel look faint, even though their intensity seemed similar to the previous reactions. Next, in Lane 3, the product of reaction 3 in Table 5.8 can be seen, and in Lane 4, the same product after agarose gel extraction with the Ultrafree®-DA DNA Extraction Kit can be observed. There is an observable difference, since there is no blurring in the whole lane, because the salts, the initial template, and the primers are removed. Lane 5 contained the aPCR reaction product of reaction 1 in Table 5.9. This band is fainter compared to the previous 3. If the exposure to the UV was in-

creased, 4 bands could be seen, just like the bands of Lane 2 in Figure 7.4b. Lane 6 contained one extracted band of the aPCR product, and only this band appeared on the gel. From this result two assumptions can be made: either the conformation is strong enough and the bands which didn't appear didn't exist in a sufficient concentration, or each band was a different PCR product.

A change in the intensity of the four bands of the asymmetric PCR product of reaction 1, Table 5.9, occurred after a change in the Taq buffer used. As can be seen in Figure 7.6, when a Taq buffer containing KCl & 15 mM MgCl₂ was used, the 2 top bands appeared more intense, while on the use of (NH₄)₂SO₄ Taq buffer, the two lower bands were more intense and the 600 bp band disappeared. MgCl₂ affects the efficiency of Taq polymerase and also decreases the electrostatic repulsions between DNA strands. [90]. Additionally, (NH₄)₂SO₄ destabilizes weak Hydrogen bonds, while KCl makes DNA more reluctant in separation [91]. Therefore, a slight change in salts concentration could eventually lead to making some conformations of the ssDNA preferable to others.

8.2.4 DNA Origami-like Structure Annealing

For the annealing procedure of the DNA origami-like structure, two annealing protocols were tested, obtained from a previous thesis of Steffan Møller Sønderskov [92].

AGE For the DNA Origami-like Structure

Initially, AGE was used for the identification of the DNA origami structure, but as can be seen in Figure 7.7, no remarkable changes could be observed. In Sønderskov's thesis, a slight change in the band migration was made in the DNA origami structure and its free scaffold. However, the length of the scaffold used was approximately 5 times bigger compared to the one used in this project. In the case of Figure 7.7, there is a slight increase in intensity and decrease in migration for the 500 bp bands, the ones falling on the red line, of lanes 5 and 9, compared to the 500 bp bands of lanes 4 and 8. It can be assumed that these changes occur due to DNA origami formation since the amounts of the scaffold on each lane are the same. For better observation of the DNA origami structure, the origami formation would probably not be able to be observed through AGE, and for that reason, AFM was used.

AFM For the DNA Origami-like Structure

During the AFM imaging, it was observed that all the origami structures reached a maximum height of 1.6 nm, while their height, obtained from oxDNA2 simulations, was 15 nm. It was hypothesized that the origami structures were compressed vertically during deposition on the mica substrate. This seems plausible since the structure

is not as compact as a regular DNA origami cylinder, and the structures observed are broader than expected, while their diameter matches the simulations.

During AFM imaging, the scaffold intended to be used for the origami annealing was run on its own, as can be seen in Figure 7.9. The small dots appearing are probably loops formed on the ssDNA scaffold, which are comparable to a report from Shlyakhtenko et al. [93]. In this report, except for the dots, thin DNA strands were also observable. However, in the AFM experiments performed here, the quality was not high enough to visualise such thin structures.

A comparison was also made between the two different protocols of Table 5.10, which contained scaffold DNA obtained by using two different Taq buffers in the asymmetric PCR reaction. As can be seen in Figure 7.11, the figure which seems to have the most compact and biggest structures is Figure 7.11c. Therefore, for further experiments, protocol 2 of Table 5.10, containing a scaffold obtained from an aPCR reaction which had Taq buffer with KCl and MgCl₂, was used.

In an attempt to increase the stability of the structure, different concentrations of positively charged spermine replaced the MgCl₂ in the annealing reaction, in a similar procedure as in the report of Aradhana Chopra et al. [50], where spermidine was used instead of spermine. The AFM visualization of three different concentrations of spermine, 100 μM, 200 μM, and 500 μM, can be seen in Figure 7.12. Unfortunately, none of these three concentrations appeared to produce a structure of sufficient size.

In order to cover the origami structures with a positive charge, for a more efficient transfection, PLL was implemented. Three different annealing mixtures were tested, and they can be seen in Figure 7.13. The least promising mixture contained spermine instead of MgCl₂, and no structures of sufficient size appeared on AFM. This was probably caused by the positively charged spermine molecules, which were blocking the wrapping of PLL around the origami. Additionally, as it was also seen in Figure 7.12, spermine was not assisting enough for the formation of an origami structure. On the other hand, both Figure 7.13a and Figure 7.13b, which contained 10 mM and 20 mM of MgCl₂, respectively, formed structures of a probable match with the origami's expected size.

Two other factors tested were the volume of scaffold added and the concentration of MgCl₂. While observing the figures, which were obtained two weeks after the initial annealing of the structure, most of the structures are unfolded, and it can be concluded that the origami structure is not stable for a long period at 4°C. Even in this case though, it can be observed that the increased amount of scaffold in the mixture did not influence the maintenance of the origami structure, and only on the 5 μL scaf-

fold of Figure 7.15a one compact DNA origami molecule can be observed. Regarding the different concentrations of MgCl_2 , the 5 mM mixture appeared to be the least unfolded compared to the other mixtures, while the 20 mM mixture appeared to contain the structures closer to the expected size. Since the structures appearing in the 5 mM, 10 mM, and 15 mM mixtures could be loops of the ssDNA scaffold due to their small height, the most efficient concentration was concluded to be the 20 mM of MgCl_2 .

In both Figure 7.14 and Figure 7.15, the unfolded structures appear to be double-stranded. An explanation is that the staples were un-binded over time, while the single-stranded fragments, which were binding continuously for 55 bp, were stable enough to maintain their double-stranded nature along with the scaffold.

Two origami mixtures, containing either 10 mM or 20 mM of MgCl_2 , were annealed with oligomer-conjugated cholesterol molecules and their results are seen in Figure 7.16. There is not an observable difference between the two samples, but the molecules also appear smaller than the expected origami size. This could be caused due to the annealing procedure of cholesterol onto origami, where the latter may have unfolded due to heating. The origami molecules which were annealed with DNA origami were the only ones not tested for transfection since cholesterol arrived close to the hand-in of the thesis, and there was not enough time to complete the transfection protocol.

8.2.5 Transfection of HeLa Cells

In order to check the transfection efficiency of the origami structures, HeLa cells were cultured for 24 h or 48 h with transfecting molecules, either plasmid or origami structures, and were afterwards observed on the Enspire Microplate Reader and the AxioObserver Z1 microscope. For both cases, the excitation and emission used were 555 nm and 584 nm, respectively [59]. Regarding the Enspire microplate reader, the signal produced from the cultures was not sufficient enough to be observed. Consequently, only the AxioObserver Z1 microscope was used for detecting the transfection.

A negative control, a culture containing only the HeLa cells and culture medium, was used. Any indications in Figure 7.17 appearing are not produced due to fluorescence but due to the reflection of dead cells or buddings. Therefore, no transfection was observed in the negative culture.

The TagRFP gene was also attempted to be transfected through the free pTagRFP-C, Figure 7.18, or the pTagRFP-C plasmid mixed with PLL, Figure 7.19, in a protocol similar to one performed by Daniel Joubert et al. [75]. The free plasmid showed no

indications of transfection, which was expected since the negatively charged DNA molecule would be repelled from the negatively charged membrane of the cell [7]. On the other hand, transfection was successful for the plasmid DNA mixed with PLL since the molecule had obtained a positive charge and was able to interact with the membrane. It can also be seen in Figure 7.19 that the culture containing 500 ng of plasmid (Figure 7.19c and Figure 7.19d) was more efficient than the culture containing 300 ng of plasmid (Figure 7.19a and Figure 7.19b). A higher transfection efficiency would be probably achieved if chloroquine and PLL molecules of around 300 residues, instead of the 500-1000 residues used in this thesis, were utilized.

Regarding the origami structure, different annealing protocols were tested for transfection efficiency, but none of them appeared to have efficient transfection. Two indicative cultures can be seen, one for free DNA origami containing 200 μM of spermine in Figure 7.20 and DNA origami mixed with PLL in Figure 7.21. For the PLL case, which was the only positively charged origami structure tested, the inefficient transfection could be caused either by the small amount of actual DNA origami transfected or by a destabilization of the origami structure, caused by its mixing with the PLL molecules. Regarding the small amount of DNA, the results obtained from the Picodrop may not be accurate, because the un-binded staples contained in the mixture may not be completely discarded during dialysis, leading to an increased concentration signal.

9 Conclusion

This Master's thesis aimed to design and produce a DNA origami-like structure, able to *in vivo* transfect a gene which expresses a fluorescent protein into mammalian cells. Initially, an attempt was made with the pHAGE-EF1 α L-eGFP-W plasmid, but as it was proven later, its sequencing was insufficient for an effective design of primers. Therefore, a different plasmid was chosen. Regarding the pTagRFP-C plasmid, a set of primers produced through aPCR reactions to the antisense strand of the TagRFP gene, and ten different fragments, which would make the promoter of the gene accessible for the transcription factors to attach, were designed.

The design of the staples and the overall structure, based on the aforementioned primers, was obtained through the aid of caDNA2 and Maya's vHelix plugin. The final structure was a ten-stranded honeycomb cylinder, in which staples bind to the ends of the structure. The structure's stability and dimensions were tested *in silico* for a time period of 500 ns through with oxDNA2. The molecule had stable total energy for the whole duration of the simulation. Its size was approximately 50 nm x 20 nm x 15 nm, with the ends of the structure being compact and its middle part spreading up due to its lack of staples.

The ssDNA scaffold was obtained experimentally through aPCR, but the production of the ssDNA fragments was not able to be identified. Therefore, for the DNA origami annealing, these fragments were purchased externally. During the DNA origami annealing, different protocols were tested, and the most efficient one seemed to be protocol 2 of Table 5.10, containing 20 mM of MgCl₂ and 5 μ L of scaffold DNA, as it was concluded through AFM imaging.

An attempt for transfection of the TagRFP gene on HeLa cells was performed. Products of different DNA origami annealing protocols were tested, as well as DNA origami structures mixed with PLL, carrier-free plasmid DNA and plasmid DNA mixed with PLL. The only observable transfection was achieved through plasmid DNA mixed with PLL.

10 Future Considerations

To improve the origami structure, a protocol for more accurate identification of the smaller ssDNA fragments should be designed. A ssDNA ladder, combined with a more efficient denaturing protocol would increase the efficiency of the procedure. Beyond that, a ssDNA extraction protocol should be optimized for a better yield of the final product.

Some further steps could additionally be performed to initiate an efficient transfection with the DNA origami structure. Initially, transfection efficiency testing with a DNA origami structure annealed with cholesterol should be performed. If the annealing step of the cholesterol molecules with the already folded DNA origami is not efficient enough, then staples which already have cholesterol attached to them could be ordered.

Another way to increase the efficiency would be the packaging of DNA origami with PLL, with the presence of chloroquine, as was indicated by a protocol of Daniel Joubert et al. [75]. If the PLL is not disruptive enough to destroy the origami structure, then PLL would be an efficient replacement for cholesterol. Additionally, some other positively charged molecules could be used to cover the origami structure, such as polyethylene glycol conjugated with positively charged proteins or polyethylenimine [7].

One more factor which can be checked is the stability of DNA origami over time. It was observed in AFM imaging for the different volumes of scaffold in the annealing mixture, which were checked two weeks after their annealing, that the structures were unfolded. Therefore different measurements could be taken on AFM every 24 h, to check how long the DNA origami-like structures can remain stable.

Bibliography

- [1] W. Wang, W. Li, N. Ma, and G. Steinhoff, "Non-viral gene delivery methods," vol. 14, no. 1, pp. 46–60, Jan. 2013. doi: 10.2174/1389201011314010008.
- [2] N. A. Wivel and J. M. Wilson, "METHODS OF GENE DELIVERY," vol. 12, no. 3, pp. 483–501, Jun. 1998. doi: 10.1016/s0889-8588(05)70004-6.
- [3] S. Nimesh, S. Halappanavar, N. K. Kaushik, and P. Kumar, "Advances in gene delivery systems," vol. 2015, pp. 1–2, 2015. doi: 10.1155/2015/610342.
- [4] M. S. Al-Dosari and X. Gao, "Nonviral gene delivery: Principle, limitations, and recent progress," vol. 11, no. 4, Oct. 2009. doi: 10.1208/s12248-009-9143-y.
- [5] H. Sork, J. Z. Nordin, J. J. Turunen, *et al.*, "Lipid-based transfection reagents exhibit cryo-induced increase in transfection efficiency," vol. 5, e290, 2016. doi: 10.1038/mtna.2016.8.
- [6] P. A. Longo, J. M. Kavran, M.-S. Kim, and D. J. Leahy, "Transient mammalian cell transfection with polyethylenimine (PEI)," in Elsevier, 2013, pp. 227–240. doi: 10.1016/b978-0-12-418687-3.00018-5.
- [7] Y. Nie, L. Ji, H. Ding, *et al.*, "Cholesterol derivatives based charged liposomes for doxorubicin delivery: Preparation, in vitro and in vivo characterization," *Theranostics*, vol. 2, no. 11, pp. 1092–1103, 2012. doi: 10.7150/thno.4949.
- [8] K. S. Lim, D. Y. Lee, G. M. Valencia, Y.-W. Won, and D. A. Bull, "Nano-self-assembly of nucleic acids capable of transfection without a gene carrier," vol. 25, no. 34, pp. 5445–5451, Jul. 2015. doi: 10.1002/adfm.201502067.
- [9] S. A. Smith, L. I. Selby, A. P. R. Johnston, and G. K. Such, "The endosomal escape of nanoparticles: Toward more efficient cellular delivery," vol. 30, no. 2, pp. 263–272, Nov. 2018. doi: 10.1021/acs.bioconjchem.8b00732.
- [10] D. Balakrishnan, G. D. Wilkens, and J. G. Heddle, "Delivering DNA origami to cells," vol. 14, no. 7, pp. 911–925, Apr. 2019. doi: 10.2217/nnm-2018-0440.
- [11] T. Hyeon and V. Rotello, "Endocytosis at the Nanoscale," *Chemical Society reviews*, vol. 41, no. 7, pp. 2545–2561, 2012, issn: 0306-0012.

- [12] D. S. Lee, H. Qian, C. Y. Tay, and D. T. Leong, "Cellular processing and destinies of artificial DNA nanostructures," vol. 45, no. 15, pp. 4199–4225, 2016. doi: 10.1039/c5cs00700c.
- [13] I. A. Khalil, K. Kogure, H. Akita, and H. Harashima, "Uptake pathways and subsequent intracellular trafficking in nonviral gene delivery," vol. 58, no. 1, pp. 32–45, Feb. 2006. doi: 10.1124/pr.58.1.8.
- [14] E. Vivès, J. Schmidt, and A. Pèlegri, "Cell-penetrating and cell-targeting peptides in drug delivery," vol. 1786, no. 2, pp. 126–138, Dec. 2008. doi: 10.1016/j.bbcan.2008.03.001.
- [15] A. Erazo-Oliveras, N. Muthukrishnan, R. Baker, T.-Y. Wang, and J.-P. Pellois, "Improving the endosomal escape of cell-penetrating peptides and their cargos: Strategies and challenges," vol. 5, no. 11, pp. 1177–1209, Nov. 2012. doi: 10.3390/ph5111177.
- [16] A. Aissaoui, N. Oudrhiri, L. Petit, *et al.*, "Progress in gene delivery by cationic lipids : Guanidinium-cholesterol-based systems as an example," *Current Drug Targets*, vol. 3, no. 1, Feb. 2002. doi: 10.2174/1389450023348082.
- [17] J. K. Guy-Caffey, V. Bodepudi, J. S. Bishop, K. Jayaraman, and N. Chaudhary, "Novel polyaminolipids enhance the cellular uptake of oligonucleotides," *Journal of Biological Chemistry*, vol. 270, no. 52, pp. 31 391–31 396, Dec. 1995. doi: 10.1074/jbc.270.52.31391.
- [18] N. Apiratikul, T. Penglong, K. Suksen, S. Svasti, A. Chairoungdua, and B. Yingyongnarongkul, "In vitro delivery of curcumin with cholesterol-based cationic liposomes," *Russian Journal of Bioorganic Chemistry*, vol. 39, no. 4, pp. 444–450, Jul. 2013. doi: 10.1134/s1068162013030035.
- [19] A. Bajaj, P. Kondaiah, and S. Bhattacharya, "Synthesis and gene transfection efficacies of pei-cholesterol-based lipopolymers," *Bioconjugate Chemistry*, vol. 19, no. 8, pp. 1640–1651, Jul. 2008. doi: 10.1021/bc700381v.
- [20] *Idt 3'-cholesterol-teg*, <https://eu.idtdna.com/site/Catalog/Modifications/Product/2555>, Accessed: 25-4-2022.
- [21] *Cholesterol structure*, <https://pubchem.ncbi.nlm.nih.gov/compound/Cholesterol>, Accessed: 20-4-2022.
- [22] Q. Jiang, C. Song, J. Nangreave, *et al.*, "DNA origami as a carrier for circumvention of drug resistance," vol. 134, no. 32, pp. 13 396–13 403, Aug. 2012. doi: 10.1021/ja304263n.
- [23] A. K. Varkouhi, M. Scholte, G. Storm, and H. J. Haisma, "Endosomal escape pathways for delivery of biologicals," vol. 151, no. 3, pp. 220–228, May 2011. doi: 10.1016/j.jconrel.2010.11.004.

- [24] L. M. McLane and A. H. Corbett, "Nuclear localization signals and human disease," *IUBMB Life*, vol. 61, no. 7, pp. 697–706, Jul. 2009. doi: 10.1002/iub.194.
- [25] J. Mikkilä, A.-P. Eskelinen, E. H. Niemelä, *et al.*, "Virus-encapsulated DNA origami nanostructures for cellular delivery," vol. 14, no. 4, pp. 2196–2200, Mar. 2014. doi: 10.1021/nl500677j.
- [26] Y. T. L. Guen, C. Pichon, P. Guégan, *et al.*, "DNA nuclear targeting sequences for enhanced non-viral gene transfer: An in vitro and in vivo study," *Molecular Therapy - Nucleic Acids*, vol. 24, pp. 477–486, Jun. 2021. doi: 10.1016/j.omtn.2021.03.012.
- [27] A. P. Lam and D. A. Dean, "Progress and prospects: Nuclear import of nonviral vectors," *Gene Therapy*, vol. 17, no. 4, pp. 439–447, Mar. 2010. doi: 10.1038/gt.2010.31.
- [28] A. *et al.*, *Essential Cell Biology, third edition*. Garland Science, 2009.
- [29] S. T. Smale and J. T. Kadonaga, "The RNA polymerase II core promoter," vol. 72, no. 1, pp. 449–479, Jun. 2003. doi: 10.1146/annurev.biochem.72.121801.161520.
- [30] J. E. Butler, "The RNA polymerase II core promoter: A key component in the regulation of gene expression," vol. 16, no. 20, pp. 2583–2592, Oct. 2002. doi: 10.1101/gad.1026202.
- [31] J. T. Kadonaga, "Perspectives on the RNA polymerase II core promoter," vol. 1, no. 1, pp. 40–51, Dec. 2011. doi: 10.1002/wdev.21.
- [32] P. W. K. Rothmund, "Folding DNA to create nanoscale shapes and patterns," vol. 440, no. 7082, pp. 297–302, Mar. 2006. doi: 10.1038/nature04586.
- [33] S. Dey, C. Fan, K. V. Gothelf, *et al.*, "DNA origami," vol. 1, no. 1, Jan. 2021. doi: 10.1038/s43586-020-00009-8.
- [34] R. K. Jain and T. Stylianopoulos, "Delivering nanomedicine to solid tumors," vol. 7, no. 11, pp. 653–664, Sep. 2010. doi: 10.1038/nrclinonc.2010.139.
- [35] D. Han, S. Pal, J. Nangreave, Z. Deng, Y. Liu, and H. Yan, "DNA origami with complex curvatures in three-dimensional space," *Science*, vol. 332, no. 6027, pp. 342–346, Apr. 2011. doi: 10.1126/science.1202998.
- [36] E. S. Andersen, M. Dong, M. M. Nielsen, *et al.*, "DNA origami design of dolphin-shaped structures with flexible tails," *ACS Nano*, vol. 2, no. 6, pp. 1213–1218, Jun. 2008. doi: 10.1021/nl800215j.
- [37] Q. Zhang, Q. Jiang, N. Li, *et al.*, "DNA origami as an in vivo drug delivery vehicle for cancer therapy," vol. 8, no. 7, pp. 6633–6643, Jun. 2014. doi: 10.1021/nl502058j.

- [38] J. Yoo and A. Aksimentiev, "In situ structure and dynamics of DNA origami determined through molecular dynamics simulations," *Proceedings of the National Academy of Sciences*, vol. 110, no. 50, pp. 20 099–20 104, Nov. 2013. doi: 10.1073/pnas.1316521110.
- [39] H. T. Maune, S.-p. Han, R. D. Barish, *et al.*, "Self-assembly of carbon nanotubes into two-dimensional geometries using DNA origami templates," *Nature Nanotechnology*, vol. 5, no. 1, pp. 61–66, Nov. 2009. doi: 10.1038/nnano.2009.311.
- [40] A. Kuzyk, R. Schreiber, Z. Fan, *et al.*, "DNA-based self-assembly of chiral plasmonic nanostructures with tailored optical response," *Nature*, vol. 483, no. 7389, pp. 311–314, Mar. 2012. doi: 10.1038/nature10889.
- [41] P. Wang, T. A. Meyer, V. Pan, P. K. Dutta, and Y. Ke, "The beauty and utility of DNA origami," vol. 2, no. 3, pp. 359–382, Mar. 2017. doi: 10.1016/j.chempr.2017.02.009.
- [42] C. E. Castro, F. Kilchherr, D.-N. Kim, *et al.*, "A primer to scaffolded DNA origami," *Nature Methods*, vol. 8, no. 3, pp. 221–229, Feb. 2011. doi: 10.1038/nmeth.1570.
- [43] K. F. Wagenbauer, F. A. S. Engelhardt, E. Stahl, *et al.*, "How we make DNA origami," *ChemBioChem*, vol. 18, no. 19, pp. 1873–1885, Aug. 2017. doi: 10.1002/cbic.201700377.
- [44] A. Rajendran, M. Endo, Y. Katsuda, K. Hidaka, and H. Sugiyama, "Photo-cross-linking-assisted thermal stability of DNA origami structures and its application for higher-temperature self-assembly," *Journal of the American Chemical Society*, vol. 133, no. 37, pp. 14 488–14 491, Aug. 2011. doi: 10.1021/ja204546h.
- [45] J. Elbaz, P. Yin, and C. A. Voigt, "Genetic encoding of DNA nanostructures and their self-assembly in living bacteria," *Nature Communications*, vol. 7, no. 1, Apr. 2016. doi: 10.1038/ncomms11179.
- [46] V. J. Schüller, S. Heidegger, N. Sandholzer, *et al.*, "Cellular immunostimulation by CpG-sequence-coated DNA origami structures," *ACS Nano*, vol. 5, no. 12, pp. 9696–9702, Nov. 2011. doi: 10.1021/nn203161y.
- [47] M. M. C. Bastings, F. M. Anastassacos, N. Ponnuswamy, *et al.*, "Modulation of the cellular uptake of DNA origami through control over mass and shape," vol. 18, no. 6, pp. 3557–3564, May 2018. doi: 10.1021/acs.nanolett.8b00660.
- [48] A. Sharei, J. Zoldan, A. Adamo, *et al.*, "A vector-free microfluidic platform for intracellular delivery," *Proceedings of the National Academy of Sciences*, vol. 110, no. 6, pp. 2082–2087, Jan. 2013. doi: 10.1073/pnas.1218705110.
- [49] P. M. Nikolov, K. J. Koßmann, A. Schilling, *et al.*, "Cytosolic delivery of large supramolecular protein complexes arranged on DNA nanopegboards," Dec. 2017. doi: 10.1101/236729.

- [50] A. Chopra, S. Krishnan, and F. C. Simmel, "Electrotransfection of polyamine folded DNA origami structures," vol. 16, no. 10, pp. 6683–6690, Sep. 2016. doi: 10.1021/acs.nanolett.6b03586.
- [51] J. Liu, L. Song, S. Liu, *et al.*, "A DNA-based nanocarrier for efficient gene delivery and combined cancer therapy," vol. 18, no. 6, pp. 3328–3334, Apr. 2018. doi: 10.1021/acs.nanolett.7b04812.
- [52] *The ptagrfp-c vector's details page in evrogen*, <https://evrogen.com/products/vectors/pTagRFP-C/pTagRFP-C.shtml>.
- [53] "High efficiency gene transfer into mammalian cells," *Philosophical Transactions of the Royal Society of London. B, Biological Sciences*, vol. 307, no. 1132, pp. 343–346, Dec. 1984. doi: 10.1098/rstb.1984.0137.
- [54] J. Haas, E.-C. Park, and B. Seed, "Codon usage limitation in the expression of HIV-1 envelope glycoprotein," *Current Biology*, vol. 6, no. 3, pp. 315–324, Mar. 1996. doi: 10.1016/s0960-9822(02)00482-7.
- [55] M. Kozak, "An analysis of 5'-noncoding sequences from 699 vertebrate messenger RNAs," *Nucleic Acids Research*, vol. 15, no. 20, pp. 8125–8148, 1987. doi: 10.1093/nar/15.20.8125.
- [56] N. J. Proudfoot, A. Furger, and M. J. Dye, "Integrating mRNA processing with transcription," *Cell*, vol. 108, no. 4, pp. 501–512, Feb. 2002. doi: 10.1016/s0092-8674(02)00617-7.
- [57] E. M. Merzlyak, J. Goedhart, D. Shcherbo, *et al.*, "Bright monomeric red fluorescent protein with an extended fluorescence lifetime," *Nature Methods*, vol. 4, no. 7, pp. 555–557, Jun. 2007. doi: 10.1038/nmeth1062.
- [58] *The tagrfp red fluorescent protein in evrogen*, https://evrogen.com/products/TagRFP/TagRFP_Detailed_description.shtml, Accessed: 20-9-2021.
- [59] *The crystal structure of the tagrfp red fluorescent protein*, <https://www.fpbases.org/protein/tagrfp/>, Accessed: 20-9-2021.
- [60] *The ptagrfp-c vector in snapgene*, https://www.snapgene.com/resources/plasmid-files/?set=fluorescent_protein_genes_and_plasmids&plasmid=pTagRFP-C, Accessed: 20-9-2021.
- [61] D. Kobelt, J. Aumann, I. Fichtner, U. Stein, P. M. Schlag, and W. Walther, "Activation of the CMV-IE promoter by hyperthermia in vitro and in vivo: Biphasic heat induction of cytosine deaminase suicide gene expression," *Molecular Biotechnology*, vol. 46, no. 2, pp. 197–205, May 2010. doi: 10.1007/s12033-010-9292-3.
- [62] M. BOSCHART, F. WEBER, G. JAHN, K. DORSCHHLER, B. FLECKENSTEIN, and W. SCHAFFNER, "A very strong enhancer is located upstream of an immediate early gene of human cytomegalovirus," *Cell*, vol. 41, no. 2, pp. 521–530, Jun. 1985. doi: 10.1016/s0092-8674(85)80025-8.

- [63] H. Isomura and M. F. Stinski, "The human cytomegalovirus major immediate-early enhancer determines the efficiency of immediate-early gene transcription and viral replication in permissive cells at low multiplicity of infection," *Journal of Virology*, vol. 77, no. 6, pp. 3602–3614, Mar. 2003. doi: 10.1128/jvi.77.6.3602-3614.2003.
- [64] N. H. Chau, C. D. Vanson, and J. A. Kerry, "Transcriptional regulation of the human cytomegalovirus US11 early gene," *Journal of Virology*, vol. 73, no. 2, pp. 863–870, Feb. 1999. doi: 10.1128/jvi.73.2.863-870.1999.
- [65] R. Liu, J. Baillie, J. P. Sissons, and J. H. Sinclair, "The transcription factor YY1 binds to negative regulatory elements in the human cytomegalovirus major immediate early enhancer/promoter and mediates repression in nonpermissive cells," *Nucleic Acids Research*, vol. 22, no. 13, pp. 2453–2459, 1994. doi: 10.1093/nar/22.13.2453.
- [66] J. L. Meier and M. F. Stinski, "Regulation of human cytomegalovirus immediate-early gene expression," *Intervirology*, vol. 39, no. 5-6, pp. 331–342, 1996. doi: 10.1159/000150504.
- [67] K. T. Jeang, D. R. Rawlins, P. J. Rosenfeld, J. H. Shero, T. J. Kelly, and G. S. Hayward, "Multiple tandemly repeated binding sites for cellular nuclear factor 1 that surround the major immediate-early promoters of simian and human cytomegalovirus," *Journal of Virology*, vol. 61, no. 5, pp. 1559–1570, May 1987. doi: 10.1128/jvi.61.5.1559-1570.1987.
- [68] D. L. Nelson, *Lehninger Principles of Biochemistry 6th Edition*. W. H. Freeman, 2004.
- [69] *Pcr cycling parameters—six key considerations for success*, <https://www.thermofisher.com/dk/en/home/life-science/cloning/cloning-learning-center/invitrogen-school-of-molecular-biology/pcr-education/pcr-reagents-enzymes/pcr-cycling-considerations.html>, Accessed: 10-11-2021.
- [70] S. Poddar, "Symmetric vs asymmetric PCR and molecular beacon probe in the detection of a target gene of adenovirus," vol. 14, no. 1, pp. 25–32, Feb. 2000. doi: 10.1006/mcpr.1999.0278.
- [71] *The phage-ef1al-egfp-w plasmid in addgene*, <https://www.addgene.org/126686/>, Accessed: 20-9-2021.
- [72] H. Summer, R. Grämer, and P. Dröge, "Denaturing urea polyacrylamide gel electrophoresis (urea PAGE)," *Journal of Visualized Experiments*, no. 32, Oct. 2009. doi: 10.3791/1485.
- [73] *Gwyddion*, <http://gwyddion.net/>, Accessed: 22-5-2022.
- [74] *How afm works | nanosurf.com*, <https://www.nanosurf.com/en/support/history-and-background-of-afm>, Accessed: 4-5-2022.

- [75] D. Joubert, J. van Zyl, A. Hawtrey, and M. Ariatti, "A note on poly-l-lysine-mediated gene transfer in HeLa cells," *Drug Delivery*, vol. 10, no. 3, pp. 209–211, Jan. 2003. doi: 10.1080/713840395.
- [76] "Cadnano," Accessed: 25-9-2021. [Online]. Available: <https://cadnano.org/>.
- [77] "Vhelix - free-form dna nanostructure design.," Accessed: 25-9-2021. [Online]. Available: <http://vhelix.net/>.
- [78] T. E. Ouldridge, A. A. Louis, and J. P. K. Doye, "Structural, mechanical, and thermodynamic properties of a coarse-grained DNA model," *The Journal of Chemical Physics*, vol. 134, no. 8, p. 085101, Feb. 2011. doi: 10.1063/1.3552946.
- [79] E. Poppleton, R. Romero, A. Mallya, L. Rovigatti, and P. Šulc, "OxDNA.org: A public webserver for coarse-grained simulations of DNA and RNA nanostructures," *Nucleic Acids Research*, vol. 49, no. W1, W491–W498, May 2021. doi: 10.1093/nar/gkab324.
- [80] "Dna model introduction," Aug. 2019. [Online]. Available: https://dna.physics.ox.ac.uk/index.php/DNA_model_introduction.
- [81] e. a. Jonathan P. K. Doye Hannah Fowler, "The oxdna coarse-grained model as a tool to simulate dna origami," [Online]. Available: <https://arxiv.org/ftp/arxiv/papers/2004/2004.05052.pdf>.
- [82] S. Naskar and P. K. Maiti, "Mechanical properties of DNA and DNA nanostructures: Comparison of atomistic, martini and oxDNA models," *Journal of Materials Chemistry B*, vol. 9, no. 25, pp. 5102–5113, 2021. doi: 10.1039/d0tb02970j.
- [83] B. E. K. Snodin, F. Randisi, M. Mosayebi, *et al.*, "Introducing improved structural properties and salt dependence into a coarse-grained model of DNA," *The Journal of Chemical Physics*, vol. 142, no. 23, p. 234901, Jun. 2015. doi: 10.1063/1.4921957.
- [84] *Eurofins scientific*, <https://www.eurofins.com/>, Accessed: 20-2-2022.
- [85] *Dna duplex stability*, <https://atdbio.com/nucleic-acids-book/DNA-duplex-stability>, Accessed: 22-5-2022.
- [86] *Nf-kb transcription factors*, <https://www.bu.edu/nf-kb/>, Accessed: 22-4-2022.
- [87] *Input options - oxdna*, https://dna.physics.ox.ac.uk/index.php/Input_options, Accessed: 20-9-2021.
- [88] L. Verlet, "Computer "experiments" on classical fluids. i. thermodynamical properties of lennard-jones molecules," *Physical Review*, vol. 159, no. 1, pp. 98–103, Jul. 1967. doi: 10.1103/physrev.159.98.
- [89] É. Hegedüs, E. Kókai, A. Kotlyar, V. Dombrádi, and G. Szabó, "Separation of 1–23-kb complementary DNA strands by urea–agarose gel electrophoresis," *Nucleic Acids Research*, vol. 37, no. 17, e112–e112, Jun. 2009. doi: 10.1093/nar/gkp539.

- [90] *Role of mgcl₂ in pcr reaction*, <https://geneticeducation.co.in/role-of-mgcl2-in-pcr-reaction/>, Accessed: 22-5-2022.
- [91] *Role of mgcl₂ and kcl in pcr*, <https://www.biotecharticles.com/Biotech-Research-Article/Role-of-KCl-and-MgCl2-in-PCR-3271.html>, Accessed: 22-5-2022.
- [92] *Nanophotonics circuits formed by dna self-assembly*, [https://projekter.aau.dk/projekter/da/studentthesis/nanofotonisk-kredsloeb-skabt-ved-dna-selvsamling\(36f6945d-323b-4098-a4ca-89d71ca41e2a\).html](https://projekter.aau.dk/projekter/da/studentthesis/nanofotonisk-kredsloeb-skabt-ved-dna-selvsamling(36f6945d-323b-4098-a4ca-89d71ca41e2a).html), Accessed: 21-4-2022.
- [93] L. S. Shlyakhtenko, S. Dutta, J. Banga, M. Li, R. S. Harris, and Y. L. Lyubchenko, "APOBEC3g interacts with ssDNA by two modes: AFM studies," *Scientific Reports*, vol. 5, no. 1, Oct. 2015. doi: 10.1038/srep15648.

A Appendix

```
1 #####
2 ##### PROGRAM/SIM PARAMETERS #####
3 #####
4
5 backend = CPU
6 steps = 100000
7 sim_type = min
8 dt = 0.00165
9 verlet_skin = 0.15
10 diff_coeff = 2.50
11 T = 300K
12
13 #####
14 ##### INTERACTIONS #####
15 #####
16
17 interaction_type = DNA2
18 max_backbone_force = 50
19 salt_concentration = 0.2
20
21 #####
22 ##### INPUT/OUTPUT #####
23 #####
24
25 topology = pTagRFP.top
26 energy_file = energy_min.dat
27 conf_file = pTagRFP.conf
28 lastconf_file = min.conf
29 trajectory_file = min_traj.dat
30
31 print_conf_interval = 500
32 print_energy_every = 500
33 no_stdout_energy = false
34 time_scale = linear
35 restart_step_counter = 1
36 refresh_vel = 1
```

Listing A.1: The minimization script used for the pTagRFP.top and pTagRFP.conf files.

```
1 #####
2 ##### PROGRAM PARAMETERS #####
3 #####
4
5 backend = CPU
6
7 #####
8 ##### SIM PARAMETERS #####
9 #####
10
11 steps = 100000
12 sim_type = MD
13 dt = 0.00165
14 verlet_skin = 0.15
15 diff_coef = 2.50
16 T = 300K
17
18 #####
19 ##### INTERACTIONS #####
20 #####
21
22 interaction_type = DNA2
23 max_backbone_force = 20
24 salt_concentration = 0.2
25 thermostat = langevin
26
27
28 #####
29 ##### INPUT/OUTPUT #####
30 #####
31
32 topology = pTagRFP.top
33 energy_file = energy_relax.dat
34 conf_file = min.conf
35 lastconf_file = relax.conf
36 trajectory_file = relax_traj.dat
37
38 print_conf_interval = 500
39 print_energy_every = 500
40 time_scale = linear
41 restart_step_counter = 1
```

Listing A.2: The Langevin relaxation script used for the pTagRFP.top and pTagRFP.conf files.

```

1 #####
2 #####          PROGRAM PARAMETERS          #####
3 #####
4
5 backend                =                CPU
6
7 #####
8 #####          SIM PARAMETERS             #####
9 #####
10
11 steps                  =                100000
12 sim_type               =                MD
13 dt                     =                0.00165
14 verlet_skin           =                0.15
15 diff_coef              =                2.50
16 T                      =                300K
17
18 #####
19 #####          INTERACTIONS              #####
20 #####
21
22 interaction_type       =                DNA2
23 max_backbone_force    =                20
24 salt_concentration     =                0.2
25 thermostat             =                brownian
26 newtonian_steps        =                103
27
28
29 #####
30 #####          INPUT/OUTPUT              #####
31 #####
32
33 topology               =                pTagRFP.top
34 energy_file            =                energy_relax.dat
35 conf_file              =                min.conf
36 lastconf_file          =                relax.conf
37 trajectory_file        =                relax_traj.dat
38
39 print_conf_interval    =                500
40 print_energy_every     =                500
41 time_scale             =                linear
42 restart_step_counter   =                1

```

Listing A.3: The Brownian relaxation script used for the pTagRFP.top and pTagRFP.conf files.

```
1 #####
2 ##### PROGRAM PARAMETERS #####
3 #####
4
5 backend = CPU
6
7 #####
8 ##### SIM PARAMETERS #####
9 #####
10
11 steps = 2500000
12 sim_type = MD
13 newtonian_steps = 103
14 dt = 0.005
15 verlet_skin = 0.05
16 diff_coef = 2.50
17 T = 300K
18
19 #####
20 ##### INTERACTIONS #####
21 #####
22
23 interaction_type = DNA2
24 salt_concentration = 0.2
25 thermostat = langevin
26
27 #####
28 ##### INPUT/OUTPUT #####
29 #####
30
31 topology = pTagRFP.top
32 energy_file = energy_go_1.dat
33 conf_file = relax.conf
34 lastconf_file = sim_1.conf
35 trajectory_file = sim_traj_1.dat
36
37 print_conf_interval = 50000
38 print_energy_every = 50000
39 time_scale = linear
40 restart_step_counter = 1
```

Listing A.4: The Langevin Molecular Dynamics script used for the pTagRFP.top and pTagRFP.conf files.

```

1 #####
2 ##### PROGRAM PARAMETERS #####
3 #####
4
5 backend = CPU
6
7 #####
8 ##### SIM PARAMETERS #####
9 #####
10
11 steps = 250000
12 sim_type = MD
13 newtonian_steps = 103
14 dt = 0.005
15 verlet_skin = 0.05
16 diff_coef = 2.50
17 T = 300K
18
19 #####
20 ##### INTERACTIONS #####
21 #####
22
23 interaction_type = DNA2
24 salt_concentration = 0.2
25 thermostat = brownian
26
27 #####
28 ##### INPUT/OUTPUT #####
29 #####
30
31 topology = pTagRFP.top
32 energy_file = energy_go_1.dat
33 conf_file = relax.conf
34 lastconf_file = sim_1.conf
35 trajectory_file = sim_traj_1.dat
36
37 print_conf_interval = 5000
38 print_energy_every = 5000
39 time_scale = linear
40 restart_step_counter = 1

```

Listing A.5: The Brownian Molecular Dynamics script used for the pTagRFP.top and pTagRFP.conf files.

B Appendix

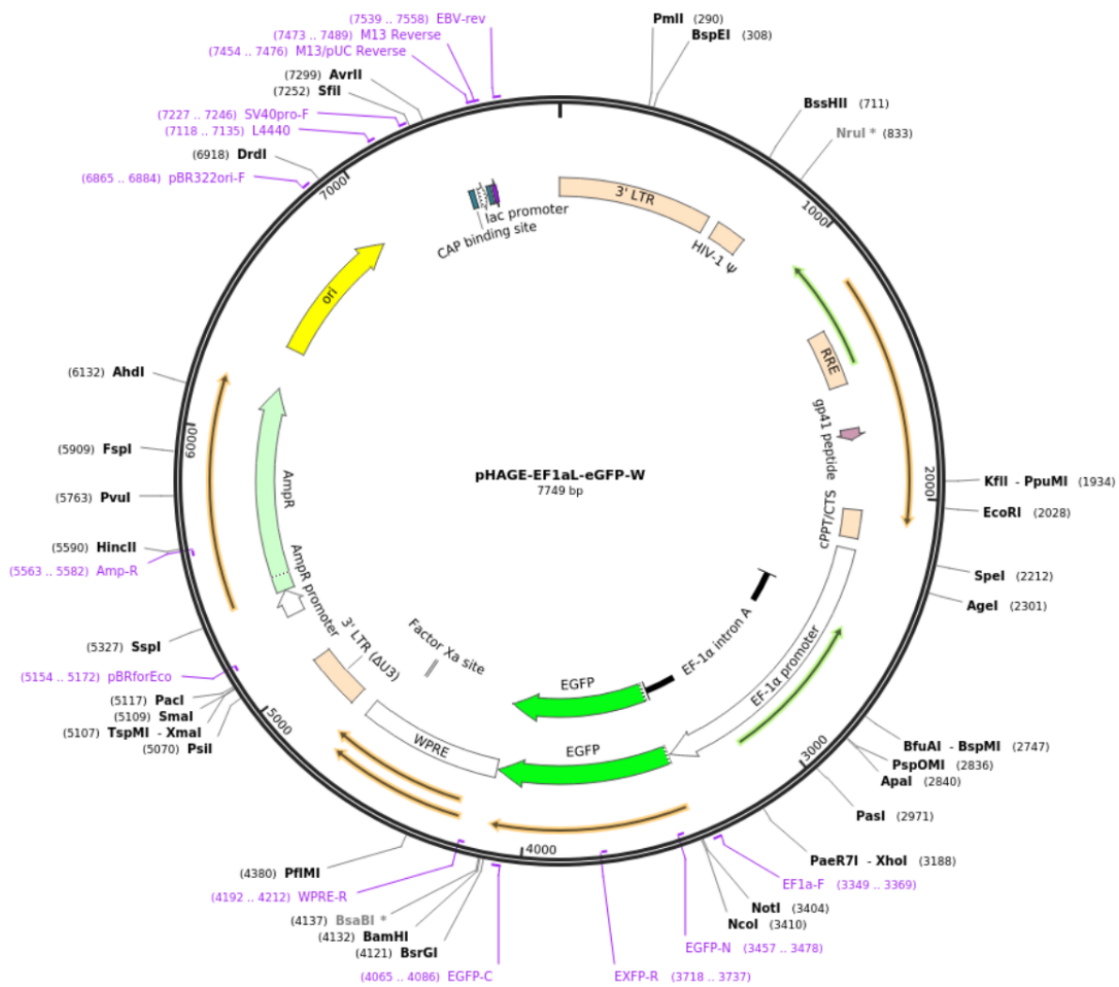


Figure B.1: The pHAGE-EF1 α L-eGFP-W plasmid. Obtained from [71].

Table B.1: 1677 nt sequence obtained from the asymmetric PCR reaction with pTagRFP-C vector as a template. This sequence is the complementary, 5' to 3', sequence of the asymmetric PCR product, when the first three primers of Table 5.5 are utilized. **Green sequence:** CMV_{IE} promoter's enhancer sequence. **Red sequence:** CMV_{IE} promoter sequence. **Blue sequence:** TATA box. **Yellow sequence:** TagRFP gene.

1	CC CCT GAT TCT GTG GAT AAC CGT ATT ACC GCC ATG CAT TAG TTA	44
45	TTA ATA GTA ATC AAT TAC GGG GTC ATT AGT TCA TAG CCC ATA TAT	89
90	GGA GTT CCG CGT TAC ATA ACT TAC GGT AAA TGG CCC GCC TGG CTG	134
135	ACC GCC CAA CGA CCC CCG CCC ATT GAC GTC AAT AAT GAC GTA TGT	179
180	TCC CAT AGT AAC GCC AAT AGG GAC TTT CCA TTG ACG TCA ATG GGT	224
225	GGA GTA TTT ACG GTA AAC TGC CCA CTT GGC AGT ACA TCA AGT GTA	269
270	TCA TAT GCC AAG TAC GCC CCC TAT TGA CGT CAA TGA CGG TAA ATG	314
315	GCC CGC CTG GCA TTA TGC CCA GTA CAT GAC CTT ATG GGA CTT TCC	359
360	TAC TTG GCA GTA CAT CTA CGT ATT AGT CAT CGC TAT TAC CAT GGT	404
405	GAT GCG GTT TTG GCA GTA CAT CAA TGG GCG TGG ATA GCG GTT TGA	449
450	CTC ACG GGG ATT TCC AAG TCT CCA CCC CAT TGA CGT CAA TGG GAG	494
495	TTT GTT TTG GCA CCA AAA TCA ACG GGA CTT TCC AAA ATG TCG TAA	539
540	CAA CTC CGC CCC ATT GAC GCA AAT GGG CGG TAG GCG TGT ACG GTG	584
585	GGA GGT CTA TAT AAG CAG AGC TGG TTT AGT GAA CCG TCA GAT CCG	629
630	CTA GCG CTA CCG GTC GCC ACC ATG GTG TCT AAG GGC GAA GAG CTG	674
675	ATT AAG GAG AAC ATG CAC ATG AAG CTG TAC ATG GAG GGC ACC GTG	719
720	AAC AAC CAC CAC TTC AAG TGC ACA TCC GAG GGC GAA GGC AAG CCC	764
765	TAC GAG GGC ACC CAG ACC ATG AGA ATC AAG GTG GTC GAG GGC GGC	809
810	CCT CTC CCC TTC GCC TTC GAC ATC CTG GCT ACC AGC TTC ATG TAC	854
855	GGC AGC AGA ACC TTC ATC AAC CAC ACC CAG GGC ATC CCC GAC TTC	899
900	TTT AAG CAG TCC TTC CCT GAG GGC TTC ACA TGG GAG AGA GTC ACC	944
945	ACA TAC GAA GAC GGG GGC GTG CTG ACC GCT ACC CAG GAC ACC AGC	989
990	CTC CAG GAC GGC TGC CTC ATC TAC AAC GTC AAG ATC AGA GGG GTG	1034
1035	AAC TTC CCA TCC AAC GGC CCT GTG ATG CAG AAG AAA ACA CTC GGC	1079
1080	TGG GAG GCC AAC ACC GAG ATG CTG TAC CCC GCT GAC GGC GGC CTG	1124
1125	GAA GGC AGA AGC GAC ATG GCC CTG AAG CTC GTG GGC GGC GGC CAC	1169
1170	CTG ATC TGC AAC TTC AAG ACC ACA TAC AGA TCC AAG AAA CCC GCT	1214
1215	AAG AAC CTC AAG ATG CCC GGC GTC TAC TAT GTG GAC CAC AGA CTG	1259
1260	GAA AGA ATC AAG GAG GCC GAC AAA GAG ACC TAC GTC GAG CAG CAC	1304
1305	GAG GTG GCT GTG GCC AGA TAC TGC GAC CTC CCT AGC AAA CTG GGG	1349
1350	CAC AAA CTT AAT TCC GGA CTC AGA TCT CGA GCT CAA GCT TCG AAT	1394
1395	TCT GCA GTC GAC GGT ACC GCG GGC CCG GGA TCC ACC GGA TCT AGA	1439
1440	TAA CTG ATC ATA ATC AGC CAT ACC ACA TTT GTA GAG GTT TTA CTT	1484
1485	GCT TTA AAA AAC CTC CCA CAC CTC CCC CTG AAC CTG AAA CAT AAA	1529
1530	ATG AAT GCA ATT GTT GTT GTT AAC TTG TTT ATT GCA GCT TAT AAT	1574
1575	GGT TAC AAA TAA AGC AAT AGC ATC ACA AAT TTC ACA AAT AAA GCA	1619
1620	TTT TTT TCA CTG CAT TCT AGT TGT GGT TTG TCC AAA CTC ATC AAT	1664
1665	GTA TCT TAA CGC G	1677